

**Supporting Information For:**

**Post-synthetic Modification of a Macrocyclic  
Receptor via Regioselective Imidazolium Ring-  
opening**

Jia Shang,<sup>a</sup> Brett M. Rambo,<sup>b</sup> Xiang Hao,<sup>c</sup> Jun-Feng Xiang,<sup>c</sup> Han-Yuan Gong,<sup>\*a</sup> and Jonathan L. Sessler<sup>\*b,d</sup>

<sup>a</sup> College of Chemistry, Beijing Normal University, Xijiekouwaidajie 19, Beijing 100875, P. R. China;

<sup>b</sup> Department of Chemistry, The University of Texas at Austin, 105 East 24th Street, Stop A5300, Austin, Texas 78712-1224, United States;

<sup>c</sup> Institute of Chemistry, Chinese Academy of Sciences, Zhongguancunbeiyijie 2, Beijing 100190, P. R. China;

<sup>d</sup> Department of Chemistry, Shanghai University, Shanghai 200444, China

\*e-mail: [hanyuangong@bnu.edu.cn](mailto:hanyuangong@bnu.edu.cn); [ssessler@cm.utexas.edu](mailto:ssessler@cm.utexas.edu)

## Materials and Methods

**Section S1:** *General considerations (pp. S3-S4)*

**Section S2:** *Synthesis, characterization, and conformational study of  $[2^{2+} \cdot 2PF_6^-]$  and  $[3^{2+} \cdot 2PF_6^-]$  in solution (pp. S5-S33)*

**Section S3:** *Single crystal X-ray diffraction analysis of  $[2^{2+} \cdot 2PF_6^- \cdot 4\text{dioxane}]$ ,  $[2^{2+} \cdot 2PF_6^- \cdot CH_3CN \cdot H_2O]$  and  $[3^{2+} \cdot 2PF_6^- \cdot CH_3CN]$  (pp. S34-S39)*

**Section S4:** *Solution binding studies and characterization of the host-guest complexes formed between  $[2^{2+} \cdot 2PF_6^-]$  and dianionic guests 2,6-naphthalenedicarboxylate (**4**), 2,6-naphthalenedisulfonate (**5**) or 1,5-naphthalenedisulfonate (**6**) (pp. S40-S54)*

**Section S5:** *Single crystal X-ray analysis of the complexes formed between  $2^{2+}$  and dianionic guest **5** or **6** (pp. S55-S59)*

**Section S6:** *Mass spectrometric analysis of the complexes formed between  $2^{2+}$  and dianionic guest **4**, **5** or **6** (p. S60-S63)*

**Section S7:** *Solution binding studies and characterization of the OH ring-opening process leading to the irreversible disassembly of the interpenetrated structures  $[1^{4+} \cdot 4]$  and  $[1^{4+} \cdot 5]$  (pp. S64-S69)*

**Section S7:** *Comparative analysis of the conformation of  $[2^{2+} \cdot 2PF_6^-]$  and  $[1^{4+} \cdot 4PF_6^-]$ , and the associated complexes formed with anionic guest **4**, **5**, or **6** (pp. S70-S72)*

**Section S8:** *References (pp. S73)*

### *Section S1: General considerations*

All solvents were dried before use according to standard protocols.<sup>1</sup> For this study, all reagents were purchased commercially (Aldrich, Acros, or Fisher) and used without further purification. Deuterated solvents were purchased from Cambridge Isotope Laboratory (Andover, MA). NMR spectra were recorded on Bruker AVANCE III 400, AVANCE III 500WB or AVANCE 600 spectrometers. The <sup>1</sup>H and <sup>13</sup>C NMR chemical shifts are reported relative to residual solvent signals (<sup>1</sup>H: DMSO-*d*<sub>6</sub> at 2.50 ppm).<sup>2</sup> ESI-MS data was acquired by infusion on a Thermo LTQ-XL linear ion trap mass spectrometer operating in positive ion mode.

All single crystals used to obtain the X-ray diffraction structures grew as colorless prisms or needles, or yellow prisms. The .cif documents are available as separate supporting information files, which provide details regarding the specific crystals used for the analysis, along with the structure in question. Diffraction grade crystals were obtained *via* slow evaporation or liquid-liquid diffusion from solution in a mixture of water/acetonitrile/DMF or water/acetonitrile or dioxane/acetonitrile as described below.

The specific liquid-liquid diffusion conditions for crystal cultivation are shown below: a solvent mixture (DMF/water, 1/1, v/v; 2 mL), used as the second layer, was added to a first layer of guest **5** or **6** in water (0.400 mL of a 0.01 M solution). Then, 1 mL of **2**<sup>2+</sup> (0.05 M) in a mixture of DMF/acetonitrile/water (1/1/1, v/v/v; 1 mL) was added as the third layer to the clear solution. The anion guest was produced from 2H<sup>+</sup>·**5** or 2H<sup>+</sup>·**6** in situ *via* the addition of two molar equiv. of tetramethylammonium hydroxide (TMA<sup>+</sup>·OH<sup>-</sup>) such that tetramethylammonium was the counter cation.

The crystals used for single crystal analyses were cut from clusters of the corresponding crystals and had the approximate dimensions given in the .cif documents. The data were collected on a D8 Venture, Rigaku Mercury2 (2x2 bin mode) or Saturn724+ (2x2 bin mode) CCD diffractometers using a graphite monochromator with *MoKα* radiation ( $\lambda = 0.71073 \text{ \AA}$ ). Data reduction was performed using CrystalClear or APEX II. The structures were solved by

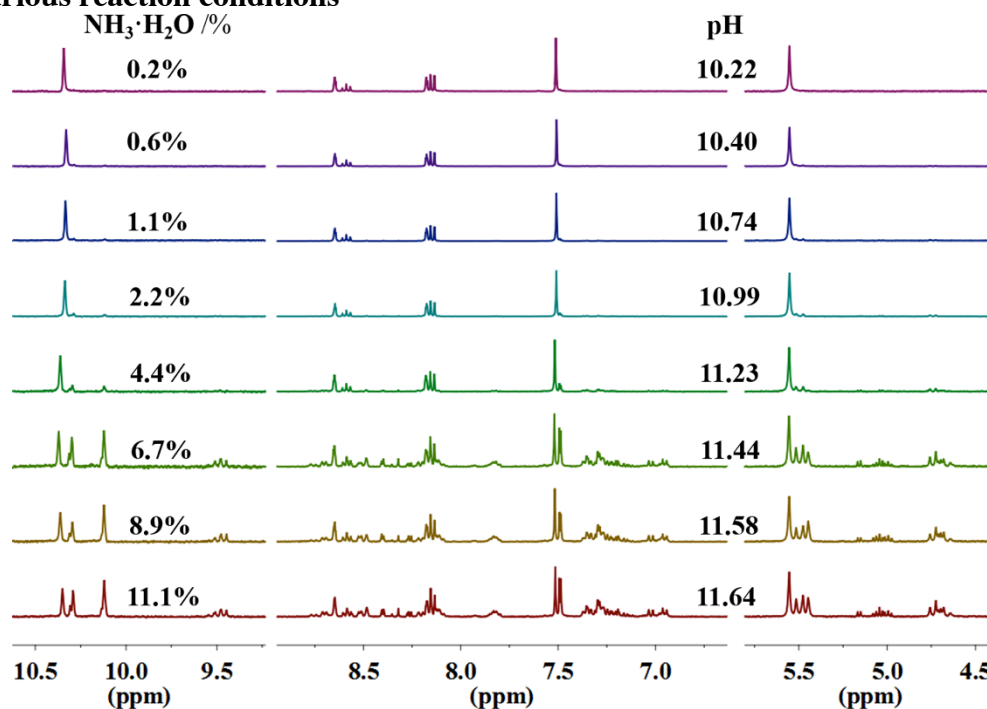
direct methods using SIR97<sup>3</sup> and refined by full-matrix least-squares on  $F^2$  with anisotropic displacement parameters for the non-H atoms using SHELXL-97.<sup>4</sup> The hydrogen atoms were calculated in idealized positions with isotropic displacement parameters set to 1.2 x Ueq of the attached atom (1.5 x Ueq for methyl hydrogen atoms). The utility ROTAX<sup>5</sup> in the program WinGX<sup>6</sup> was used to look for possible twins. R(F), Rw(F2) and the goodness of fit, S, are given below and in the .cif documents. All ellipsoid figures were generated using SHELXTL/PC.<sup>7</sup> Tables of positional and thermal parameters, bond lengths and angles, torsion angles, figures and lists of observed and calculated structure factors are located in the .cif documents available from the Cambridge Crystallographic Centre and may be obtained by quoting the CCDC ref. numbers 1433722, 1433723, 1433724, 1433725 and 1433726. The documents also contain details of the crystal data, data collection, and structure refinement for each structure.

**Section S2: Synthesis, characterization, and conformational study of  $[2^{2+} \cdot 2PF_6^-]$  and  $[3^{2+} \cdot 2PF_6^-]$  in solution**

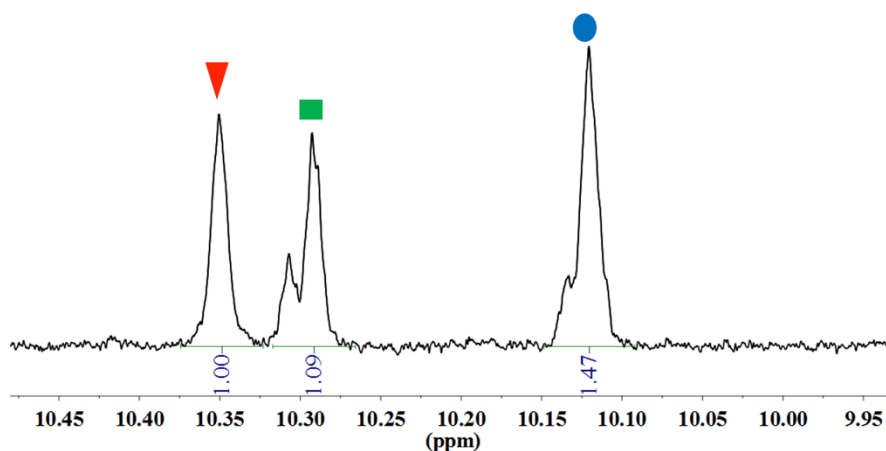
**General procedure for the synthesis of  $[2^{2+} \cdot 2PF_6^-]$  and  $[3^{2+} \cdot 2PF_6^-]$**

In a typical procedure, a 25ml small vial was charged with 50 mg (0.041 mmol)  $1^{4+} \cdot 4PF_6^-$  ( $1^{4+}$ : cyclo[2](2,6-di(1H-imidazol-1-yl)pyridine)[2](1,4-dimethylenebenzene)) in a mixture containing 1 mL aqueous ammonia (between 25-28% by mass), 3.5 mL water and 4.5 mL acetonitrile. This solution was stirred hermetically at 313K for 24h. The reaction was then cooled to room temperature and acetonitrile was removed *via* blowing with compressed air, which gave rise to a light yellow precipitate (the crude product). The product was then collected via filtration and washing with 2 ml of water. Herein, reference to %NH<sub>3</sub>·H<sub>2</sub>O is meant to represent the volume fraction of NH<sub>3</sub>·H<sub>2</sub>O (25-28% by mass) used in the final solution. The reaction solvent consists of acetonitrile (4.5 mL) and dilutes aqueous ammonia (4.5 mL). The latter was obtained by mixing concentrated aqueous ammonia (25-28% by weight) with water to give the final stated concentration of ammonia. The ratio of the initial organic and aqueous phases was 1:1 in all experiments. It is suggested that the crude product mainly contains  $1^{4+} \cdot 4PF_6^-$ , the single ring-opened product  $I^{3+} \cdot 3PF_6^-$ , the two ring opened product  $II^{2+} \cdot 2 PF_6^-$  (*i.e.*,  $2^{2+} \cdot 2PF_6^-$  and  $3^{2+} \cdot 2PF_6^-$ ) (cf. Figure S2 and S3).

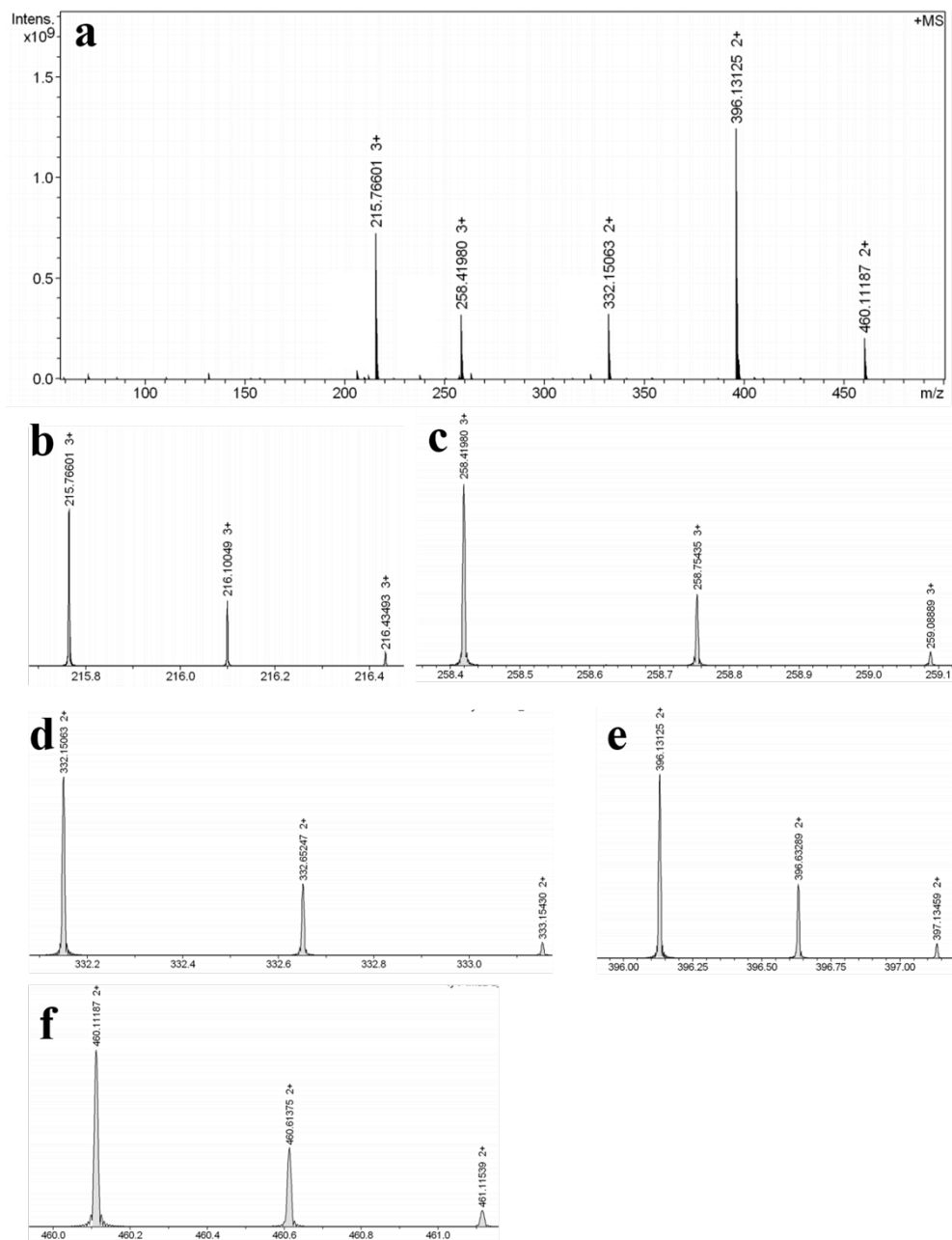
**$^1\text{H}$  NMR and ESI mass spectrometric analysis of the synthesis of  $[2^{2+}\cdot 2\text{PF}_6^-]$  and  $[3^{2+}\cdot 2\text{PF}_6^-]$  under various reaction conditions**



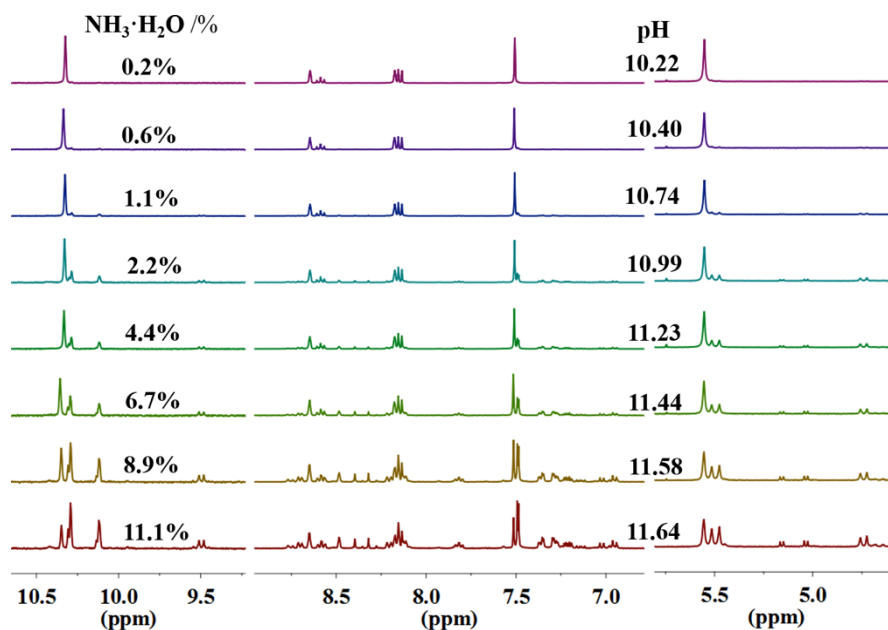
**Figure S1.**  $^1\text{H}$  NMR spectra recorded in  $\text{DMSO-}d_6$  (400 MHz, 300K) representing the crude products obtained from the ring-opening reaction of  $1^{4+}\cdot 4\text{PF}_6^-$  using different concentrations of  $\text{NH}_3\cdot\text{H}_2\text{O}$  at 288K for 45h. Here  $\text{NH}_3\cdot\text{H}_2\text{O} \%$  represents the volume fraction of  $\text{NH}_3\cdot\text{H}_2\text{O}$  (25-28% by weight) in the final solution. The pH value shown is that of the initial solvent system.



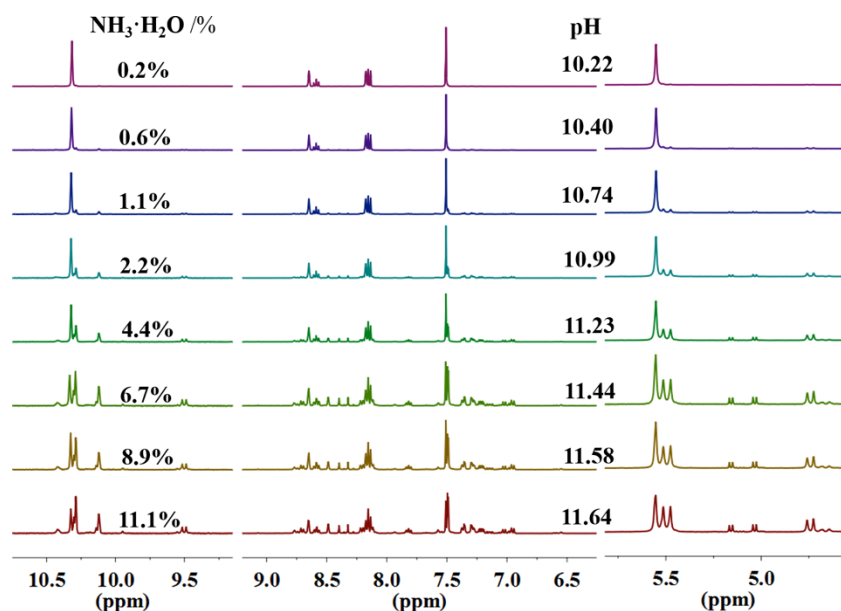
**Figure S2.** The expanded  $^1\text{H}$  NMR spectrum recorded in  $\text{DMSO-}d_6$  (400 MHz, 300K) of the crude product obtained from the reaction wherein the initial solvent pH was 11.64 and the reaction was run at 288K for 45 h. The proton signals of the C-H protons between the two nitrogen atoms on the imidazolium rings of  $1^{4+}$  (labeled as “ $\blacktriangledown$ ”),  $1^{3+}$  (labeled as “ $\blacksquare$ ”) and  $11^{2+}$  (labeled as “ $\bullet$ ”). The relative amounts of each independent component in the crude product were obtained from the integrated areas.



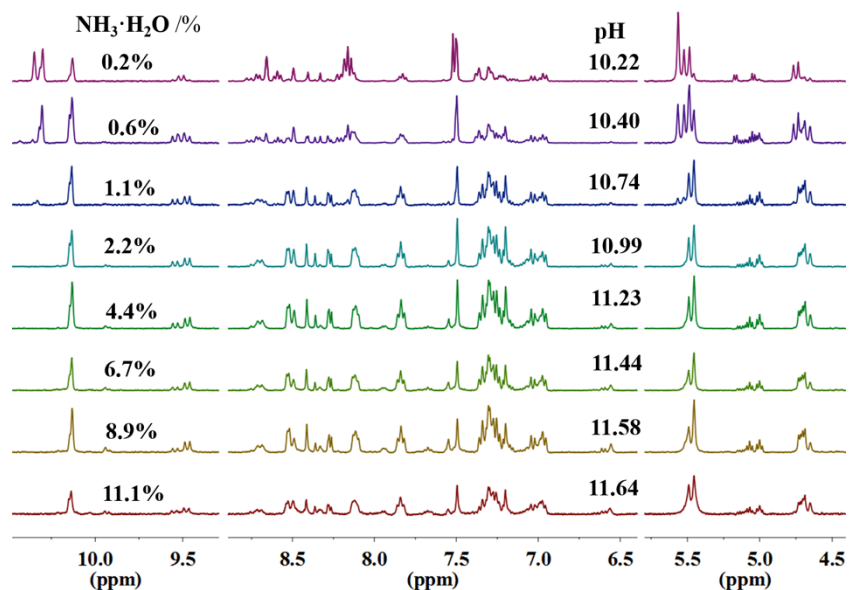
**Figure S3.** The full view (a) and expanded view (b) of the ESI high resolution mass spectrum of the crude product obtained from the ring-opening reaction of  $\mathbf{1}^{4+} \cdot 4\text{PF}_6^-$  which was conducted at 288K for 45h at an initial pH of 11.64. It is implied that the crude product contained at least three components  $\mathbf{1}^{4+}$ ,  $\mathbf{I}^{3+}$  and  $\mathbf{II}^{2+}$ : calcd. for  $\text{C}_{38}\text{H}_{34}\text{N}_{10}\text{PF}_6$  ( $[\mathbf{1}^{4+} \cdot \text{PF}_6^-]^{3+}$ ) 258.4203. Found: 258.4198; calcd. for  $([\mathbf{1}^{4+} \cdot 2\text{PF}_6^-]^{2+})$  460.1126. Found: 460.1119; calcd. for  $\text{C}_{38}\text{H}_{35}\text{N}_{10}\text{O}$  ( $[\mathbf{I}^{3+}]$ ) 215.7665. Found: 215.7660; calcd. for  $\text{C}_{38}\text{H}_{36}\text{N}_{10}\text{O}_2$  ( $[\mathbf{II}^{2+}]$ ) 332.1512. Found: 332.1506; calcd. for  $\text{C}_{36}\text{H}_{36}\text{N}_{10}\text{PF}_6\text{K}$  ( $[\mathbf{II}^{2+} \cdot 2\text{CHO} + \text{K} + 2\text{H} + \text{PF}_6^-]^{2+}$ ) 396.1202. Found: 396.1313.



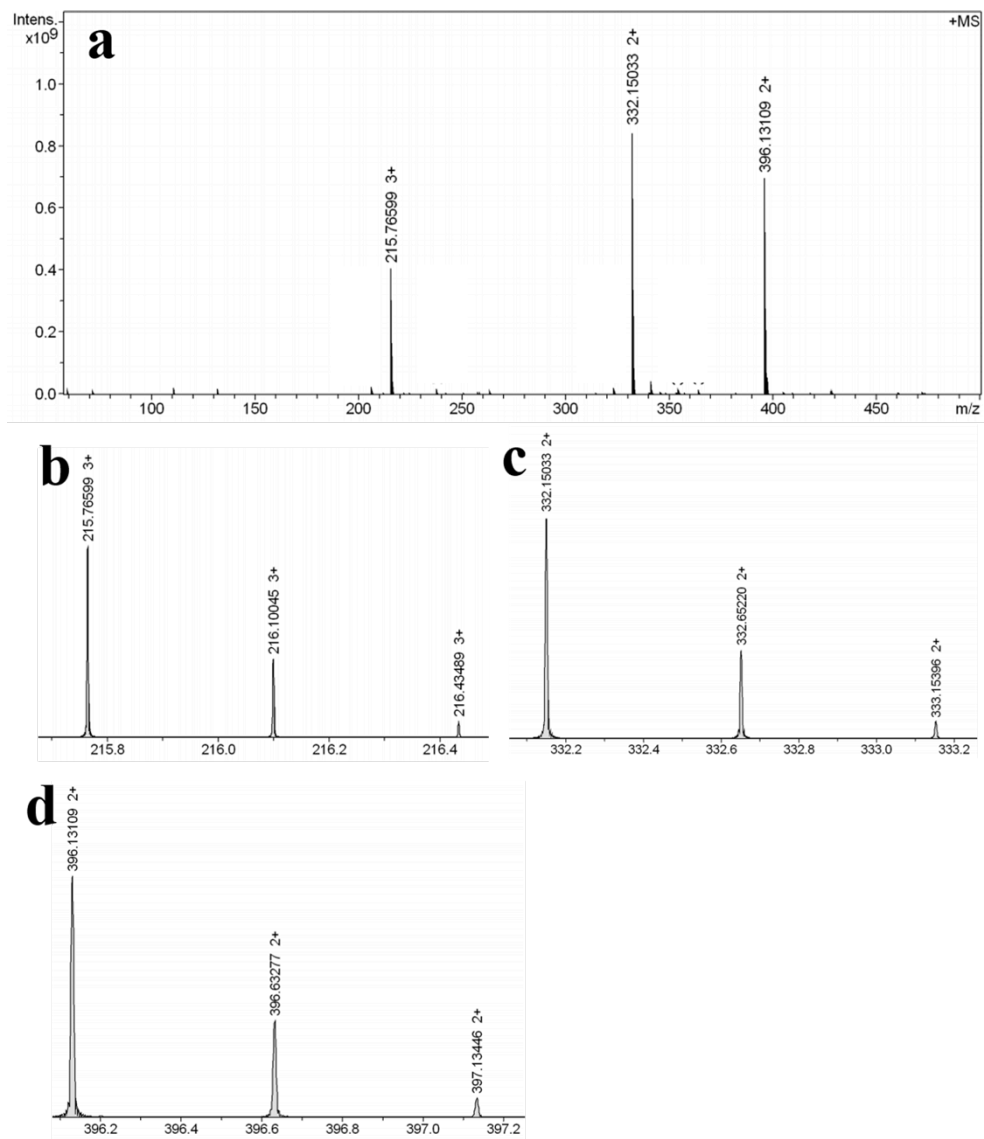
**Figure S4.**  $^1\text{H}$  NMR spectra recorded in  $\text{DMSO-}d_6$  (400 MHz, 300K) representing the crude products obtained from the ring-opening reaction of  $1^{4+}\cdot 4\text{PF}_6^-$  using different concentrations of  $\text{NH}_3\cdot\text{H}_2\text{O}$  at 288K for 96 h. Here,  $\text{NH}_3\cdot\text{H}_2\text{O}\%$  represents the volume fraction of  $\text{NH}_3\cdot\text{H}_2\text{O}$  (25-28% by weight) in the final solution. The pH value shown is that of the initial solvent system.



**Figure S5.**  $^1\text{H}$  NMR spectra recorded in  $\text{DMSO-}d_6$  (400 MHz, 300K) representing the crude products obtained from the ring-opening reaction of  $1^{4+}\cdot 4\text{PF}_6^-$  using different concentrations of  $\text{NH}_3\cdot\text{H}_2\text{O}$  at 288K for 120h. Here  $\text{NH}_3\cdot\text{H}_2\text{O}\%$  represents the volume fraction of  $\text{NH}_3\cdot\text{H}_2\text{O}$  (25-28% by weight) in final solution. The pH value shown is that of the initial solvent system.



**Figure S6.** <sup>1</sup>H NMR spectra recorded in DMSO-*d*<sub>6</sub> (400 MHz, 300K) representing the crude products obtained from the ring-opening reaction of **1**<sup>4+</sup>·4PF<sub>6</sub><sup>-</sup> using different concentrations of NH<sub>3</sub>·H<sub>2</sub>O at 298K for 45 h. Here NH<sub>3</sub>·H<sub>2</sub>O% represents the volume fraction of NH<sub>3</sub>·H<sub>2</sub>O (25-28% by weight) in the final solution. The pH value shown is that of the initial solvent system.



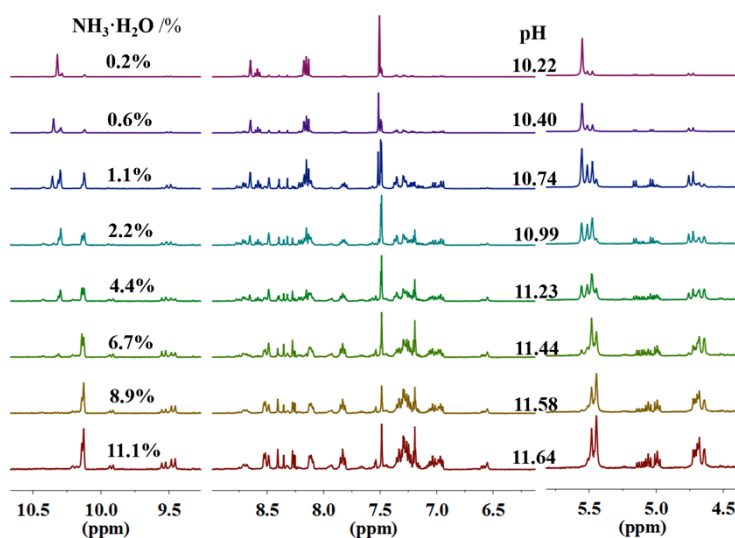
**Figure S7.** Full view (a) and expanded view (b) of the ESI high resolution mass spectrum of the crude product obtained from the ring-opening reaction of  $\mathbf{I}^{4+} \cdot 4\text{PF}_6^-$ , which was conducted at 298K for 45 h at an initial pH of 10.40. It was found that signals for  $\mathbf{I}^{4+}$  disappeared in the crude product, and only the signals related to component  $\mathbf{I}^{3+}$  and  $\mathbf{II}^{2+}$  could be detected as follows: calcd. for  $\text{C}_{38}\text{H}_{35}\text{N}_{10}\text{O}$  ( $[\mathbf{I}^{3+}]$ ) 215.7665. Found: 215.7660; calcd. for  $\text{C}_{38}\text{H}_{36}\text{N}_{10}\text{O}_2$  ( $[\mathbf{II}^{2+}]$ ) 332.1512. Found: 332.1503; calcd. for  $\text{C}_{36}\text{H}_{36}\text{N}_{10}\text{PF}_6\text{K}$  ( $[\mathbf{II}^{2+} - 2\text{CHO} + \text{K} + 2\text{H} + \text{PF}_6^-]^{2+}$ ) 396.1202. Found: 396.1311.

Table S1 below compiles and summarizes the above results.

**Table S1.** Optimization of the ring-opening reaction conditions for  $1^{4+}$ .

Entry	$\text{NH}_3 \cdot \text{H}_2\text{O}$ [a] /%	pH <sub>a</sub> [b]	Total percent conversion/% (288 K, 45h)	Total percent conversion/% (288 K, 96h)	Total percent conversion/% (288 K, 120h)	Total percent conversion/% (298 K, 45h)
1	0.2	10.22	≤ 4.0	≤ 4.0	≤ 4.0	79
2	0.6	10.40	11	9	11	98
3	1.1	10.74	12	20	26	99
4	2.2	10.99	19	46	46	100
5	4.4	11.23	33	49	60	100
6	6.7	11.44	78	62	77	100
7	8.9	11.58	78	78	75	100
8	11.1	11.64	81	87	85	100

[a] Volume fraction of  $\text{NH}_3 \cdot \text{H}_2\text{O}$  used in the final solution. The mixture of reaction solvents consisted of acetonitrile (4.5 mL) and dilute aqueous ammonia (4.5 mL). The latter was obtained by mixing concentrated aqueous ammonia (25-28% by weight) with water to give the final stated concentration of ammonia. The ratio of the initial organic and aqueous phases was 1:1 in all experiments. [b] pH of the initial solvent system.



**Figure S8.**  $^1\text{H}$  NMR spectra recorded in  $\text{DMSO}-d_6$  (400 MHz, 300K) representing the crude products obtained from the ring-opening reaction of  $1^{4+} \cdot 4\text{PF}_6^-$  using different concentrations of  $\text{NH}_3 \cdot \text{H}_2\text{O}$  at 333K for 2 h. Here  $\text{NH}_3 \cdot \text{H}_2\text{O}\%$  represents the volume fraction of  $\text{NH}_3 \cdot \text{H}_2\text{O}$  (25-28% by weight) in final solution. The pH value shown is that of the initial solvent system.

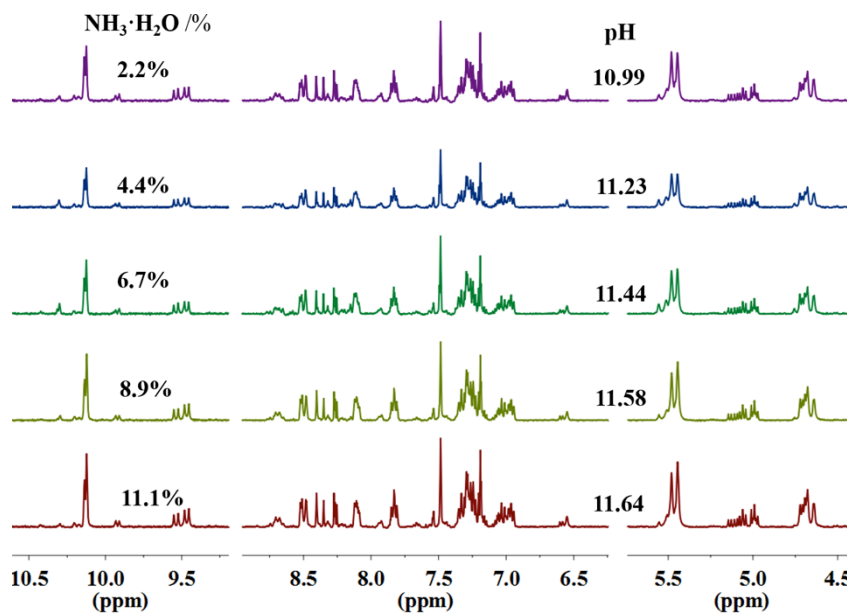


**Figure S9.**  $^1\text{H}$  NMR spectra recorded in  $\text{DMSO-}d_6$  (400 MHz, 300K) representing the crude products obtained from the ring-opening reaction of  $\mathbf{1}^{4+}\cdot 4\text{PF}_6^-$  using different concentrations of  $\text{NH}_3\cdot\text{H}_2\text{O}$  at 313K for 24h. Here  $\text{NH}_3\cdot\text{H}_2\text{O}\%$  represents the volume fraction of  $\text{NH}_3\cdot\text{H}_2\text{O}$  (25-28% by weight) in the final solution. The pH value shown is that of the initial solvent system.

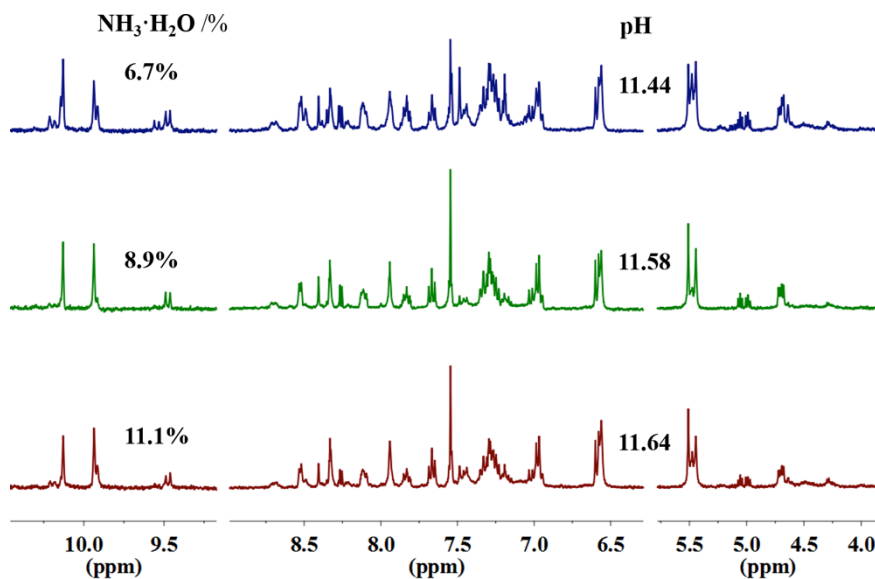


**Figure S10.**  $^1\text{H}$  NMR spectra recorded in  $\text{DMSO-}d_6$  (400 MHz, 300K) representing the crude products obtained from the ring-opening reaction of  $\mathbf{1}^{4+}\cdot 4\text{PF}_6^-$  using different concentrations of  $\text{NH}_3\cdot\text{H}_2\text{O}$  at 313K for 48h. Here  $\text{NH}_3\cdot\text{H}_2\text{O}\%$  represents the volume fraction of  $\text{NH}_3\cdot\text{H}_2\text{O}$  (25-28% by weight) in the final solution. The pH value shown is that of the initial solvent system.

### Simulated ratio of $2^{2+} \cdot 2PF_6^-$ and $3^{2+} \cdot 2PF_6^-$ in the mixture

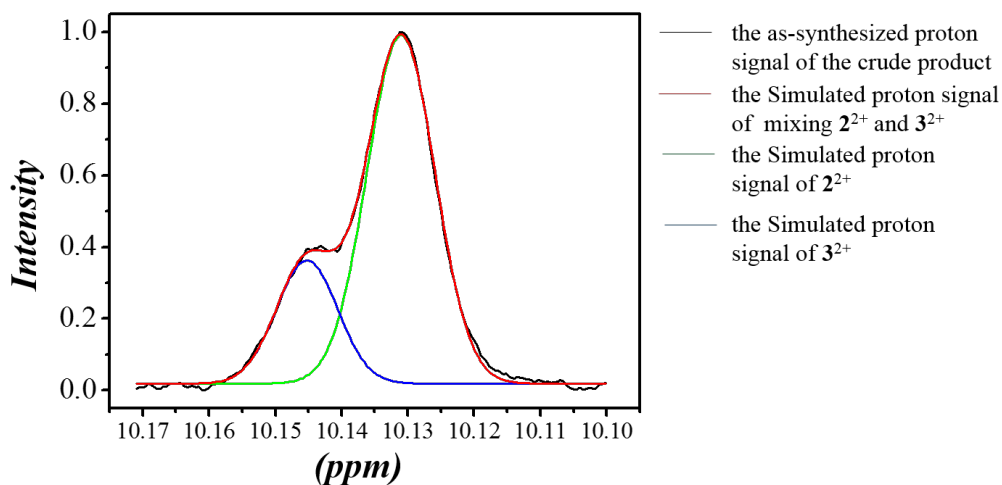
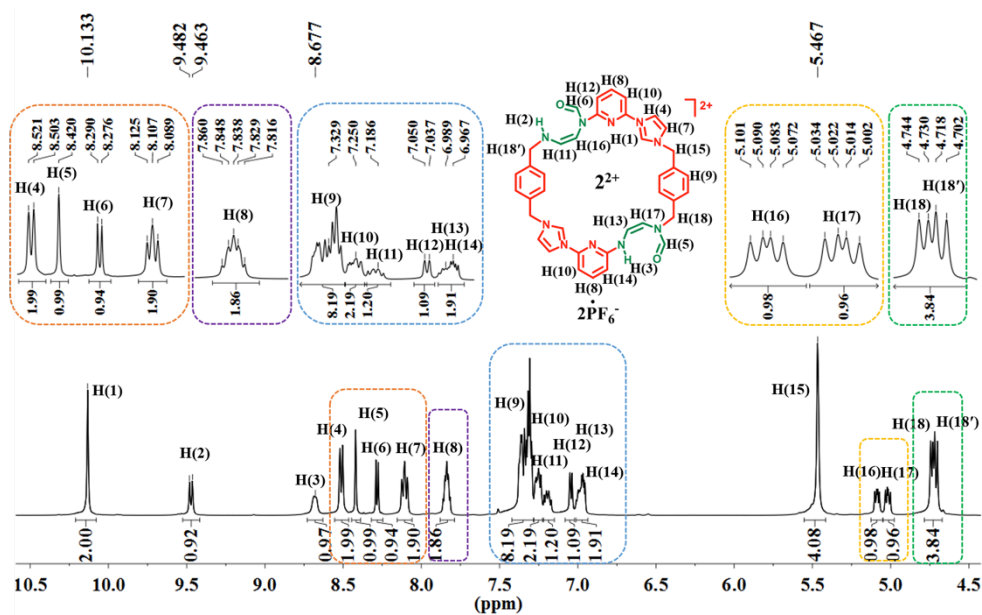


**Figure S11.** Expanded view of signals for H(1) (the proton signals with most lowest chemical shift on  $2^{2+} \cdot 2PF_6^-$  and  $3^{2+} \cdot 2PF_6^-$ ) in the crude product (i.e., the mixture of  $2^{2+}$  and  $3^{2+}$  obtained via the general reaction conditions) in DMSO- $d_6$  at 300K (400 MHz). The black curve is the as-synthesized peak data for H(1) in  $2^{2+}$  and  $3^{2+}$ . The red curve is the simulated peak data for H(1) in the mixture of  $2^{2+}$  and  $3^{2+}$ . The green curves is the simulated peak data for the H(1) signals in  $2^{2+}$ . The blue curves is the simulated peak data for the H(1) signals of  $3^{2+}$ . The mathematical area ratio, consistent with the molar ratio of  $2^{2+} \cdot 2PF_6^-$  and  $3^{2+} \cdot 2PF_6^-$  in the crude product, is approximately 3:1.

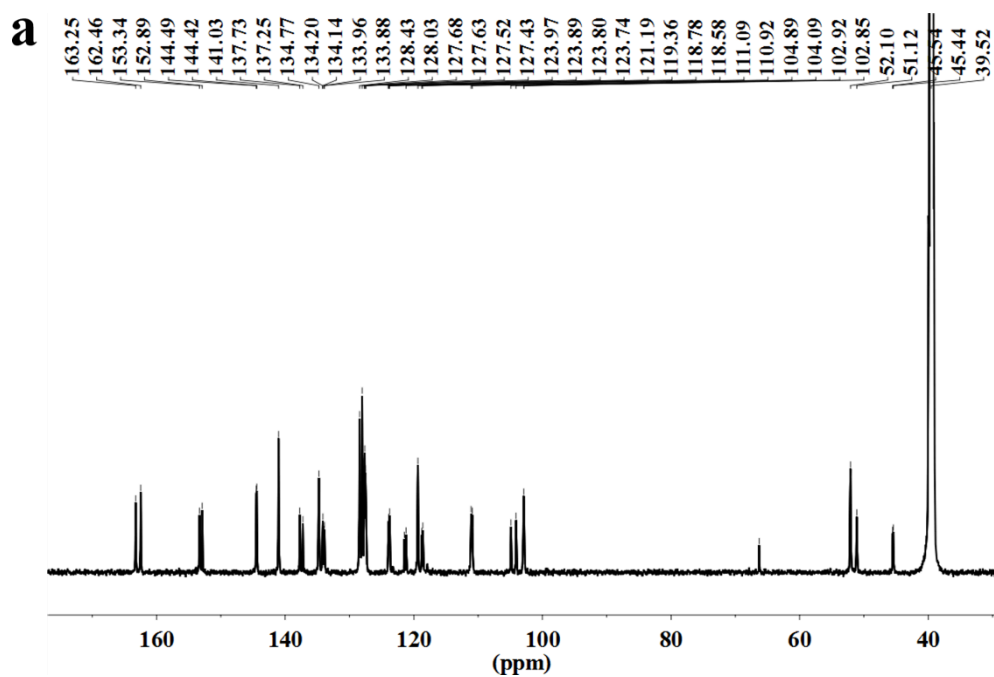
### Synthesis of *trans*-cyclo[2]((*Z*)-*N*-(2-((6-(1*H*-imidazol-1-yl)pyridin-2-yl)amino)vinyl)formamide)[2](1,4-bismethylbenzene)hexafluorophosphate [ $2^{2+} \cdot 2PF_6^-$ ]:

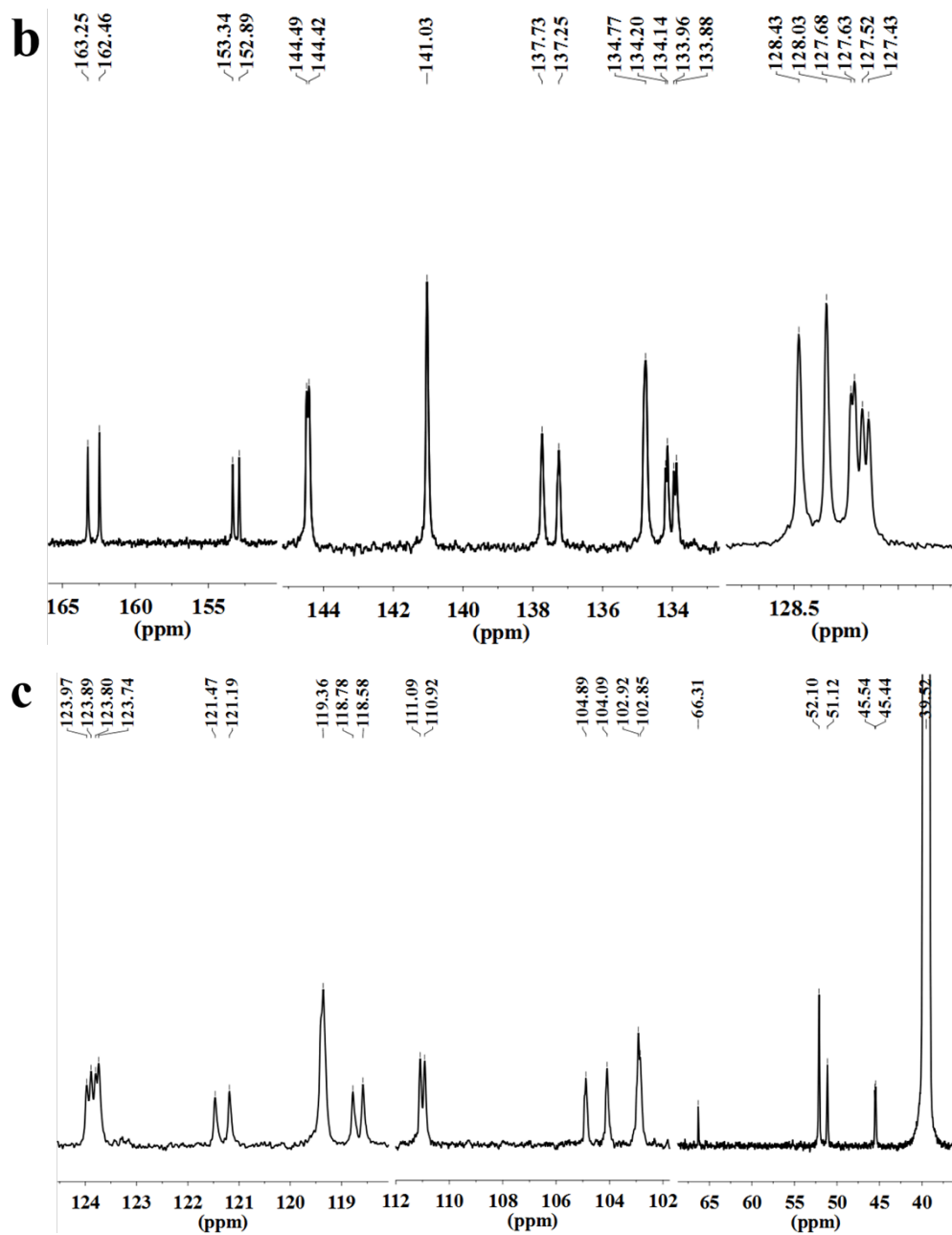
Using the aforementioned procedure, a 25 ml small vial was charged with 50.0 mg (0.041 mmol) of  $1^{4+} \cdot 4PF_6^-$  in aqueous ammonia (between 25-28% by mass), water, and acetonitrile (v/v/v, 1/3.5/4.5, 9 mL). The pH of the initial solvent system was 11.64. The solution was stirred in the absence of air at 313 K for 24 h. The reaction mixture was then cooled to room temperature and the solvent was subsequently removed by blowing the sample with compressed air. Subsequently, a light yellow precipitate (86%-93% crude yield of  $2^{2+} \cdot 2PF_6^-$  plus  $3^{2+} \cdot 2PF_6^-$ ) was collected and then washed with 2 mL water. This crude product was recrystallized from a

mixture of acetonitrile and dioxane (2:1, v/v), resulting in isolation of the pure product  $2^{2+} \cdot 2PF_6^-$  as a light yellow solid in 42% overall yield (37 mg);  $^1H$  NMR (600MHz, DMSO- $d_6$ , 300K)  $\delta$  10.13 (br, 2H, imidazolium ring  $-N=CH-N-$ ), 9.47 (d,  $J = 11.1$  Hz, 1H, ring-opened imidazolium  $-CH=CH-NH-CH_2-$ ), 8.67 (m, 1H, ring-opened imidazolium  $-CH=CH-NH-Py$ ), 8.51 (d, 2H, imidazolium ring  $-CH=CH-N-CH_2-$ ) 8.42 (s, 1H,  $-CH=CH-N(CHO)-CH_2-$  on ring-opened imidazolium group), 8.28 (d,  $J = 8.5$  Hz, 1H,  $-CH=CH-N(CHO)-Py$  on ring-opened imidazolium group), 8.11 (t, 2H, imidazolium ring  $-CH=CH-N-CH_2-$ ), 7.84 (m, 2H,  $H_\gamma-Py$ ), 7.33 (m, 8H, ArH), 7.25 (m, 2H,  $H_\beta-Py-N(imidazolium\ ring)$ ), 7.19 (m, 1H,  $-CH=CH-N(CHO)-Py$  on ring-opened imidazolium group), 7.04 (d,  $J = 8.2$  Hz, 1H,  $H_{\beta 1}-Py-N-CHO$ ), 6.99 (m, 1H,  $-CH=CH-N(CHO)-CH_2-$  on ring-opened imidazolium group), 6.98 (m, 1H,  $H_{\beta 2}-Py-NH$ ), 5.46 (s, 4H,  $-C-CH_2-N(imidazolium\ ring)$ ), 5.08 (m, 1H,  $-CH=CH-N(CHO)-Py$  on ring-opened imidazolium group), 5.02 (m, 1H,  $-CH=CH-N(CHO)-CH_2-$  on ring-opened imidazolium group), 4.72 (m, 4H,  $-C-CH_2-N(ring-opened\ imidazolium\ group)$ );  $^{13}C$  NMR (150 MHz, DMSO- $d_6$ , 300K)  $\delta$  163.3, 162.5, 153.3, 152.9, 144.5, 144.4, 141.0, 137.7, 137.3, 134.8, 134.2, 134.1, 134.0, 133.9, 128.4, 128.0, 127.7, 127.6, 127.5, 127.4, 124.0, 123.9, 123.8, 123.7, 121.5, 121.2, 119.4, 118.8, 118.6, 111.1, 110.9, 104.9, 104.1, 102.9, 102.9, 66.3, 52.1, 51.1, 45.5, 45.4; FT-ICRMS: calcd. for  $C_{38}H_{36}N_{10}O_2PF_6$  ( $[2^{2+} \cdot PF_6^-]^+$ ) 809.2665. Found: 809.2657; calcd. for  $C_{38}H_{35}N_{10}O_2$  ( $[(2^{2+}-H)]^+$ ) 663.2944. Found: 663.2934.

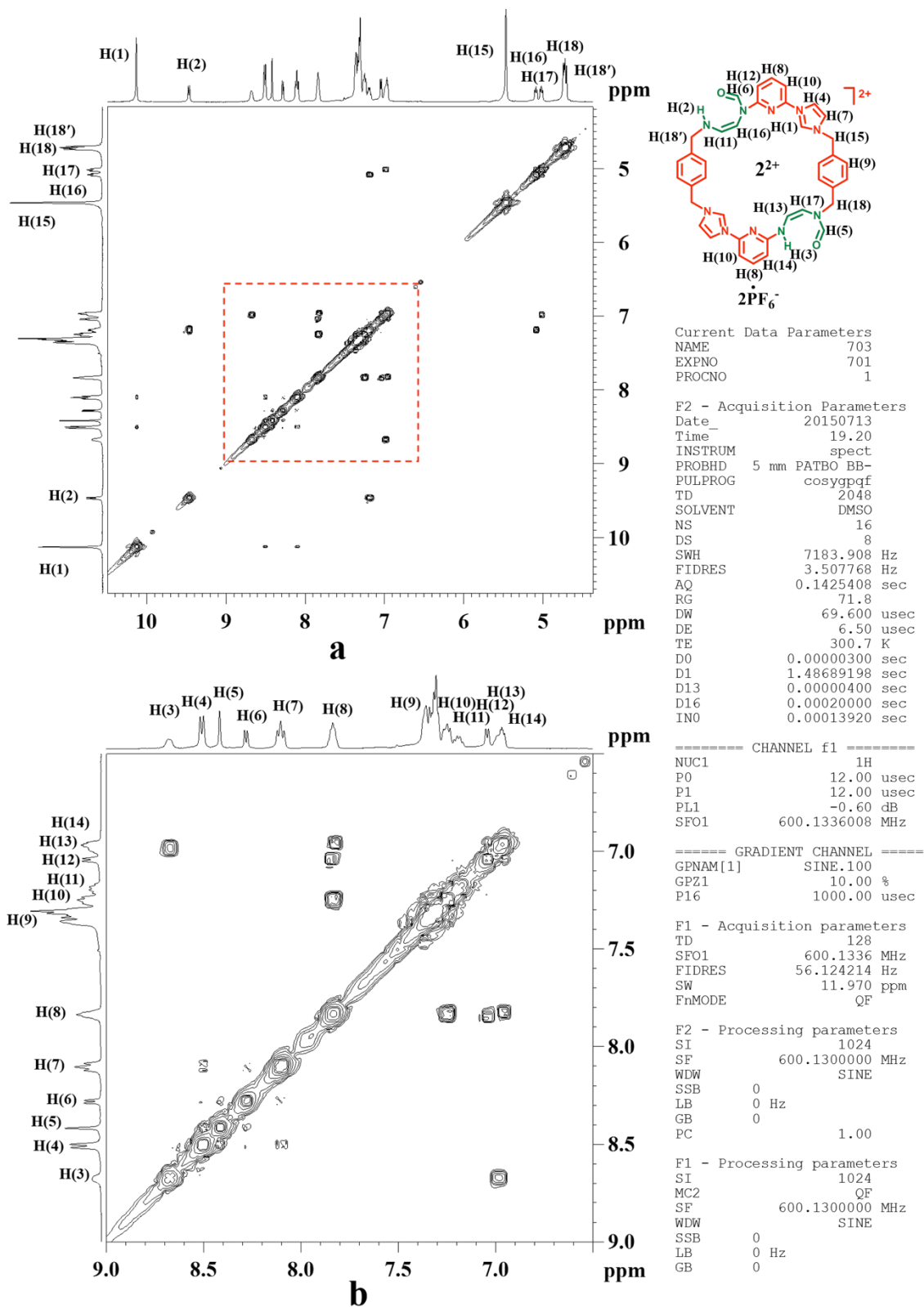


**Figure S12.**  $^1\text{H}$  NMR spectrum of  $2^{2+}\cdot 2\text{PF}_6^-$  ( $6.0 \times 10^{-2}\text{M}$ ) collected in  $\text{DMSO-}d_6$  at 300K (600 MHz).

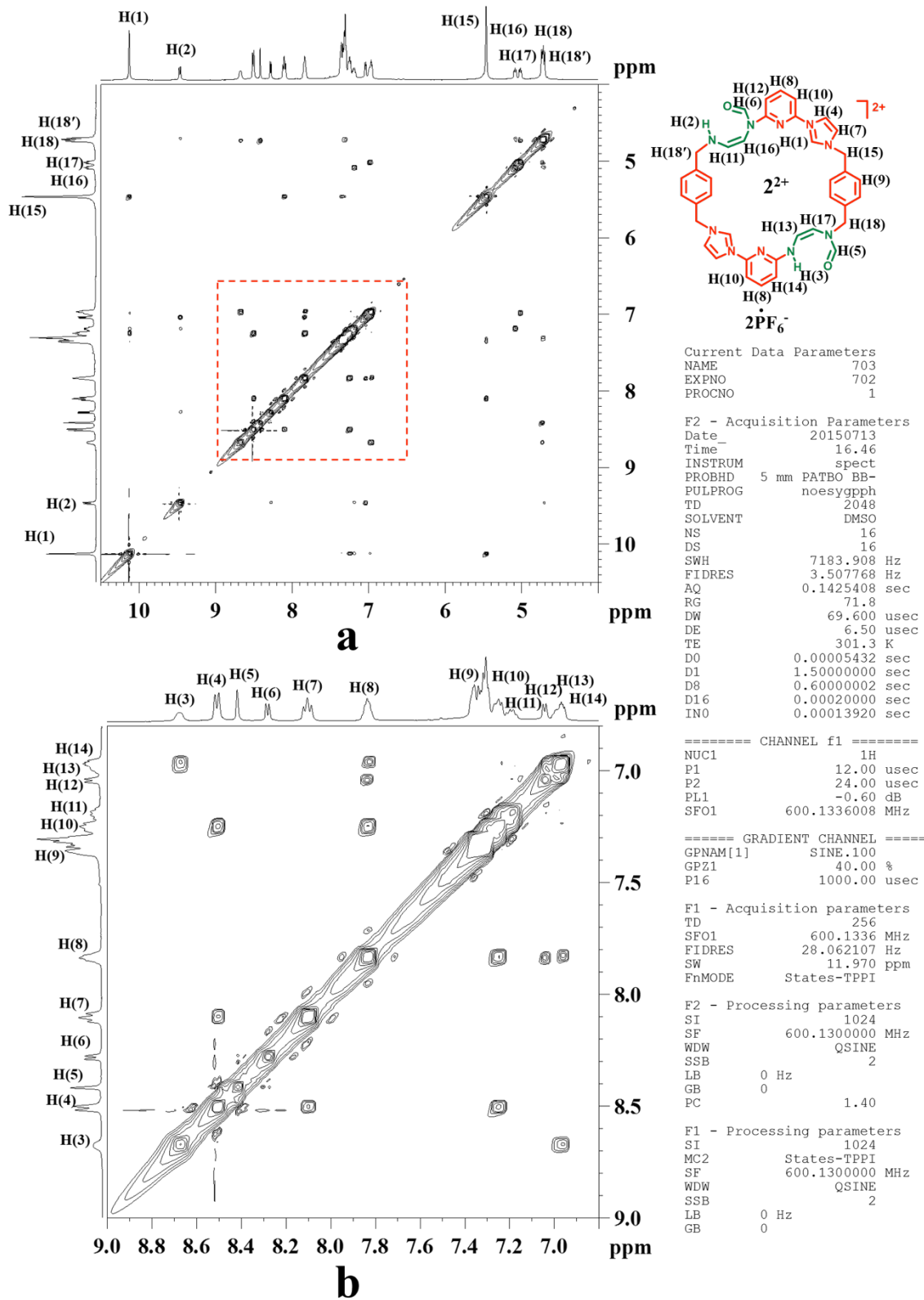




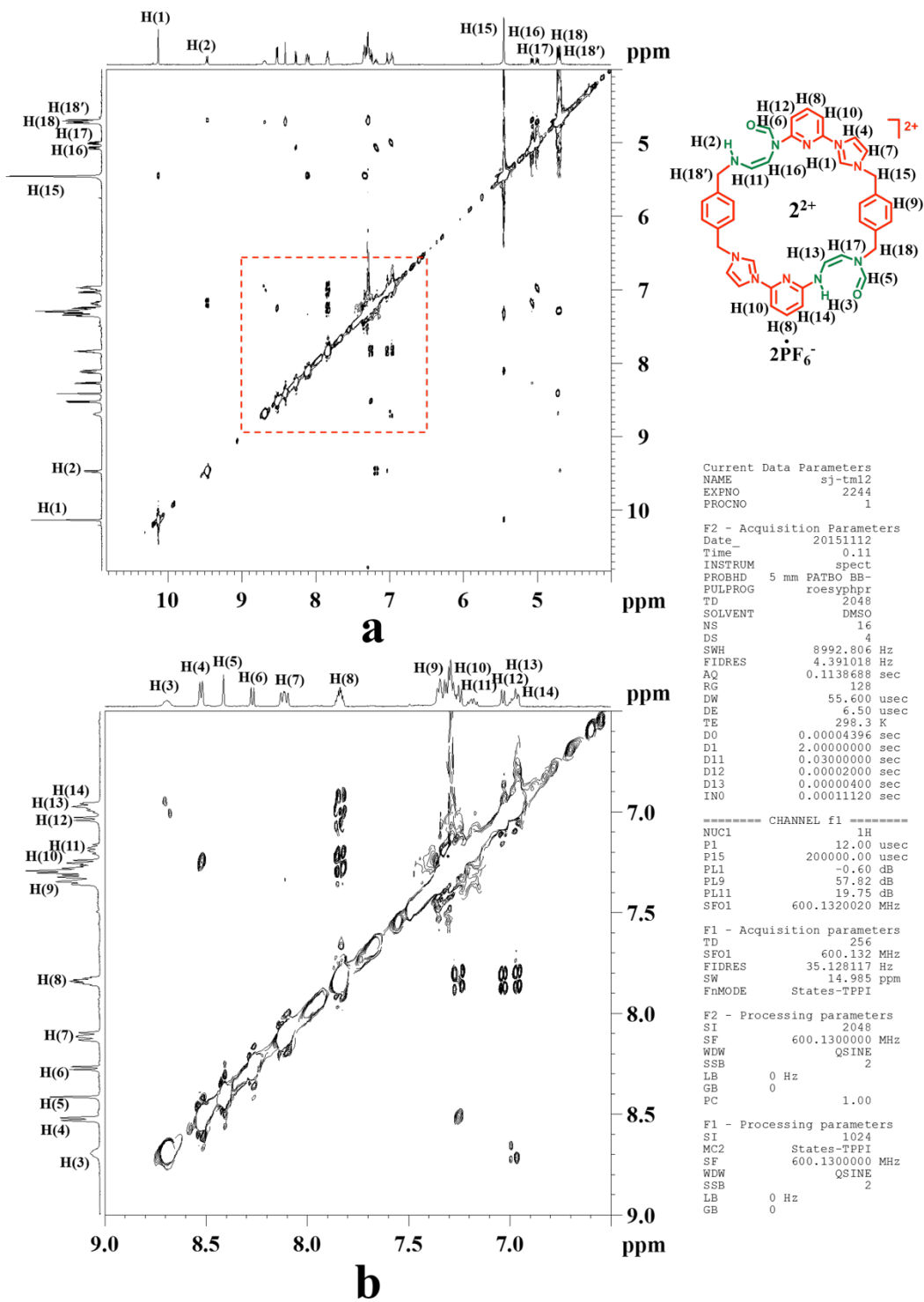
**Figure S13.** Full view (a) and expanded views (b), (c) of the  $^{13}\text{C}$  NMR spectrum of  $2^{2+}\cdot 2\text{PF}_6^-$  ( $6.0 \times 10^{-2}\text{M}$ ) collected in  $\text{DMSO-}d_6$  at 300K (150 MHz).



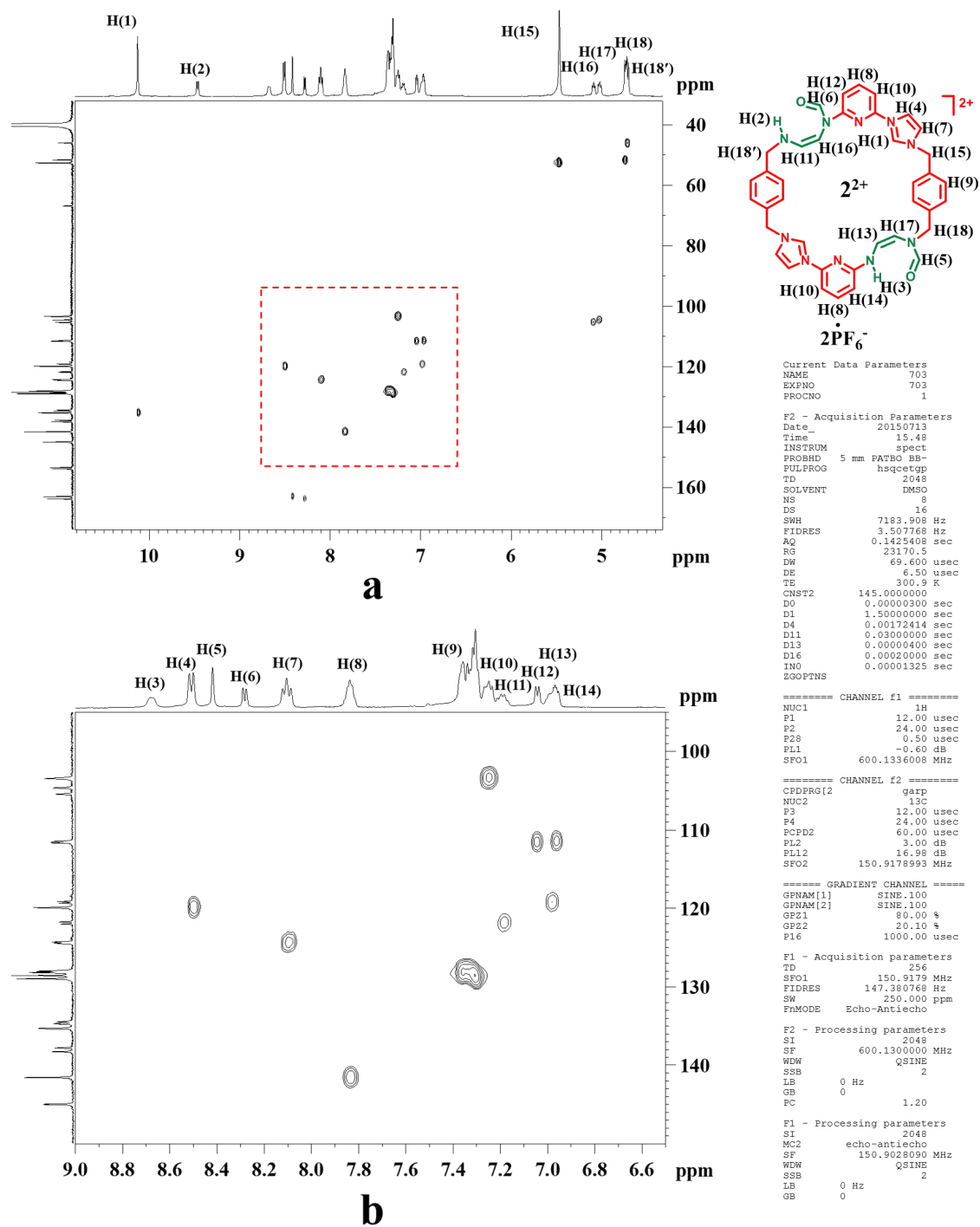
**Figure S14.** Full view (a) and expanded view (b) of the 2D COSY NMR spectrum of  $2^{2+} \cdot 2PF_6^{-}$  ( $6.0 \times 10^{-2}$  M) collected in DMSO- $d_6$  at 300K (600 MHz).



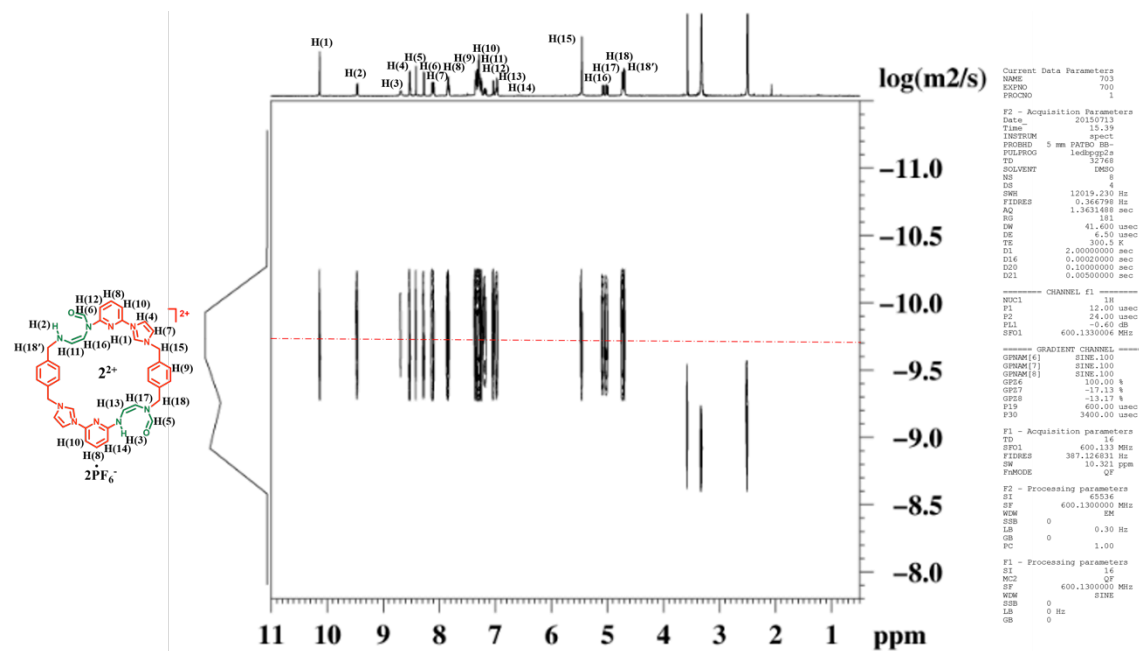
**Figure S15.** Full view (a) and expanded view (b) of the 2D NOESY NMR spectrum of  $2^{2+} \cdot 2PF_6^{-}$  ( $6.0 \times 10^{-2} M$ ) collected in  $DMSO-d_6$  at 300K (600 MHz).



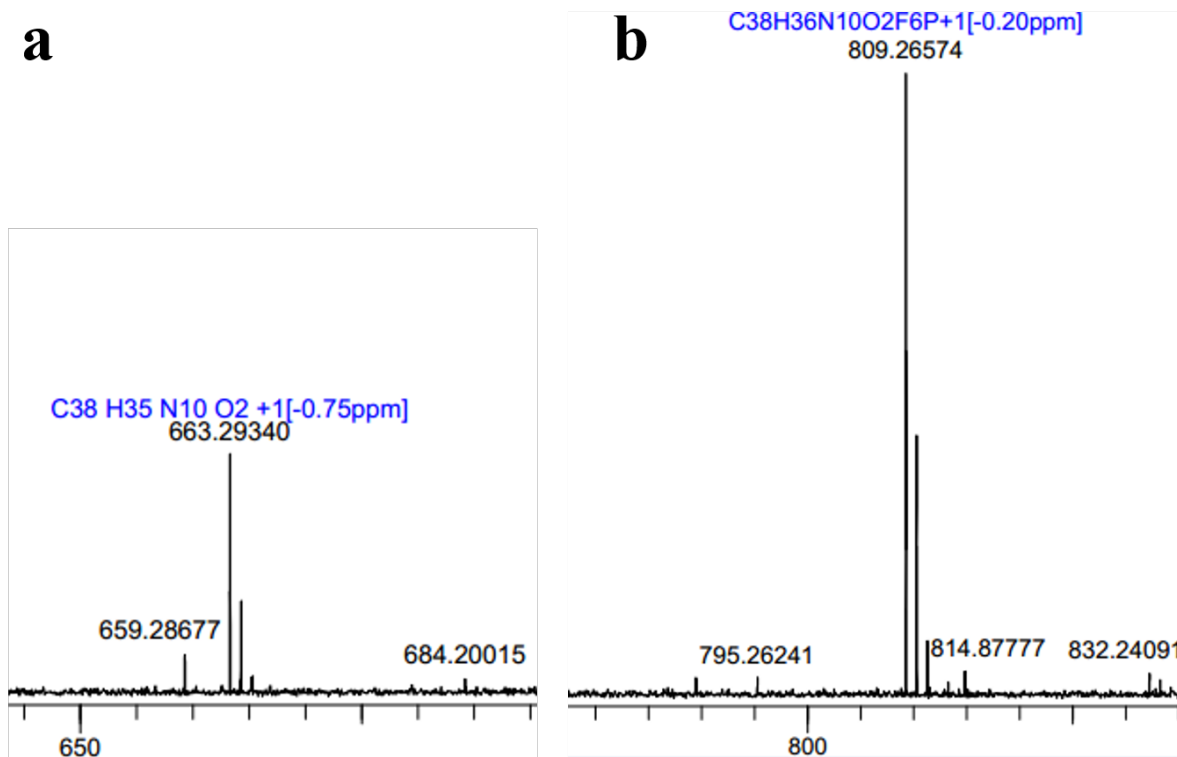
**Figure S16.** Full view (a) and expanded view (b) of the 2D ROESY NMR spectrum of  $2^{2+} \cdot 2PF_6^{-}$  ( $6.0 \times 10^{-2}$  M) collected in DMSO- $d_6$  at 300K (600 MHz).



**Figure S17.** Full view (a) and expanded view (b) of the HSQC NMR spectrum of  $2^{2+} \cdot 2PF_6^-$  ( $6.0 \times 10^{-2}$  M) collected in DMSO- $d_6$  at 300K (600 MHz).

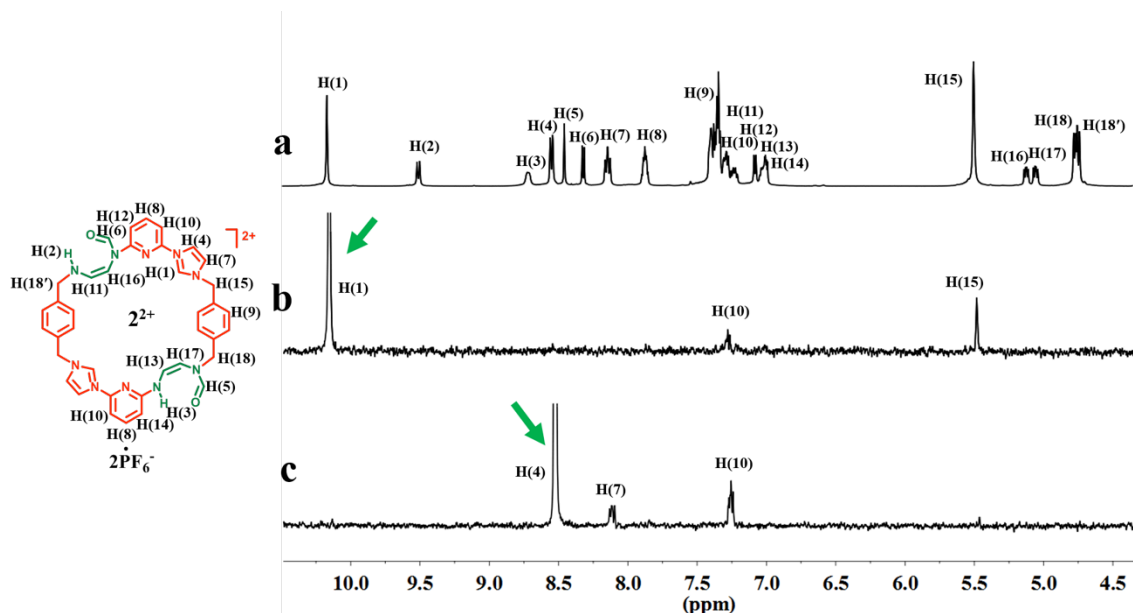


**Figure S18.** 2D DOSY NMR spectrum of  $2^{2+} \cdot 2PF_6^{-}$  ( $6.0 \times 10^{-2} M$ ) collected in  $DMSO-d_6$  at 300K (600 MHz).

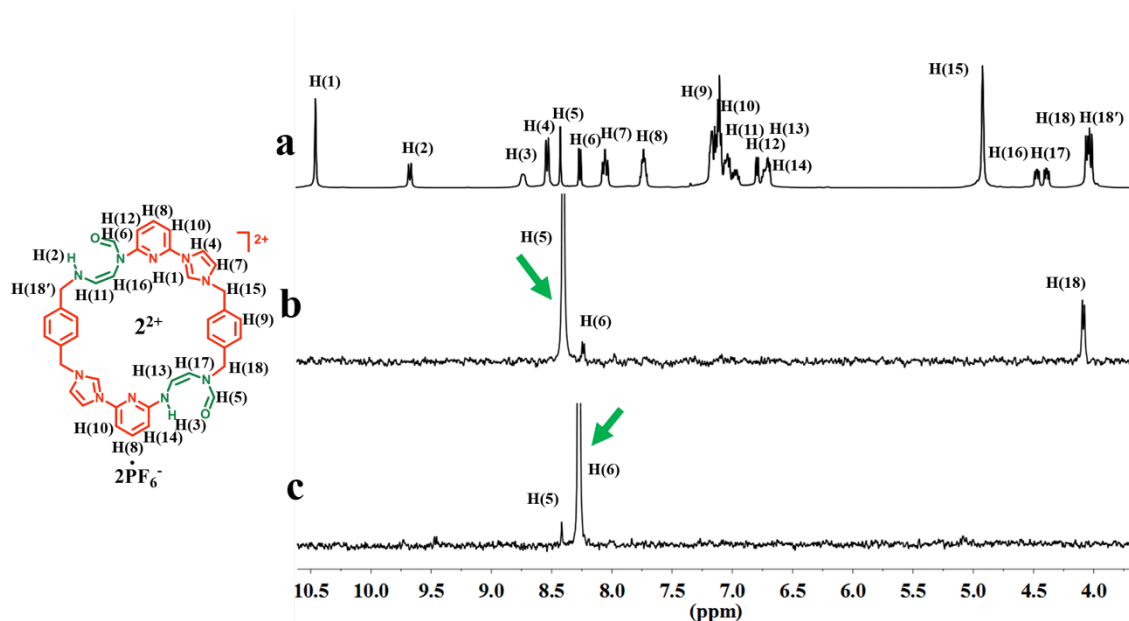


**Figure S19.** Expanded views (i.e., (a) and (b)) of the ESI high-resolution mass spectrum of  $2^{2+} \cdot 2PF_6^{-}$ .

Structural analysis of  $2^{2+} \cdot 2PF_6^-$  in DMSO- $d_6$  at 300K

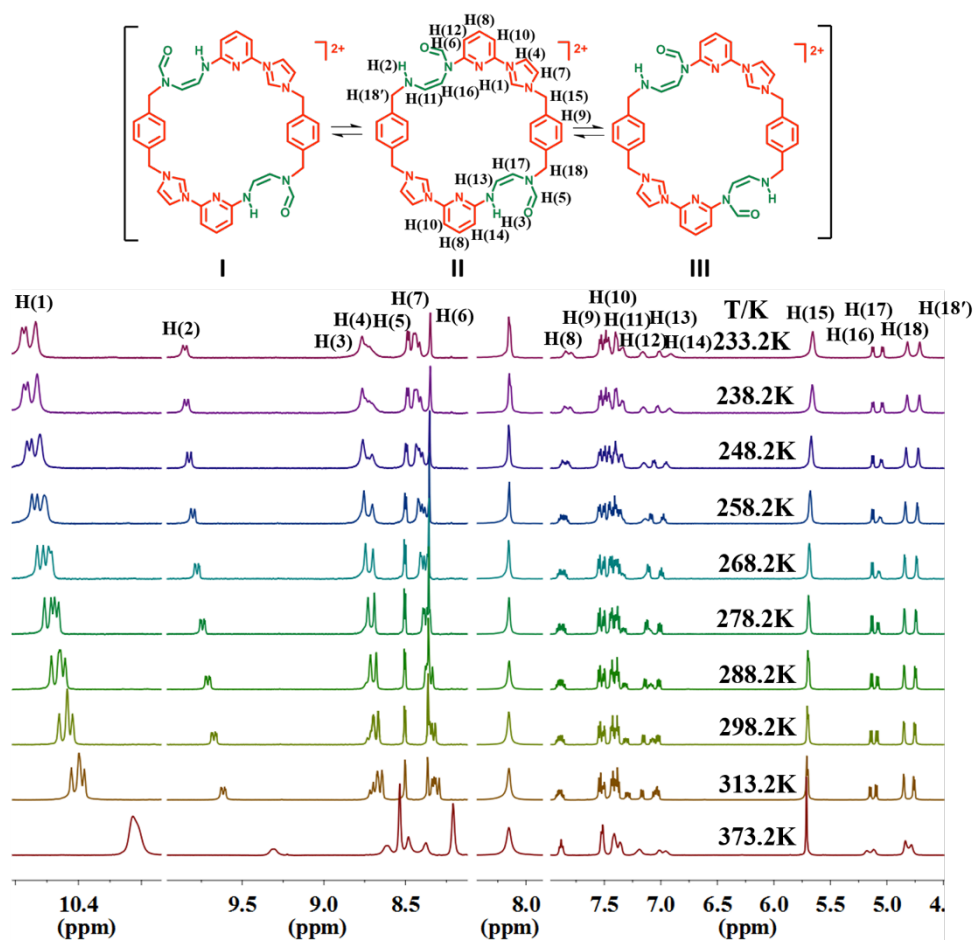


**Figure S20.**  $^1H$  NMR (a), as well as the 1D-NOE NMR ((b) and (c)) spectra of  $2^{2+} \cdot 2PF_6^-$  as recorded in DMSO- $d_6$  at 300 K (600 MHz). The green arrow in (b) and (c) indicates irradiation at the frequency of H(1) and H(4) on  $2^{2+}$ . It is suggested that macrocycle  $2^{2+}$  has a flexible structure as inferred from the observed correlations between H(1), H(4) and H(10).

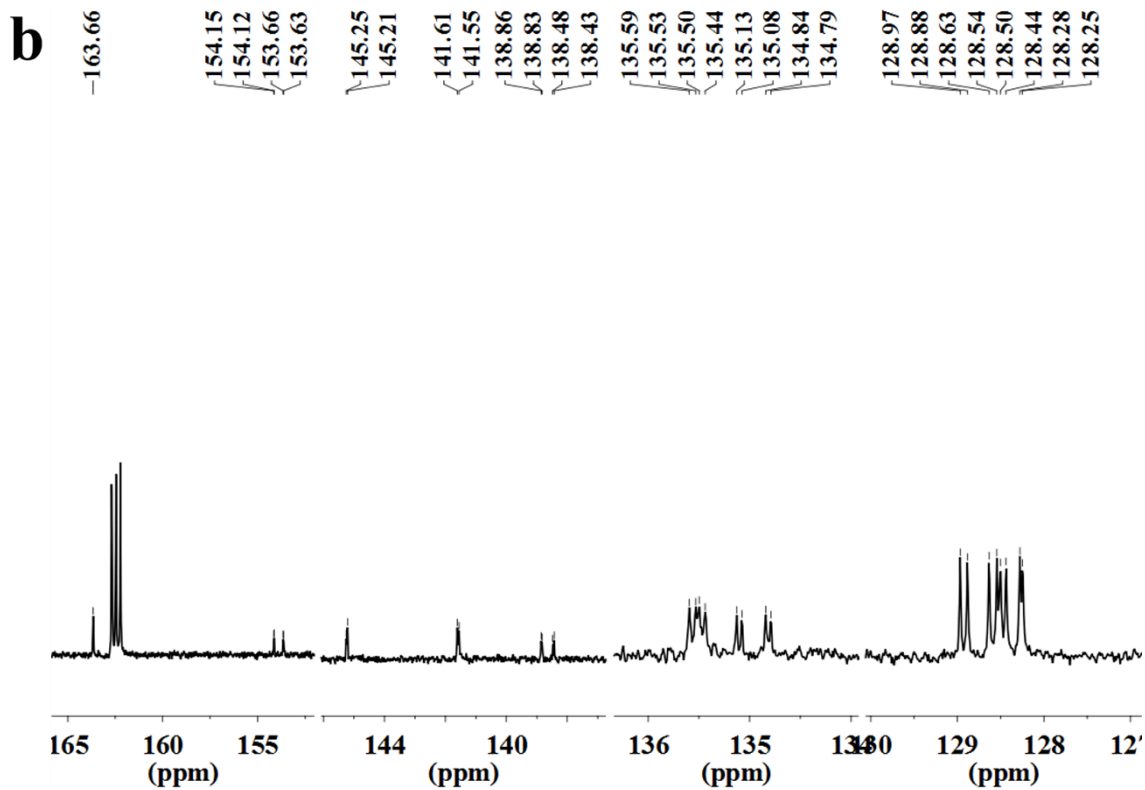
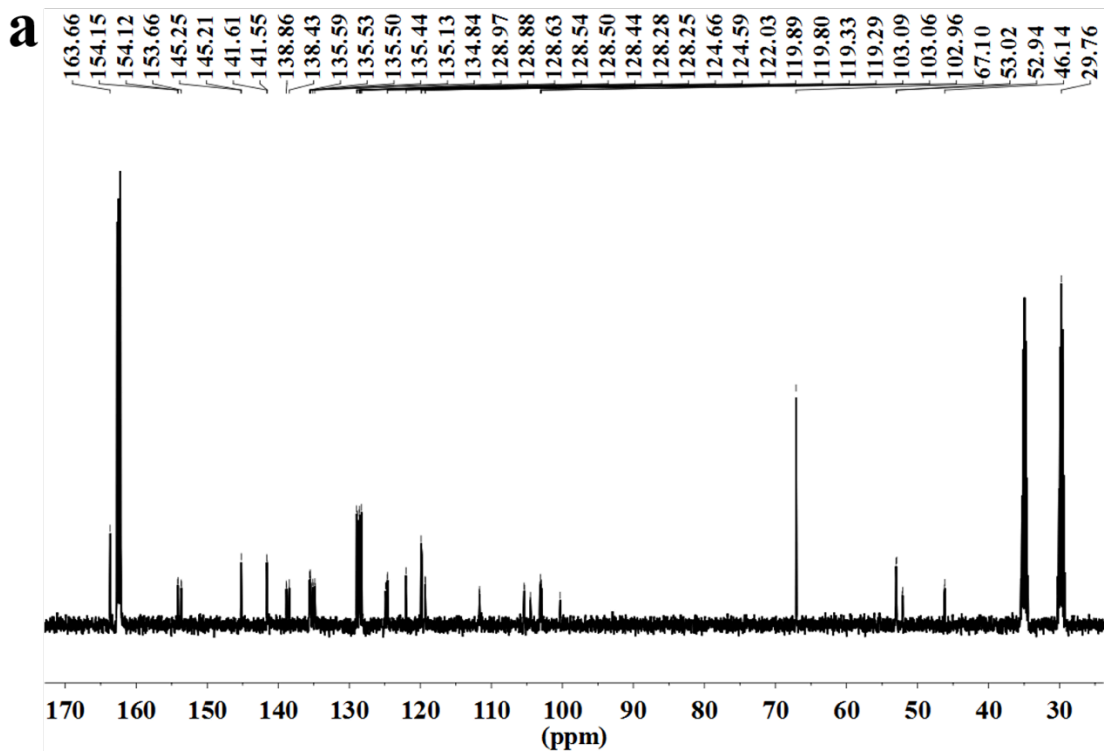


**Figure S21.**  $^1H$  NMR (a), as well as the 1D-NOE NMR ((b) and (c)) spectra of  $2^{2+} \cdot 2PF_6^-$  in DMSO- $d_6$  at 300 K (600 MHz). The green arrow in (b) and (c) indicates irradiation at the frequency of H(5) and H(6) on  $2^{2+}$ .

Structural analysis of  $2^{2+} \cdot 2PF_6^-$  in  $DMF-d_7$



**Figure S22.** Three possible isomeric structural conversions of  $2^{2+} \cdot 2PF_6^-$ , as well as the  $^1H$  NMR spectra of  $2^{2+} \cdot 2PF_6^-$  in  $DMF-d_7$  at different temperatures (500 MHz). At 278K, three isomers exists in  $DMF-d_7$  solution in a ratio of about 1:2:1 (I:II:III).



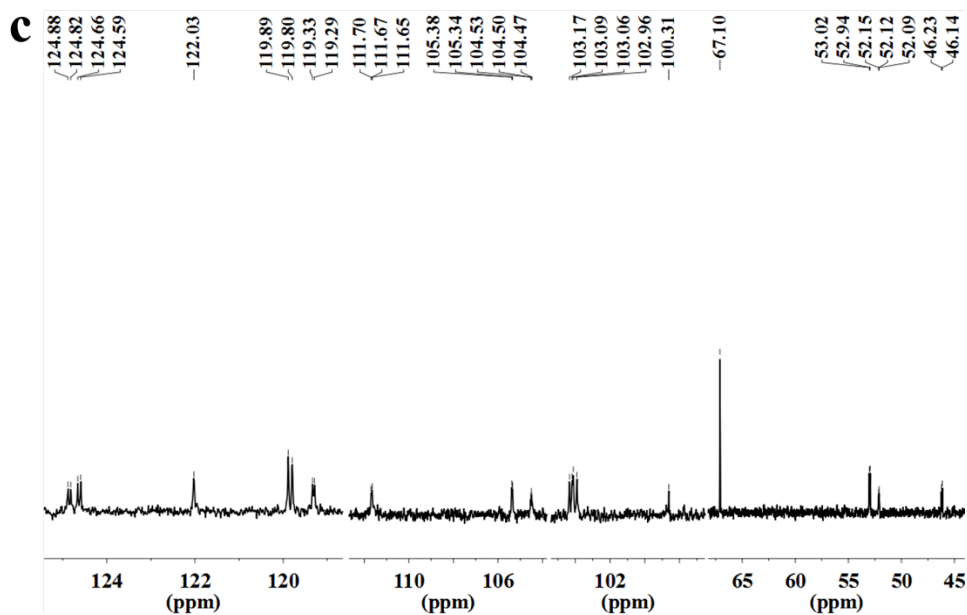


**Figure S23.** Full view (a) and expanded views ((b) and (c)) of the  $^{13}\text{C}$  NMR spectrum of  $2^{2+}\cdot 2\text{PF}_6^-$  ( $2.0 \times 10^{-2}\text{M}$ ) collected in  $\text{DMF-}d_7$  at 278K (125 MHz).

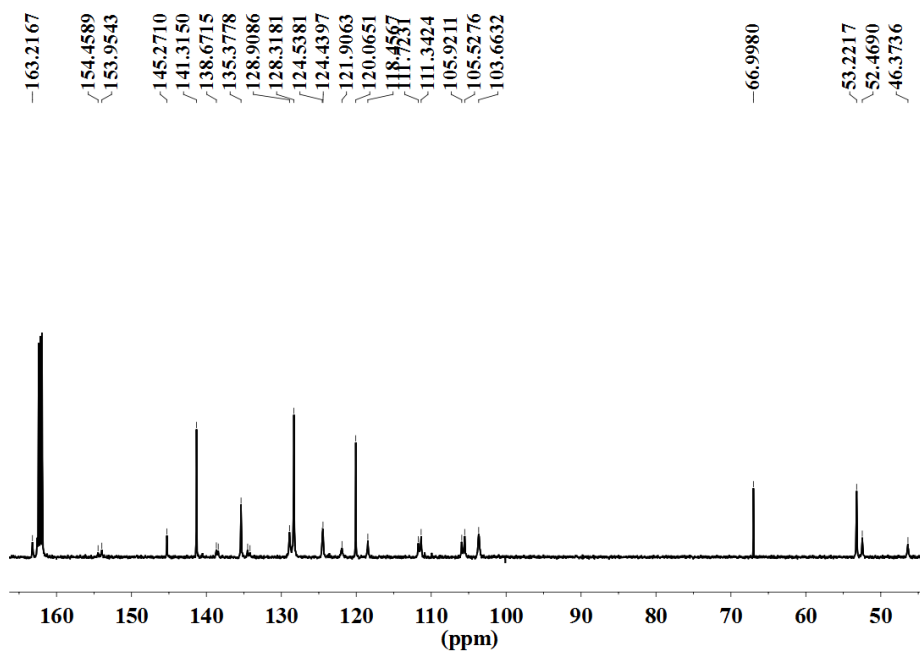


**Figure S24.** Full view of  $^{13}\text{C}$  NMR spectrum of  $2^{2+}\cdot 2\text{PF}_6^-$  ( $2.0 \times 10^{-2}\text{M}$ ) collected in  $\text{DMF-}d_7$  at 373K (125 MHz).

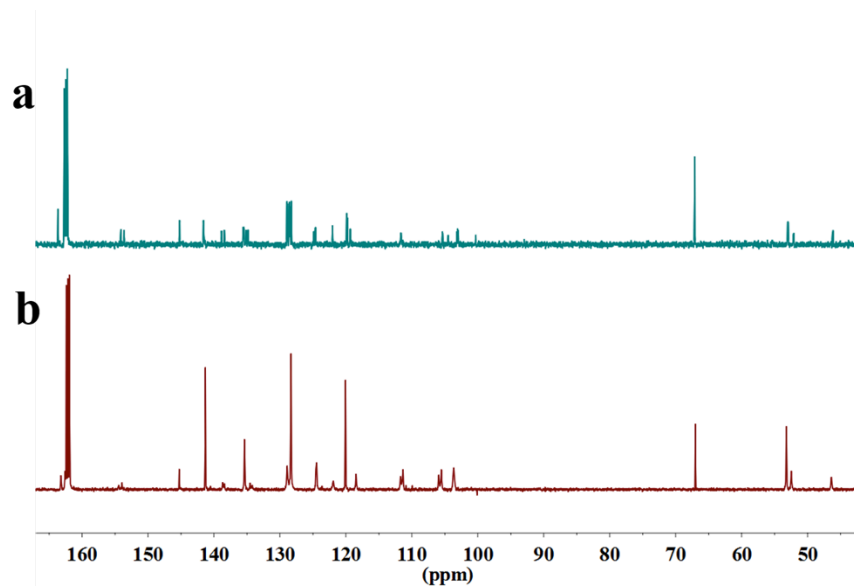


**Figure S25.** Comparison of the  $^{13}\text{C}$  NMR spectra of  $2^{2+} \cdot 2\text{PF}_6^{-}$  ( $2.0 \times 10^{-2}\text{M}$ ) collected in  $\text{DMF-}d_7$  at 278K (a) and 373K (b) (125 MHz).

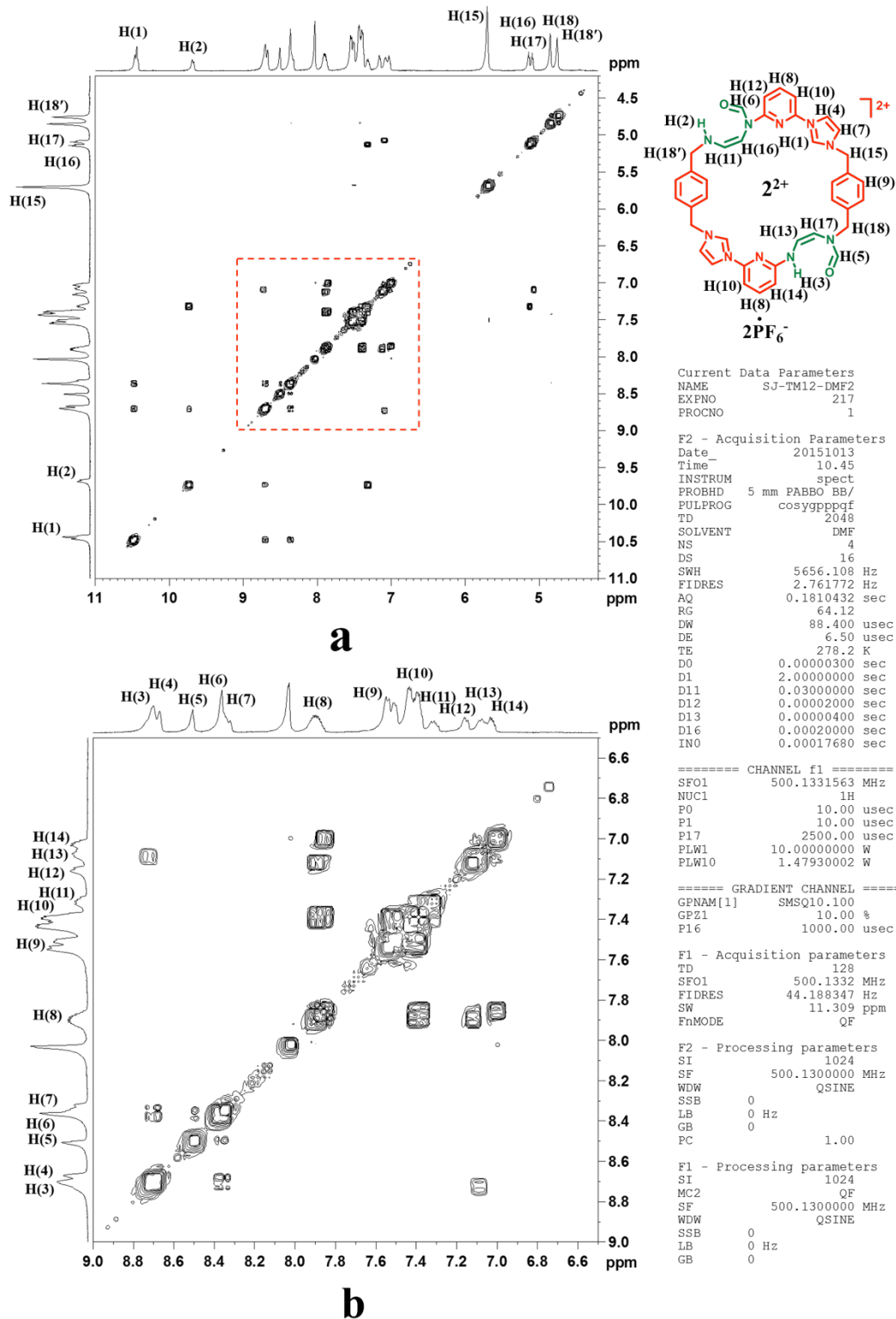


**Figure S26.** Full view (a) and expanded view (b) of the 2D COSY NMR spectrum of  $2^{2+} \cdot 2PF_6^{-}$  ( $2.00 \times 10^{-2}$  M) collected in  $DMF-d_7$  at 278K (500 MHz)

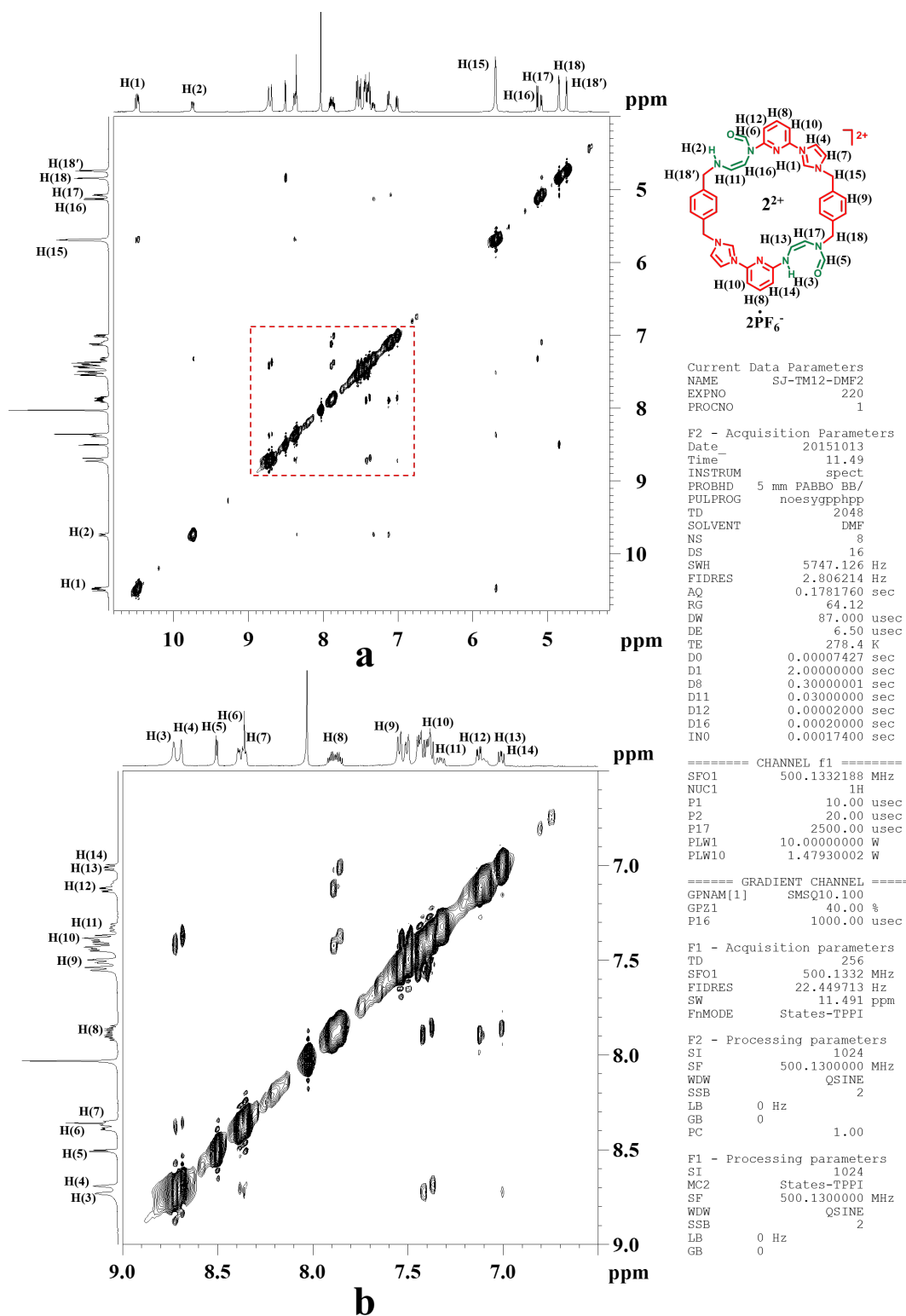


**Figure S27.** Full view (a) and expanded view (b) of the 2D NOESY NMR spectrum of  $2^{2+} \cdot 2PF_6^{-}$  ( $2.00 \times 10^{-2}$  M) collected in  $DMF-d_7$  at 278K (500 MHz).

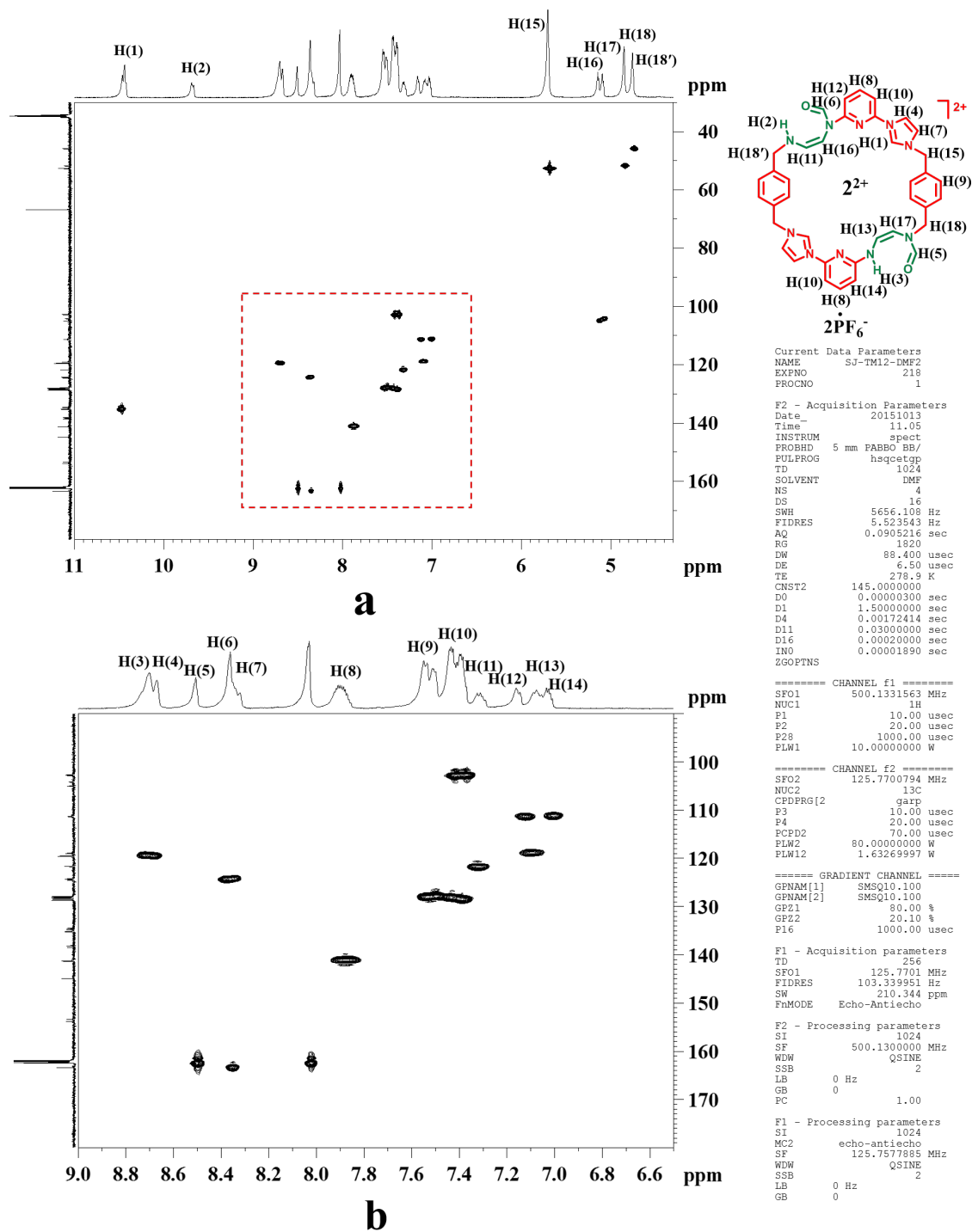


**Figure S28.** Full view (a) and expanded view (b) of the HSQC NMR spectrum of  $2^{2+} \cdot 2PF_6^{-}$  ( $2.00 \times 10^{-2}$  M) collected in DMF- $d_7$  at 278K (500 MHz).

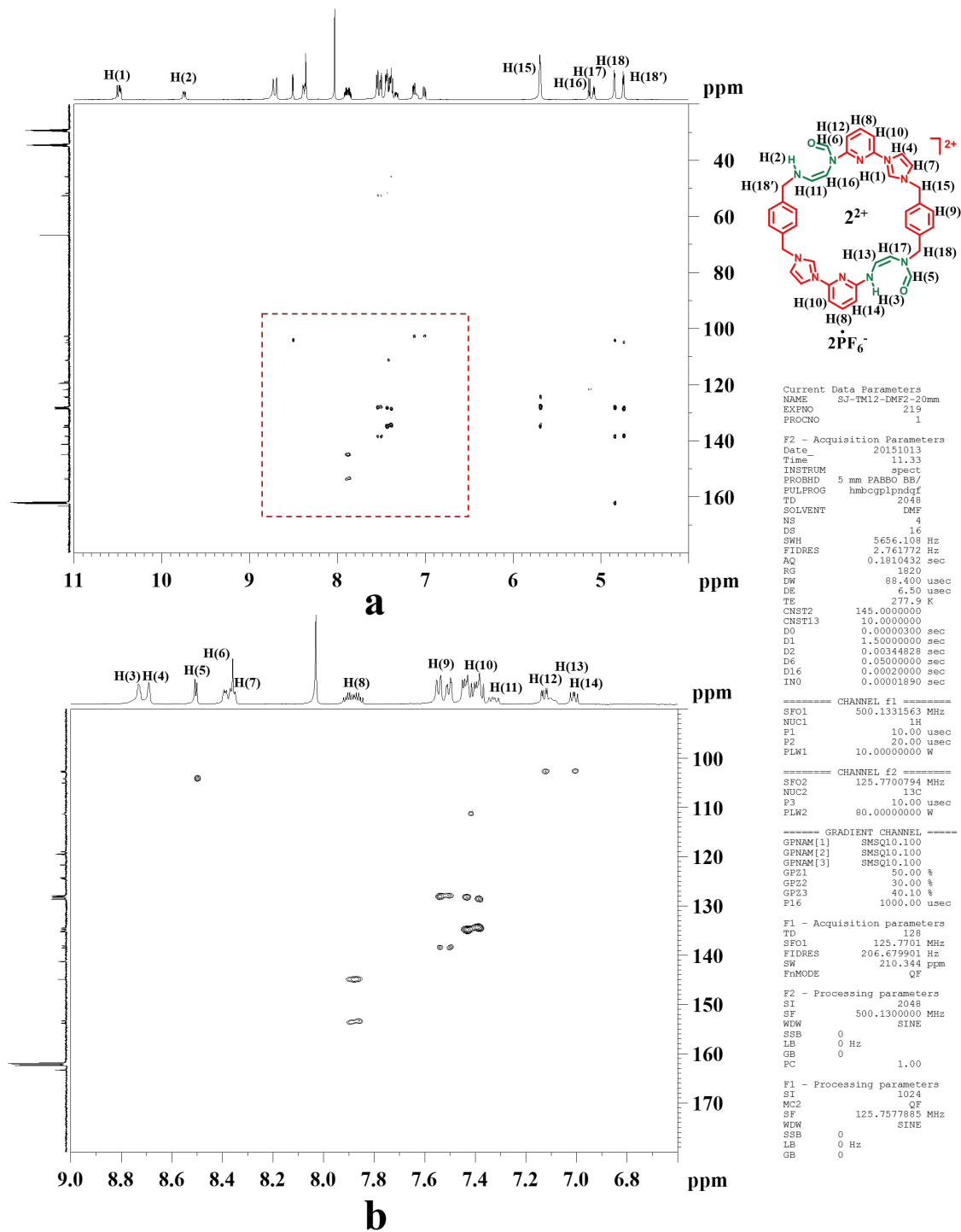


**Figure S29.** Full view (a) and expanded view (b) of the HMBC NMR spectrum of  $2^{2+} \cdot 2PF_6^{-}$  ( $2.00 \times 10^{-2}$  M) collected in  $DMF-d_7$  at 278K (500 MHz).

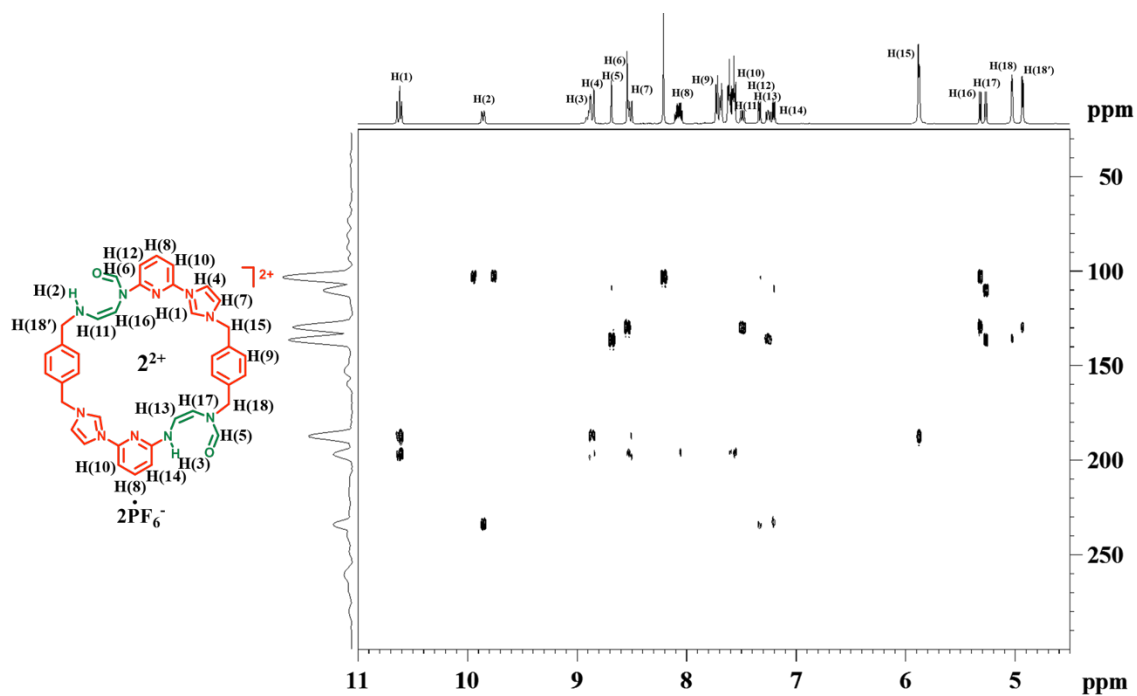


**Figure S30.** Full view of the  $^1H, ^{15}N$ -HMBC NMR spectrum of  $2^{2+} \cdot 2PF_6^-$  ( $2.00 \times 10^{-2}$  M) collected in  $DMF-d_7$  at 298K (500 MHz).

Characterization of the by-product: *Cis-cyclo[2]((Z)-N-(2-((6-(1H-imidazol-1-yl)pyridin-2-yl)amino)vinyl)formamide)[2](1,4-bismethylbenzene)hexafluorophosphate* [ $3^{2+} \cdot 2PF_6^-$ ]:

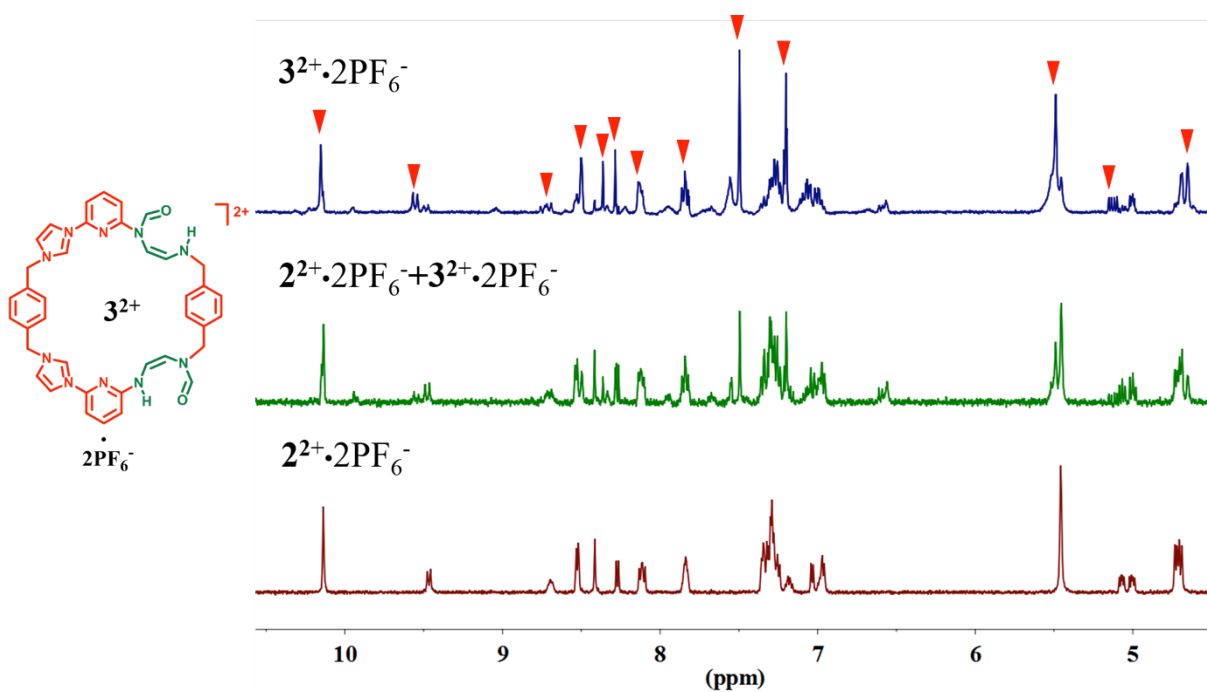


**Figure S31.**  $^1H$  NMR spectrum of impure  $3^{2+} \cdot 2PF_6^-$ , the crude product containing  $2^{2+} \cdot 2PF_6^-$  and  $3^{2+} \cdot 2PF_6^-$ , and pure  $2^{2+} \cdot 2PF_6^-$  collected in  $DMSO-d_6$  at 300K (400 MHz). The signals labeled with “ $\blacktriangledown$ ” indicate possible protons on  $3^{2+} \cdot 2PF_6^-$ .

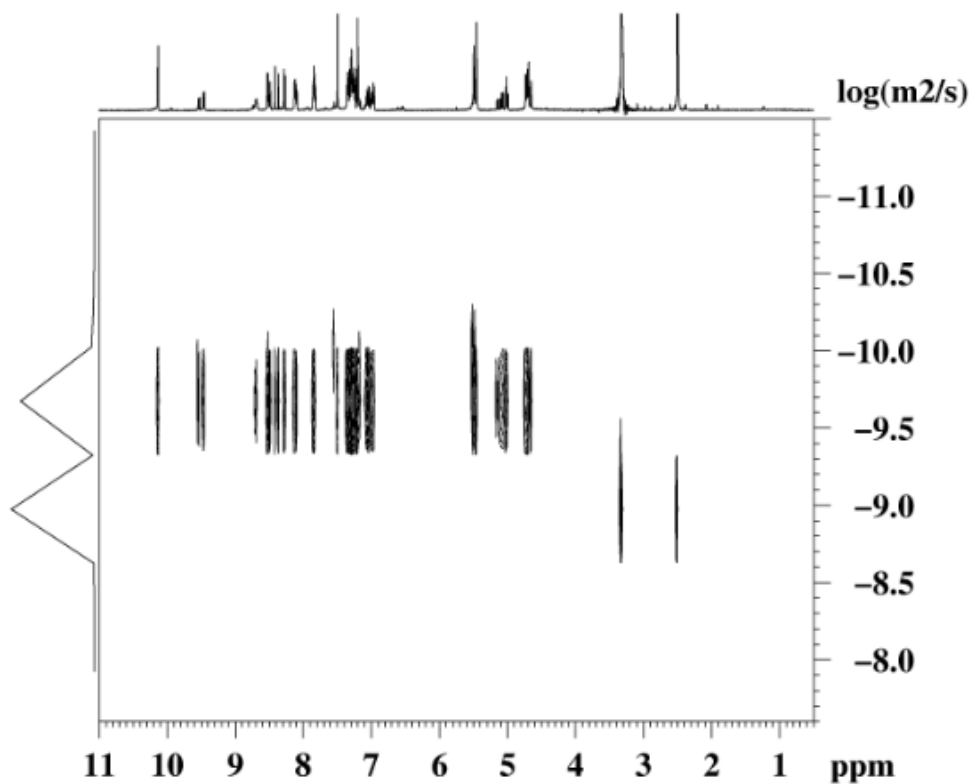


**Figure S32.** 2D DOSY NMR spectrum of crude product containing  $2^{2+} \cdot 2PF_6^-$  and  $3^{2+} \cdot 2PF_6^-$  (overall concentration as  $5 \times 10^{-3}$  M) collected in  $DMSO-d_6$  at 300K (600 MHz).

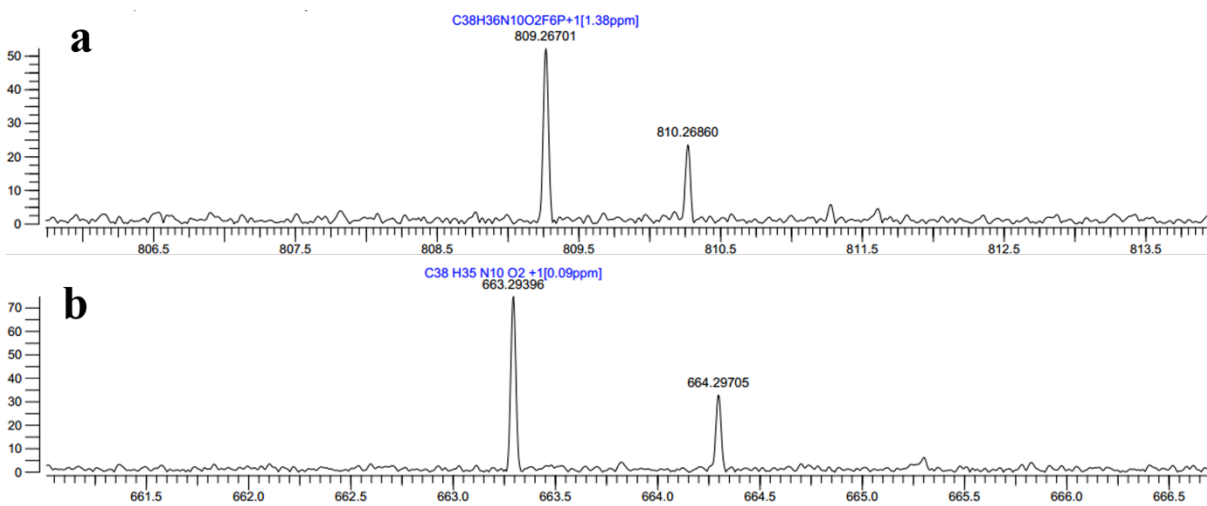


**Figure S33.** Expanded view ((a) and (b)) of ESI high resolution mass spectrum of  $3^{2+} \cdot 2PF_6^-$  generated from the single crystal sample used in X-ray diffraction analysis ( $[3^{2+} \cdot 2PF_6^- \cdot CH_3CN]$ ).

**Section S3:** Single crystal X-ray diffraction analyses of  $[2^{2+} \cdot 2PF_6^- \cdot 4dioxane]$ ,  $[2^{2+} \cdot 2PF_6^- \cdot CH_3CN \cdot H_2O]$  and  $[3^{2+} \cdot 2PF_6^- \cdot CH_3CN]$

**Table S2.** Collects X-ray crystallographic data for  $[2^{2+} \cdot 2PF_6^- \cdot 4dioxane]$ ,  $[2^{2+} \cdot 2PF_6^- \cdot CH_3CN \cdot H_2O]$ , and  $[3^{2+} \cdot 2PF_6^- \cdot CH_3CN]$ .

	$2^{2+} \cdot 2PF_6^- \cdot 4dioxane$	$2^{2+} \cdot 2PF_6^- \cdot CH_3CN \cdot H_2O$	$3^{2+} \cdot 2PF_6^- \cdot CH_3CN$
CCDC No.	1433724	1433726	1433725
description	prism	prism	prism
color	yellow	yellow	yellow
From solution	dioxane /acetonitrile	water /acetonitrile	water /acetonitrile
empirical formula	$C_{54}H_{68}F_{12}N_{10}O_{10}P_2$	$C_{40}H_{39}F_{12}N_{11}O_3P_2$	$C_{40}H_{39}F_{12}N_{11}O_2P_2$
<i>Mr</i>	1307.12	1011.76	995.76
crystal size (mm <sup>3</sup> )	0.14 × 0.09 × 0.07	0.37 × 0.10 × 0.09	0.49 × 0.07 × 0.06
crystal system	Triclinic	Monoclinic	Monoclinic
space group	P-1	C2/c	P2(1)/n
<i>a</i> [Å]	10.032(2)	28.552(6)	11.353(2)
<i>b</i> [Å]	10.288(2)	13.685(3)	20.065(4)
<i>c</i> [Å]	15.459(3)	22.641(5)	19.117(4)
<i>α</i> [deg]	80.45(3)	90.00	90.00
<i>β</i> [deg]	80.06(3)	103.63(3)	98.58(3)
<i>γ</i> [deg]	80.81(3)	90.00	90.00
<i>V</i> [Å <sup>3</sup> ]	1535.6(5)	8598(3)	4305.8(15)
<i>d</i> [g/cm <sup>3</sup> ]	1.413	1.563	1.536
<i>Z</i>	1	8	4
<i>T</i> [K]	173(2)	153(2)	153(2)
R1, wR2	0.0758	0.0798	0.0804
<i>I</i> > 2σ( <i>I</i> )	0.1585	0.1651	0.1687
R1, wR2 (all data)	0.0846 0.1643	0.1000 0.1786	0.0985 0.1791
quality of fit	1.011	1.002	1.020

Single-crystal X-ray structure of  $[2^{2+} \cdot 2PF_6^- \cdot 4dioxane]$ :

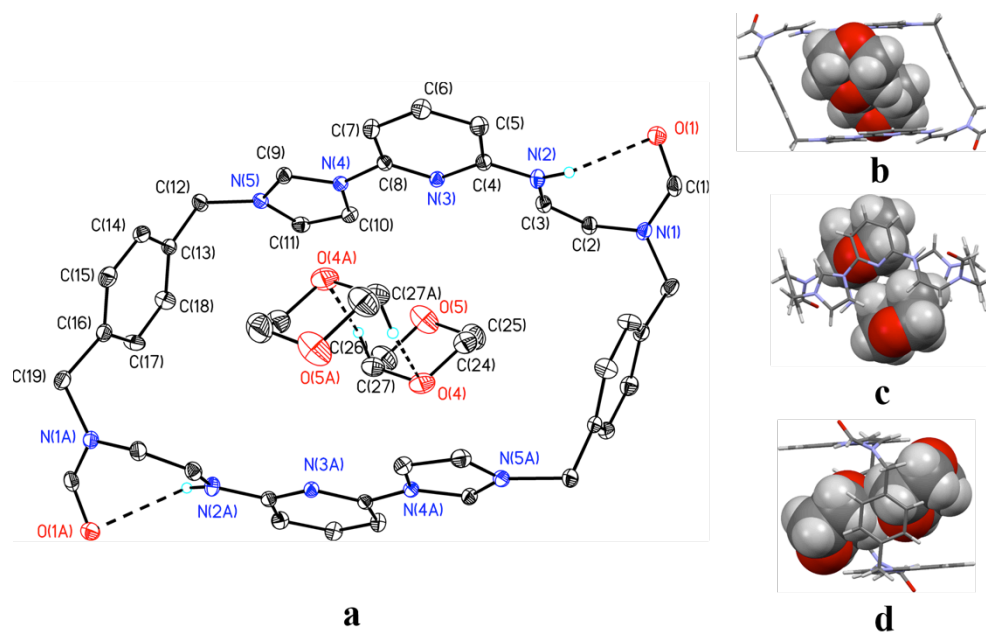


**Figure S34.** Top view of  $2^{2+}$  (a) in ellipsoid form, as well as its top view (b), side view (c), and the front view (d) in stick form. Here,  $2^{2+}$  adopts a “box” conformation containing two dioxanes in the final structure  $[2^{2+} \cdot 2PF_6^- \cdot 4dioxane]$ . Displacement ellipsoids are scaled to the 30% probability level. Some or all of the counter anions, solvent molecules and hydrogen atoms have been omitted for clarity. The symmetry transformation invoked by the additional "A" letter in the atom labels on macrocycle  $2^{2+}$  or dioxane is (1-x, 1-y, 1-z). The possible O... $\pi$  interaction was characterized with selected atomic distances between  $2^{2+}$  and dioxane are listed as below. Selected interatomic distances [ $\text{\AA}$ ]: O(4A)...N(4) 3.012(4), O(4A)...N(3) 3.754(4), O(4A)...N(5) 3.794(4), O(4A)...C(7) 3.475(5), O(4A)...C(8) 3.163(4), O(4A)...C(9) 3.197(5), O(4A)...C(10) 3.577(4). Intramolecular hydrogen bonds of  $2^{2+}$  was noted via selected interatomic distances [ $\text{\AA}$ ]: O(1)...N(2) 2.951; and selected bond angles: N(2)-H(2B)...O(1) 120.9°. Possible intermolecular hydrogen bonds between two dioxane molecules with selected interatomic distances [ $\text{\AA}$ ]: O(4)...C(27A) 3.610; and selected bond angles: C(27A)-H(27AA)...O(4) 141.2°.

**Single-crystal X-ray structure of  $[2^{2+} \cdot 2PF_6^- \cdot CH_3CN \cdot H_2O]$ :**

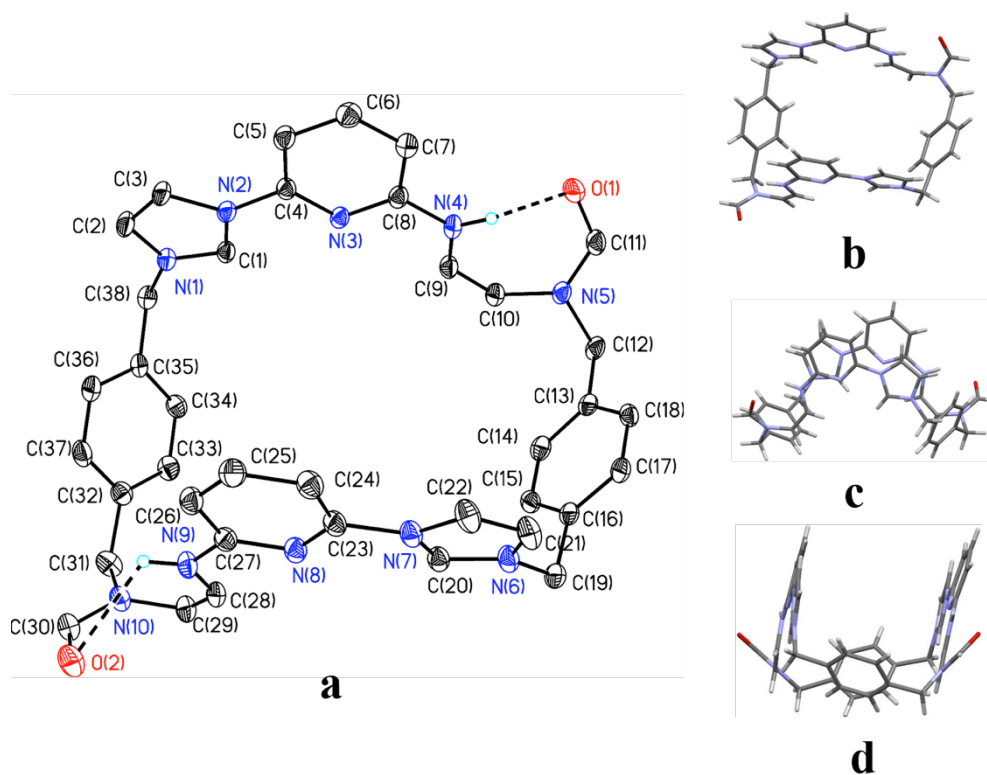


**Figure S35.** Top view of  $2^{2+}$  (a) shown in ellipsoid form, as well as top (b), side (c), and front (d) views in the stick form. Here  $2^{2+}$  adopts a “clip” conformation in the final structure  $[2^{2+} \cdot 2PF_6^- \cdot CH_3CN \cdot H_2O]$ . Displacement ellipsoids are scaled to the 25% probability level. Some or all of the counter anions, solvent molecules and hydrogen atoms have been omitted for clarity. Possible intramolecular hydrogen bonds are characterized with selected interatomic distances [Å]: O(1)...N(4) 2.720(4), O(2)...N(9) 3.061(5); selected bond angles: N(4)-H(4A)...O(1) 126.8°, N(9)-H(9B)...O(2) 118.9°.

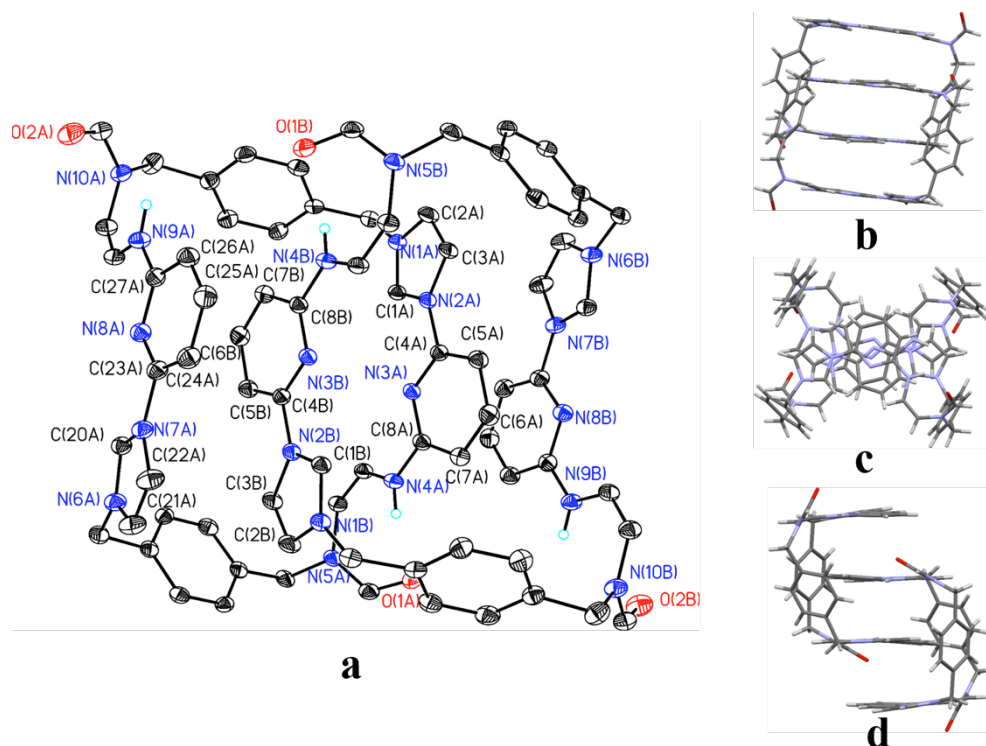


**Figure S36.** Top view of  $[2^{2+}]_2$  (a) shown in ellipsoid form, as well as top (b), side (c), and the front views (d) in stick form. Here,  $2^{2+}$  organizes into a head-to-tail racemic dimer in the final structure  $[2^{2+} \cdot 2PF_6^- \cdot CH_3CN \cdot H_2O]$ . Displacement ellipsoids are scaled to the 25% probability level. Some or all of the counter anions, solvent molecules and hydrogen atoms have been omitted for clarity. The symmetry transformation invoked by the additional "A" letter and "B" letter in the atom labels on the macrocycle  $2^{2+}$  are  $(x, y, z)$  and  $(1.5-x, 1/2-y, 1-z)$ . Possible intramolecular  $\pi \dots \pi$  interaction: Selected interatomic distances [ $\text{\AA}$ ]: N(3B)...C(24A) 3.666(5), N(3B)...C(23A) 3.741(5), C(8B)...C(26A) 3.492(6), C(8B)...C(27A) 3.565(6), C(6B)...N(8A) 3.503(5), N(3B)...N(3A) 3.304(4), C(8A)...N(3B) 3.800(5), N(3B)...C(4A) 3.441(5), C(4B)...C(8A) 3.712(6), C(5B)...C(23A) 3.788(6), C(4B)...C(23A) 3.580(6), N(7A)...N(2B) 3.697(5), C(21A)...C(2B) 3.787(7), C(21A)...C(3B) 3.728(6), N(6A)...C(3B) 3.762(6).

Single-crystal X-ray structure of  $[3^{2+} \cdot 2PF_6^- \cdot CH_3CN]$ :

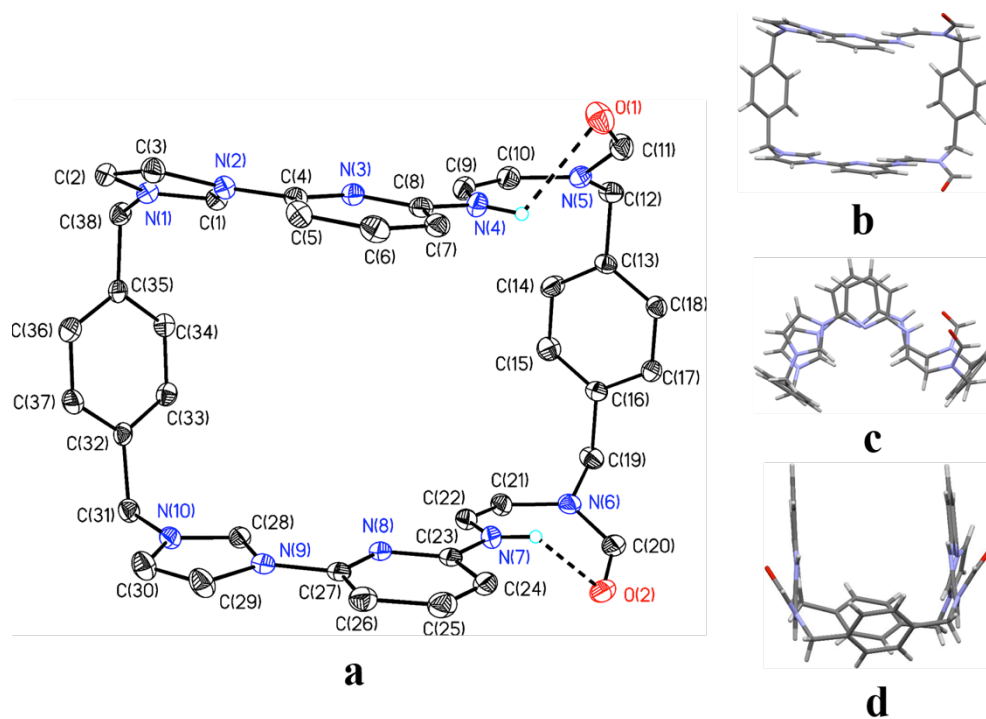


**Figure S37.** Top view of  $3^{2+}$  (a) in ellipsoid form, as well as top (b), side (c), and front views (d) in stick form. Here,  $3^{2+}$  adopts a “clip” conformation in the final structure  $[3^{2+} \cdot 2PF_6^- \cdot CH_3CN]$ . Displacement ellipsoids are scaled to the 25% probability level. Some or all of the counter anions, solvent molecules and hydrogen atoms have been omitted for clarity. Possible intramolecular hydrogen bonds are characterized with selected interatomic distances [Å]: O(1)...N(4) 2.751(5), O(2)...N(7) 2.690(5); selected bond angles: N(4)-H(4A)...O(1) 112.1°, N(7)-H(7B)...O(2) 124.1°.

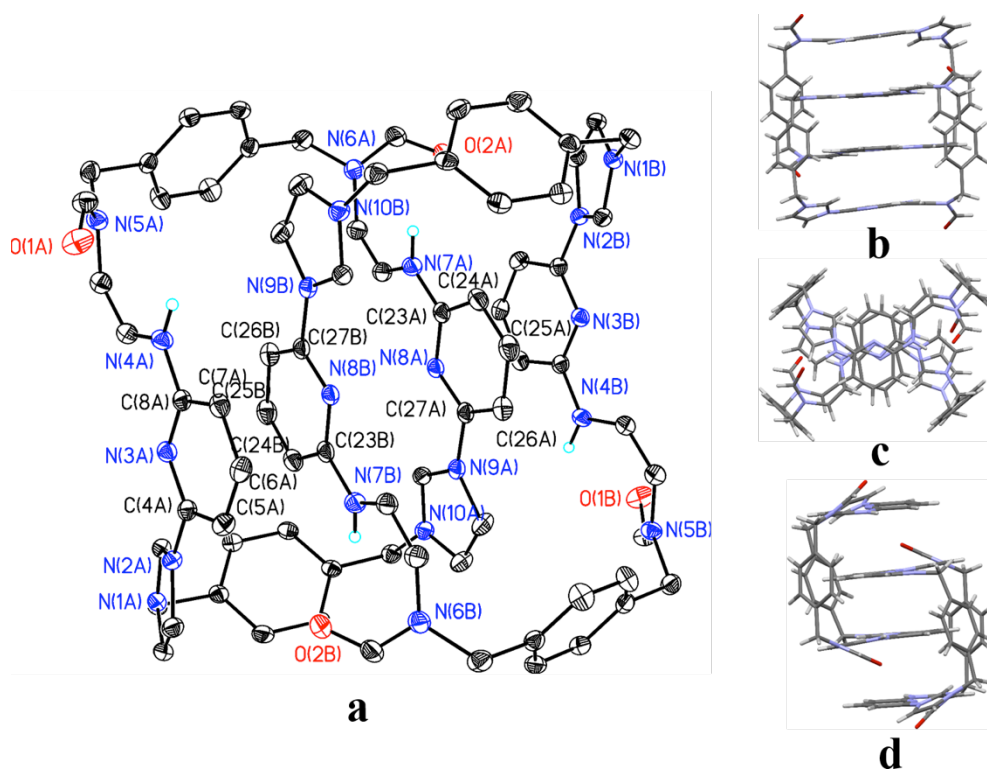


**Figure S38.** Top view of  $[3^{2+}]_2$  (a) in ellipsoid form, as well as top (b), side (c), and front views (d) in stick form. Here,  $3^{2+}$  organizes into a head-to-tail racemic dimer in the final structure  $[3^{2+} \cdot 2PF_6^- \cdot CH_3CN]$ . Displacement ellipsoids are scaled to the 25% probability level. Some or all of the counter anions, solvent molecules and hydrogen atoms have been omitted for clarity. The symmetry transformation invoked by the additional "A" letter and "B" letter in the atom labels on the macrocycle  $3^{2+}$  are  $(x, y, z)$  and  $(1-x, 1-y, 1-z)$ . Possible intramolecular  $\pi \dots \pi$  interaction: selected interatomic distances [ $\text{\AA}$ ]: N(8B)...N(3A) 3.681(5), N(8B)...C(7A) 3.491(5), N(8B)...C(8A) 3.405(5), C(23B)...C(5A) 3.792(6), C(23B)...C(4A) 3.552(6), C(24B)...C(4A) 3.791(5), C(24B)...N(3A) 3.664(5), C(27B)...C(8A) 3.438(5), N(8)...N(8B) 3.307(4), N(8B)...C(23A) 3.496(5), N(8B)...C(27A) 3.415(5), N(8B)...C(26A) 3.743(5), C(23B)...C(27A) 3.368(6).

**Section S4:** Solution binding studies and characterization of the host-guest complexes formed between  $[2^{2+} \cdot 2PF_6^-]$  and dianionic guests 2,6-naphthalenedicarboxylate (**4**), 2,6-naphthalenedisulfonate (**5**) or 1,5-naphthalenedisulfonate (**6**)

**Solution binding studies and characterization of the host-guest complex formed between  $2^{2+}$  and dianionic guest 2,6-naphthalene dicarboxylate (**4**):**

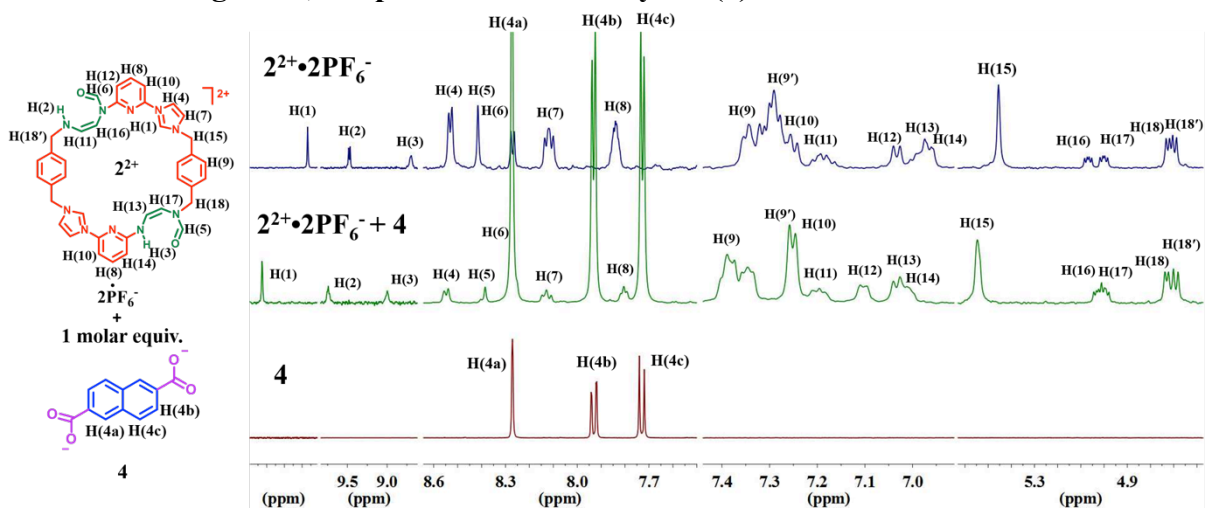


**Figure S39.** Expanded view of the  $^1H$  NMR spectra of  $2^{2+} \cdot 2PF_6^-$  ( $1.00 \times 10^{-3}$  M) recorded in the absence and presence of 1 molar equiv. of **4** in  $DMSO-d_6$  at 300 K over the indicated spectral ranges (600 MHz).

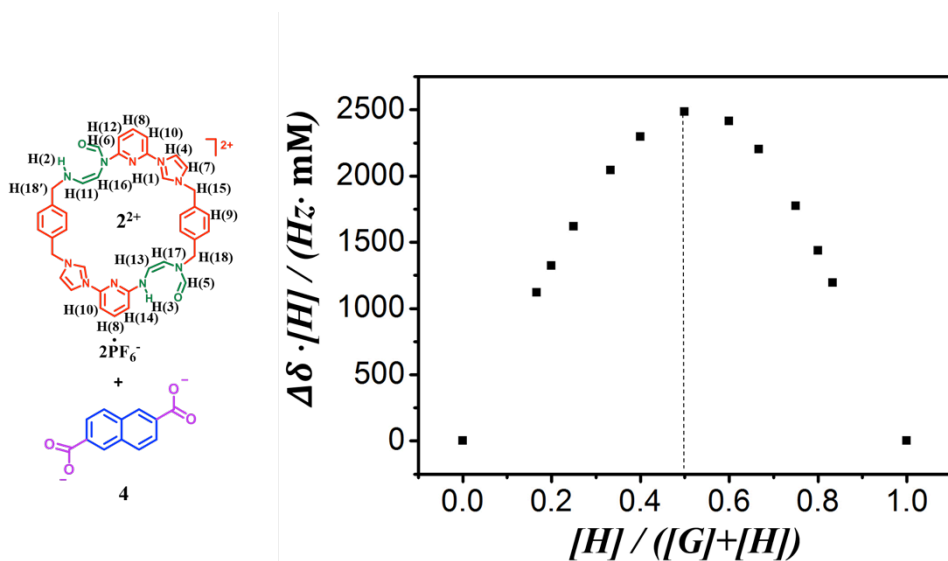


**Figure S40.**  $^1H$  NMR Job-plots (600 MHz) corresponding to the binding between  $2^{2+} \cdot 2PF_6^-$  and **4** ( $[host] + [guest] = 2.00 \times 10^{-2}$  M). The maximum value was found to be 0.5 at this concentration, a finding consistent with a 1:1 (host: guest) binding stoichiometry.<sup>8</sup>

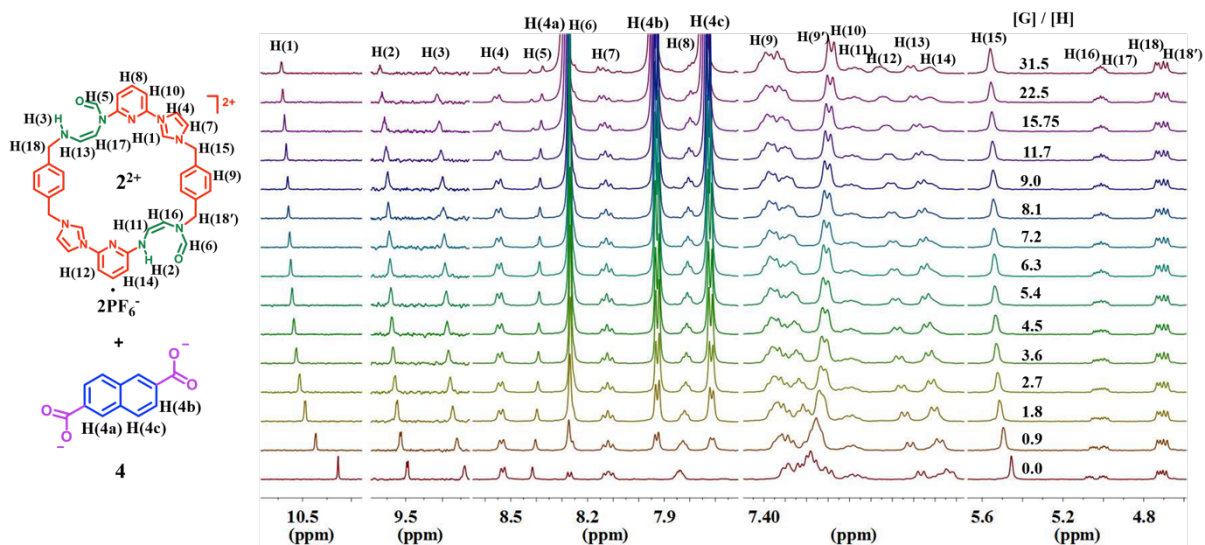


**Figure S41.**  $^1\text{H}$  NMR spectroscopic titration of  $2^{2+}\cdot 2\text{PF}_6^-$  ( $1.00 \times 10^{-3}$  M) with 2,6-naphthalenedicarboxylic acid in the presence of 2 molar equiv. of  $\text{TMA}^+\cdot\text{OH}^-$  in  $\text{DMSO-}d_6$  at 300K (600 MHz).

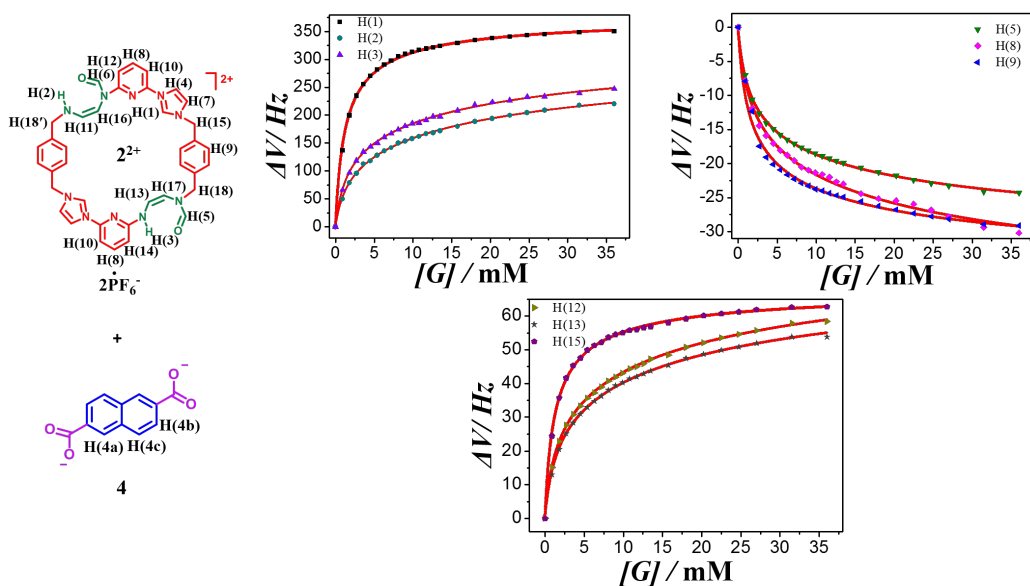


**Figure S42.**  $^1\text{H}$  NMR binding isotherms corresponding to the interaction between  $2^{2+}\cdot 2\text{PF}_6^-$  and **4** in  $\text{DMSO-}d_6$  at 300K. The chemical shift changes of (a) H(1), H(2), H(3) and (b) H(5), H(8), H(9) and (c) H(12), H(13), H(15) on  $2^{2+}$  were used for the calculation of  $K_a = (2.0 \pm 0.1) \times 10^2 \text{ M}^{-1}$  using the Hyperquad 2003 program.<sup>9</sup> The chemical shift changes of the signals of other protons present in  $2^{2+}$  and **4** overlap and thus could not be accurately fit with either a Gaussian or Lorentzian function. In other cases the change in chemical shifts were too small (less than 15.6 Hz); these signals were therefore not used in the calculation of the association constant.<sup>10</sup> The red dashed lines show the non-linear curve fit of the experimental data to the appropriate equation.

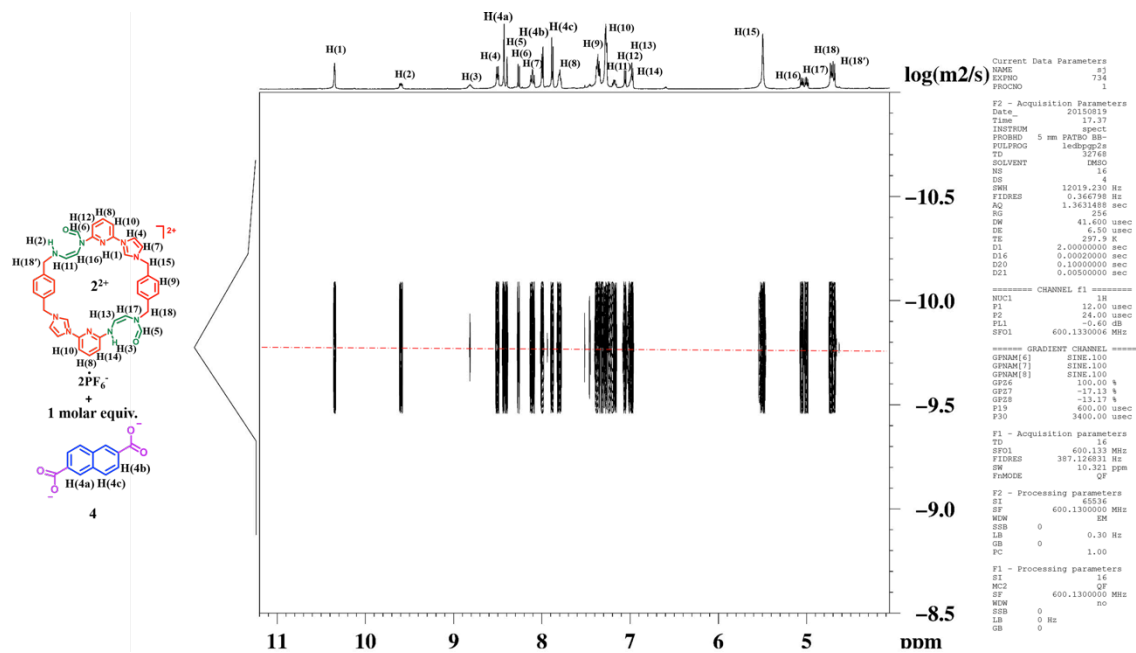


**Figure S43.** Full view of the 600 MHz 2D-DOSY NMR spectra of  $2^{2+} \cdot 2PF_6^{-}$  ( $2.00 \times 10^{-2}$  M) recorded in the presence of 1 molar equiv. of 2,6-naphthalenedicarboxylic acid and 2 molar equiv. of  $TMA^{+} \cdot OH^{-}$  collected in  $DMSO-d_6$  at 300K.

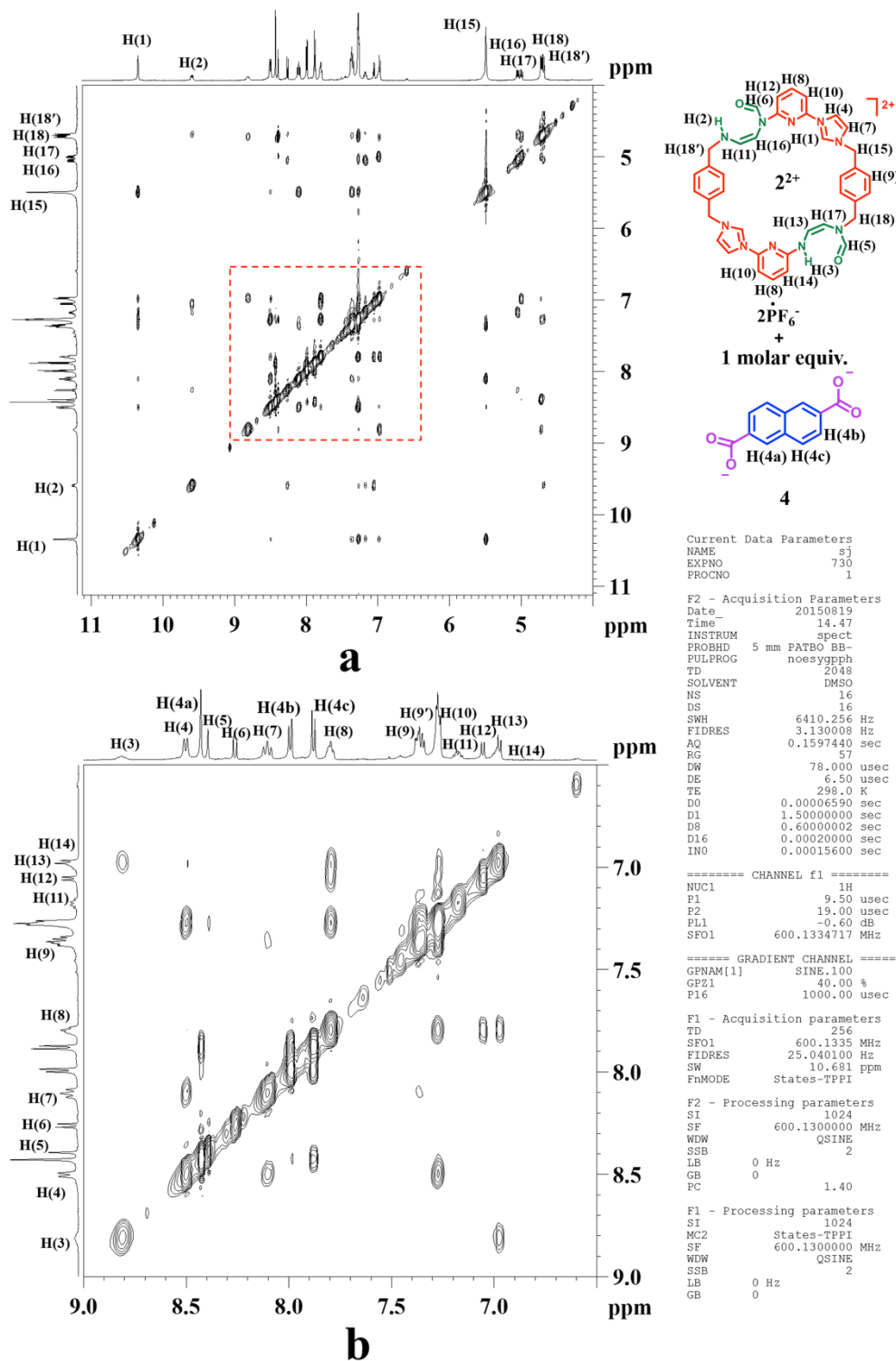


**Figure S44.** Full view (a) and expanded view (b) of the 600 MHz NOESY NMR spectrum of  $2^{2+} \cdot 2PF_6^-$  ( $2.0 \times 10^{-2}$  M) recorded in the presence of 1 molar equiv. of 2,6-naphthalenedicarboxylic acid and 2 molar equiv. of  $TMA^+ \cdot OH^-$  collected in  $DMSO-d_6$  at 300K.

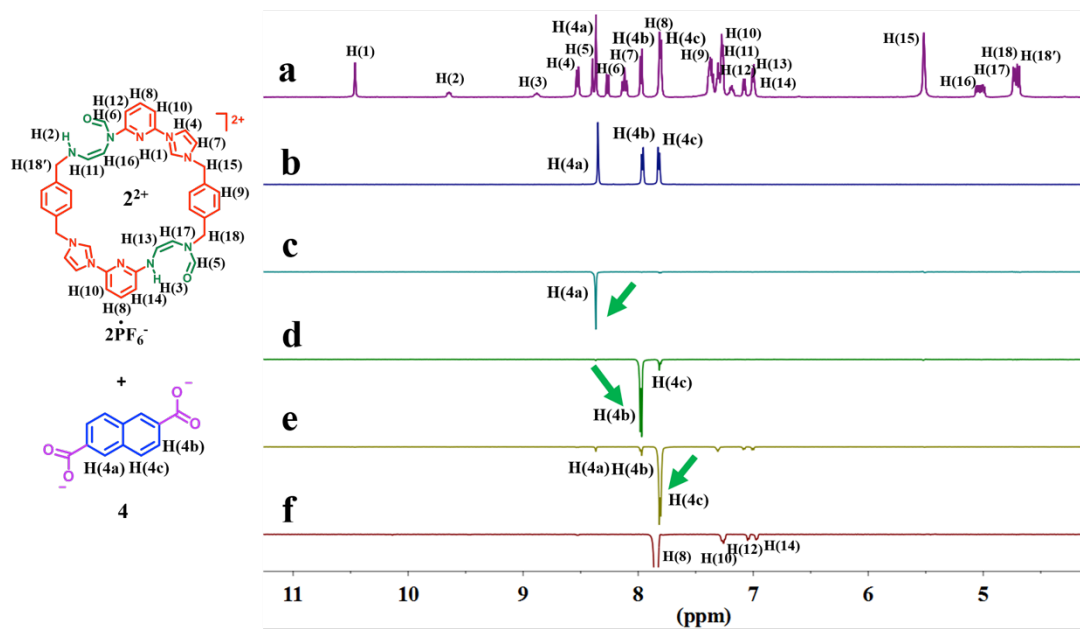


**Figure S45.** 600 MHz  $^1\text{H}$  NMR and 1D NOE NMR spectra recorded in  $\text{DMSO-}d_6$  at 300K: (a)  $^1\text{H}$  NMR of  $2^{2+}\cdot 2\text{PF}_6^-$  in the presence of 1 molar equiv. of 2,6-naphthalenedicarboxylic acid and 2 molar equiv. of  $\text{TMA}^+\cdot\text{OH}^-$  ( $[\text{host}] = [\text{guest}] = 1.00 \times 10^{-2} \text{ M}$ ), (b)  $^1\text{H}$  NMR of the 2,6-naphthalenedicarboxylic acid in the presence of 2 molar equiv. of  $\text{TMA}^+\cdot\text{OH}^-$ , (c-e) 1D-NOE NMR spectra of  $2^{2+}\cdot 2\text{PF}_6^-$  in the presence of 1 molar equiv. of 2,6-naphthalenedicarboxylic acid and 2 molar equiv. of  $\text{TMA}^+\cdot\text{OH}^-$  ( $[\text{host}] = [\text{guest}] = 1.00 \times 10^{-2} \text{ M}$ ). The green arrows indicate irradiation at the frequency of H(4a), H(4b) and H(4c) of **4**. Shown in (f) is the 1D NOE NMR spectrum of  $2^{2+}\cdot 2\text{PF}_6^-$  ( $1.00 \times 10^{-2} \text{ M}$ ). The green arrow indicates irradiation at the frequency of H(8) of  $2^{2+}\cdot 2\text{PF}_6^-$ .

**Solution binding studies and characterization of the host-guest complex formed between  $2^{2+}$  and dianionic guest 2,6-naphthalenedisulfonate (5):**

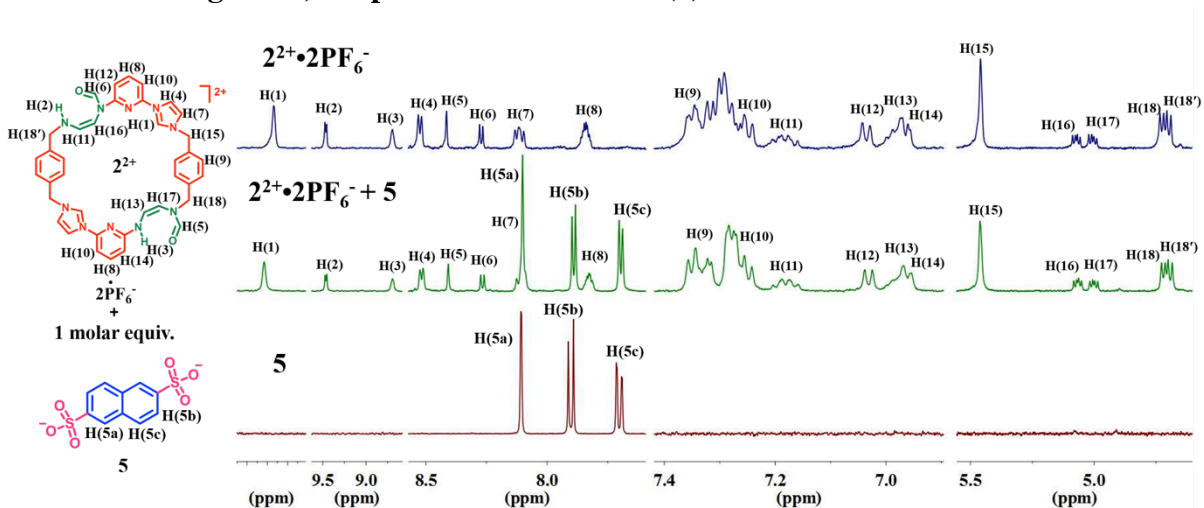


**Figure S46.** Expanded views of the  $^1\text{H}$  NMR spectra of  $2^{2+} \cdot 2\text{PF}_6^-$  ( $1.00 \times 10^{-3}$  M) recorded in the absence and presence of 1 molar equiv. of **5** in  $\text{DMSO-}d_6$  at 300 K over the indicated spectral ranges (600 MHz).

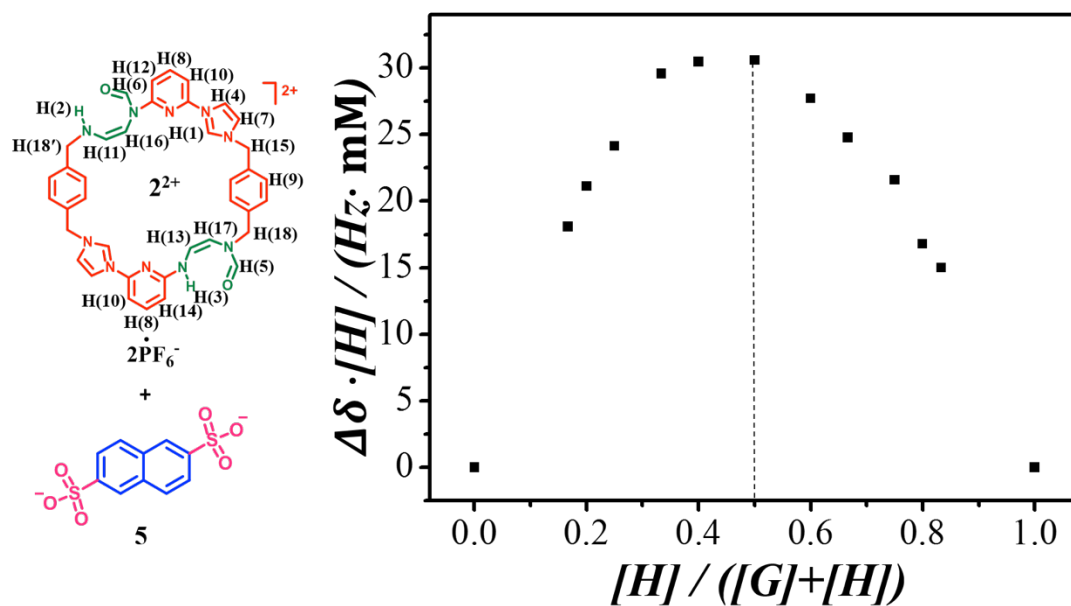


**Figure S47.**  $^1\text{H}$  NMR Job-plots (600 MHz) associated with the binding between  $2^{2+} \cdot 2\text{PF}_6^-$  and **5** ( $[\text{host}] + [\text{guest}] = 1.00 \times 10^{-2}$  M). The maximum value was determined to be 0.5 at this concentration, a finding consistent with a 1:1 (host: guest) binding stoichiometry.<sup>8</sup>

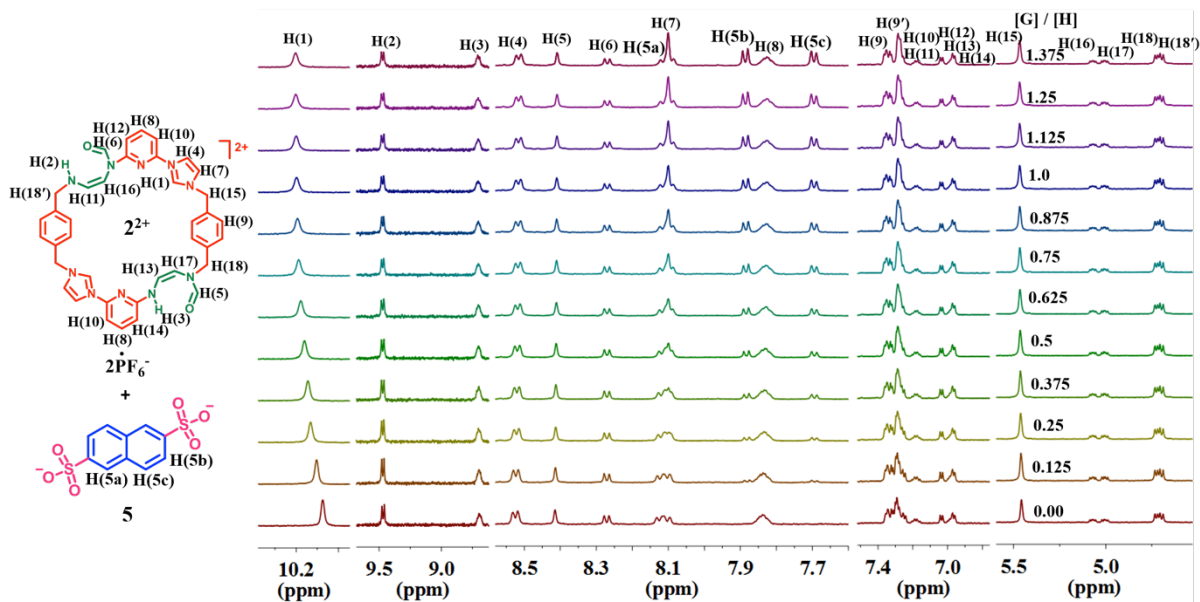


**Figure S48.**  $^1\text{H}$  NMR spectroscopic titration of  $2^{2+}\cdot 2\text{PF}_6^-$  ( $1.00 \times 10^{-3}$  M) with 2,6-naphthalenedisulfonic acid in the presence of 2 molar equiv. of  $\text{TMA}^+\cdot\text{OH}^-$  collected in  $\text{DMSO-}d_6$  at 300K (600 MHz).

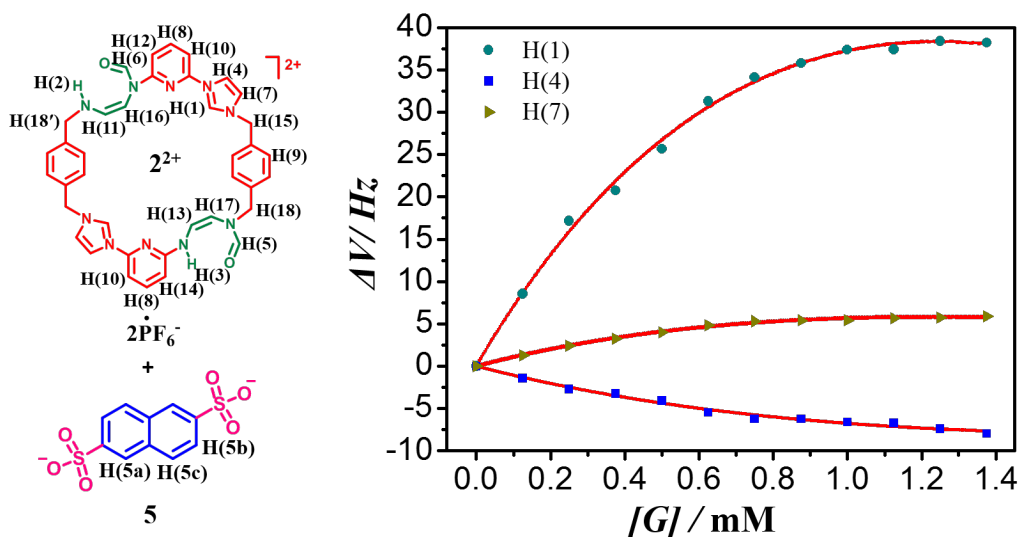


**Figure S49.**  $^1\text{H}$  NMR binding isotherms that correspond to the interaction between  $2^{2+}\cdot 2\text{PF}_6^-$  and **5** collected in  $\text{DMSO-}d_6$  at 300K. The chemical shift changes of (a) H(1), H(4) and H(7) on  $2^{2+}$  were used for the calculation of  $K_a = (1.7 \pm 0.2) \times 10^2 \text{ M}^{-1}$  for  $[2^{2+}\cdot 5]$  formation using the Hyperquad 2003 program.<sup>9</sup> The changes in chemical shift of other protons present in  $2^{2+}$  and **5** overlapped and thus could not be accurately fit with either a Gaussian or Lorentzian function. Also in some cases the chemical shift change was too small (less than 8.0 Hz); these signals were therefore not used in the calculation of the association constant.<sup>10</sup> The red dashed lines show the non-linear curve fit of the experimental data to the appropriate equation.

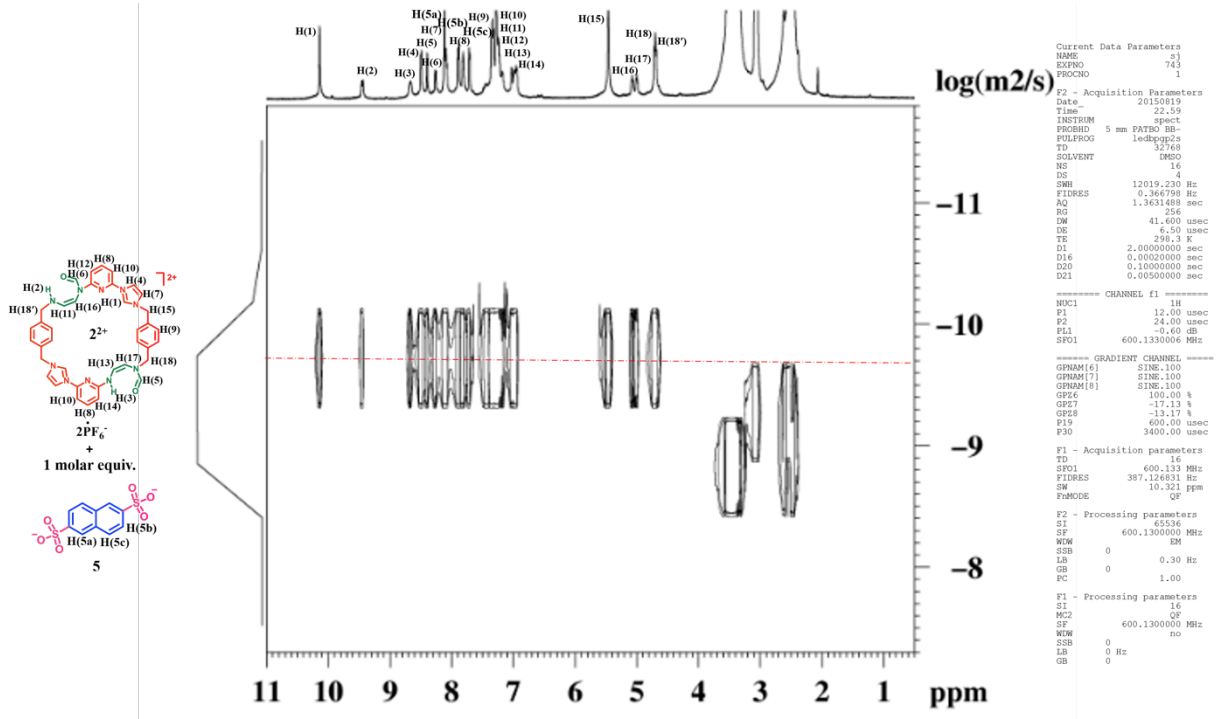


**Figure S50.** 600 MHz 2D-DOSY NMR spectra of  $2^{2+} \cdot 2PF_6^-$  ( $2.00 \times 10^{-2}$  M) recorded in the presence of 1 molar equiv. of 2,6-naphthalenedisulfonic acid and 2 molar equiv. of  $TMA^+ \cdot OH^-$  collected in  $DMSO-d_6$  at 300K.

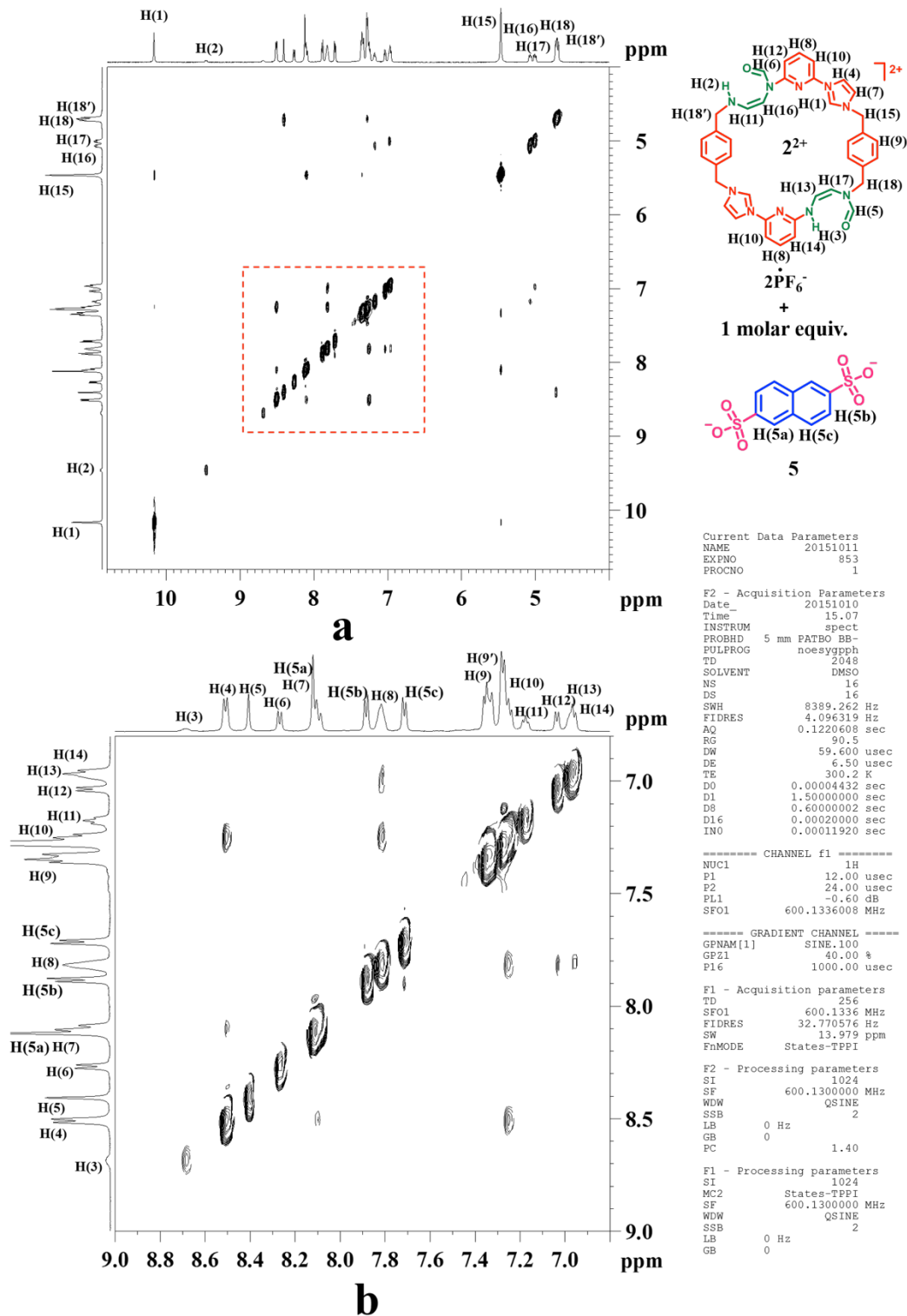


**Figure S51.** Full view (a) and expanded view (b) of the 600 MHz NOESY NMR spectrum of  $2^{2+} \cdot 2PF_6^-$  ( $2.00 \times 10^{-2}$  M) recorded in the presence of 1 molar equiv. of 2,6-naphthalenedisulfonic acid and 2 molar equiv. of  $TMA^+ \cdot OH^-$  in  $DMSO-d_6$  at 300K.

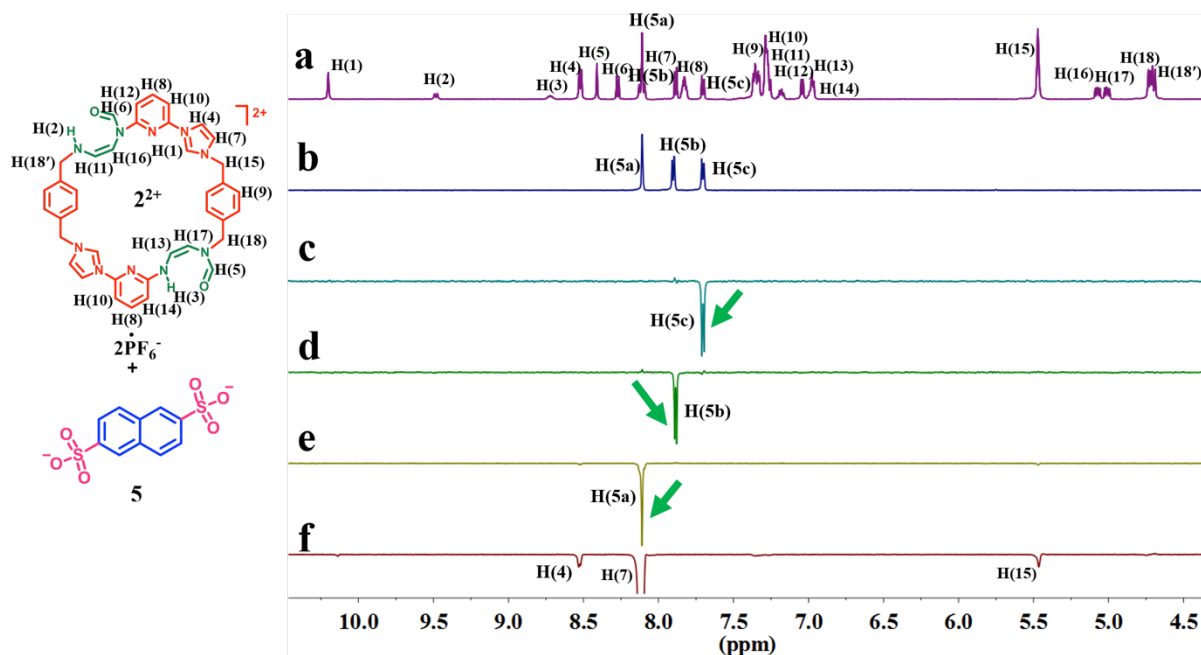


**Figure S52.** 600 MHz  $^1H$  NMR and 1D NOE NMR spectra recorded in DMSO- $d_6$  at 300K: (a)  $^1H$  NMR of  $2^{2+} \cdot 2PF_6^-$  in the presence of 1 molar equiv. of 2,6-naphthalenedisulfonic acid and 2 molar equiv. of TMA $^+$ ·OH $^-$  ([host] = [guest] =  $5.00 \times 10^{-3}$  M), (b)  $^1H$  NMR of the 2,6-naphthalenedisulfonic acid in the presence of 2 molar equiv. of TMA $^+$ ·OH $^-$ , and (c-e) 1D-NOE NMR spectra of  $2^{2+} \cdot 2PF_6^-$  in the presence of 1 molar equiv. of 2,6-naphthalenedisulfonic acid and 2 molar equiv. of TMA $^+$ ·OH $^-$  ([host] = [guest] =  $5.00 \times 10^{-3}$  M). The green arrows indicate irradiation at the frequency of H(5a), H(5b) and H(5c) of 2,6-naphthalenedisulfonate (**5**). Shown in (f) is the 1D-NOE NMR spectra of  $2^{2+} \cdot 2PF_6^-$  ( $5.00 \times 10^{-3}$  M). The green arrow indicates irradiation at the frequency of H(7) of  $2^{2+} \cdot 2PF_6^-$ .

**Solution binding studies and characterization of host-guest complex formed between  $2^{2+}$  and dianionic guest 1,5-naphthalenedisulfonate (**6**):**

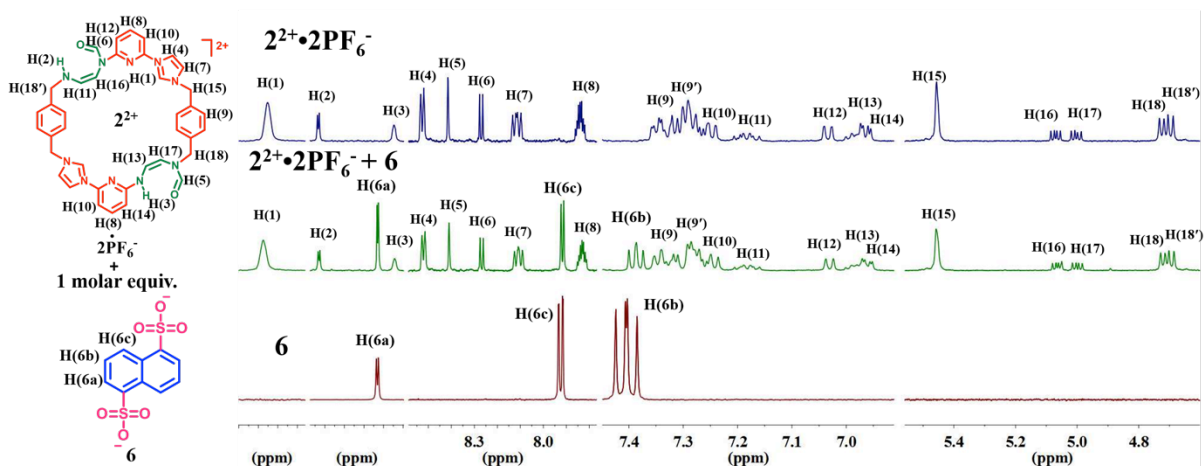


**Figure S53.** Expanded views of the  $^1\text{H}$  NMR spectra of  $2^{2+} \cdot 2\text{PF}_6^-$  ( $1.00 \times 10^{-3}$  M) recorded in the absence and presence of 1 molar equiv. of **6** in  $\text{DMSO}-d_6$  at 300 K over the indicated spectral ranges (600 MHz).

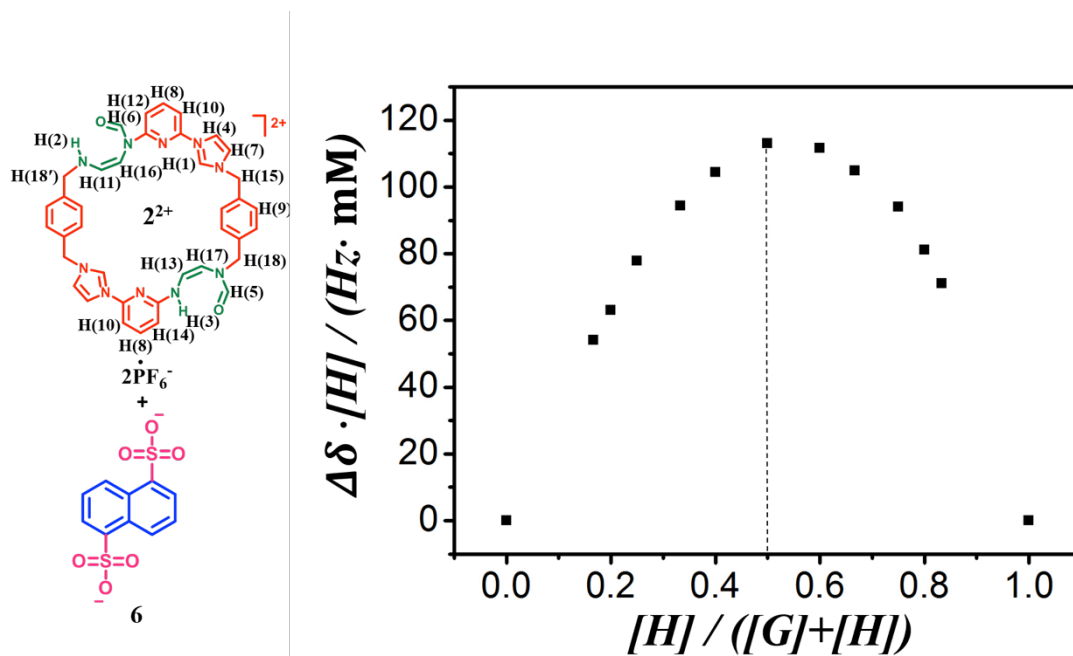


**Figure S54.**  $^1\text{H}$  NMR Job-plots (600 MHz) corresponding to the binding between  $2^{2+} \cdot 2\text{PF}_6^-$  and **6** ( $[\text{host}] + [\text{guest}] = 1.00 \times 10^{-2}$  M). The maximum value was determined to be 0.5 at this concentration, a finding that is consistent with a 1:1 (host: guest) binding stoichiometry.<sup>8</sup>

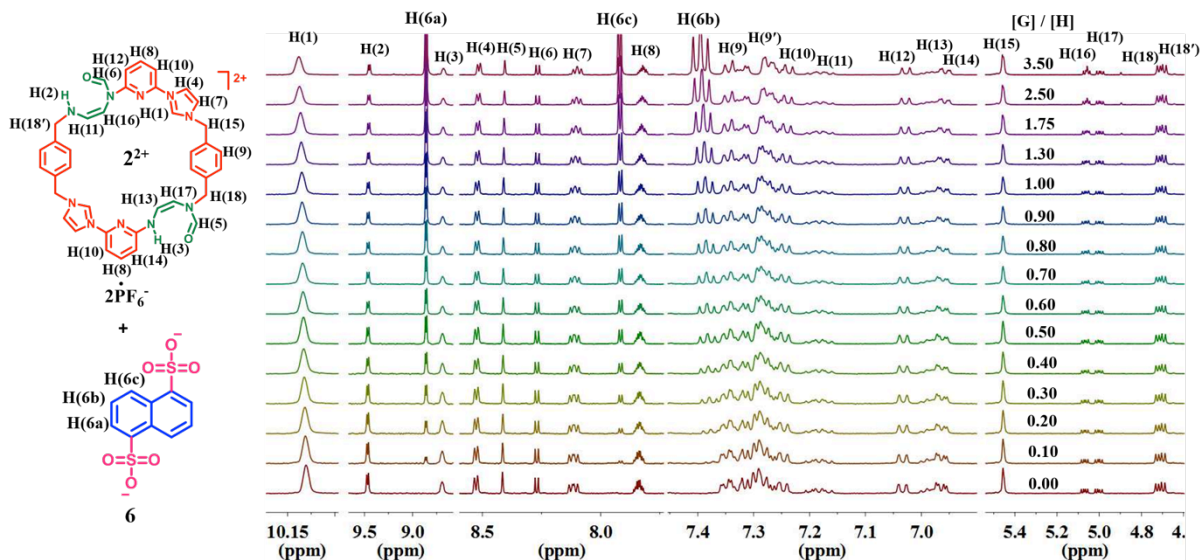


**Figure S55.**  $^1\text{H}$  NMR spectroscopic titration of  $2^{2+}\cdot 2\text{PF}_6^-$  ( $1.00 \times 10^{-3}$  M) with 1,5-naphthalenedisulfonic acid in the presence of 2 molar equiv. of  $\text{TMA}^+\cdot\text{OH}^-$  collected in  $\text{DMSO-}d_6$  at 300K (600 MHz).

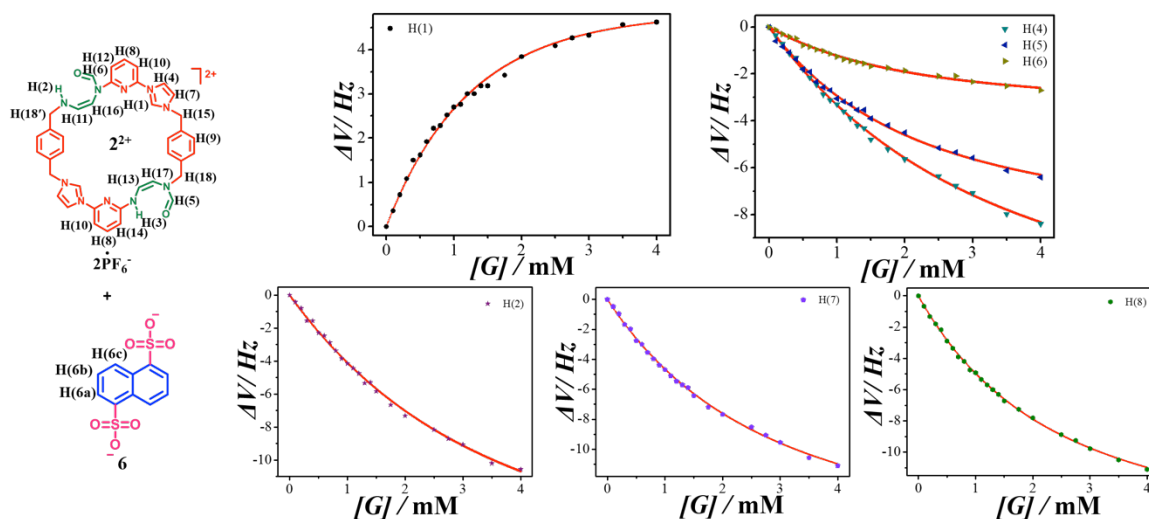


**Figure S56.**  $^1\text{H}$  NMR binding isotherms corresponding to the interaction between  $2^{2+}\cdot 2\text{PF}_6^-$  and **6** in  $\text{DMSO-}d_6$  at 300K. The chemical shift changes of H(1) and H(2), H(4), H(5), H(6), H(7) and H(8) on  $2^{2+}$  were used for the calculation of  $(4.0 \pm 0.5) \times 10^2 \text{ M}^{-1}$  using the Hyperquad 2003 program.<sup>9</sup> The changes in chemical shift of the other protons present in  $2^{2+}$  and **6** overlapped and thus could not be accurately fit with either a Gaussian or Lorentzian function. Also in some cases the chemical shift change was too small (less than 8.0 Hz); these signals were therefore not used in the calculation of the association constant.<sup>10</sup> The red dashed lines show the non-linear curve fit of the experimental data to the appropriate equation.

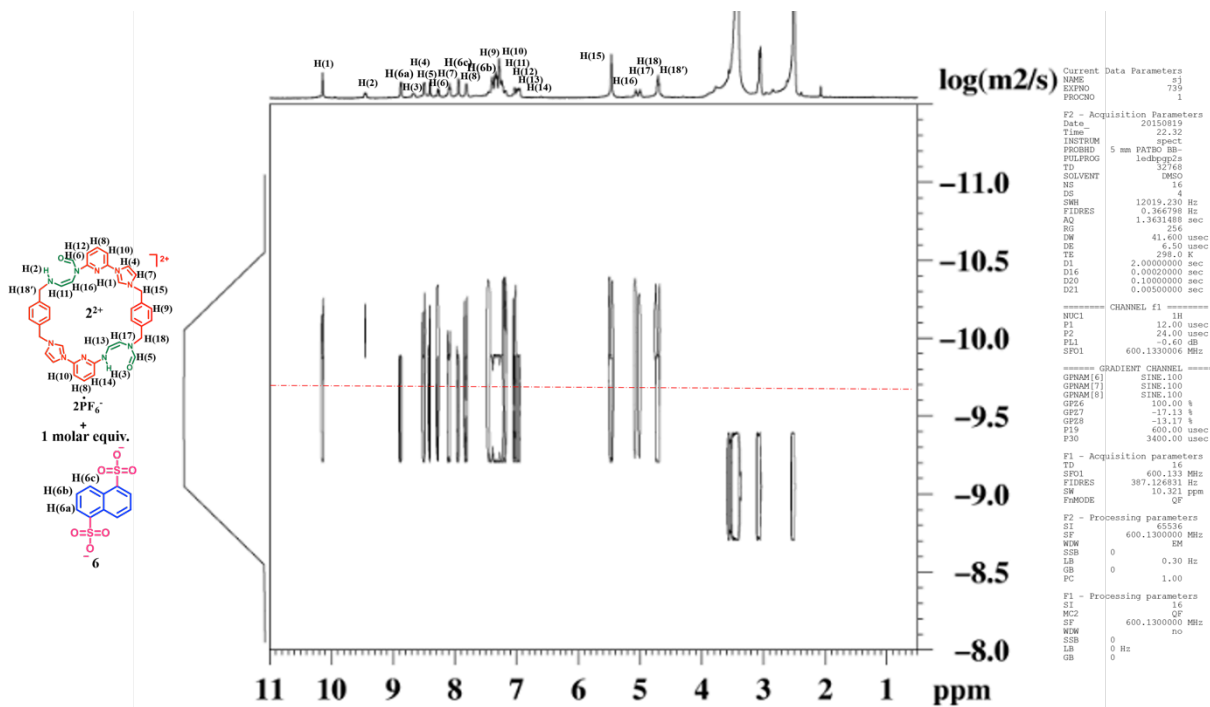


**Figure S57.** Expanded view of the 600 MHz 2D-DOSY NMR spectra of  $2^{2+} \cdot 2PF_6^-$  ( $2.00 \times 10^{-2}$  M) recorded in the presence of 1 molar equiv. of 1,5-naphthalenedisulfonic acid and 2 molar equiv. of TMA<sup>+</sup>·OH<sup>-</sup> in DMSO-*d*<sub>6</sub> at 300K.

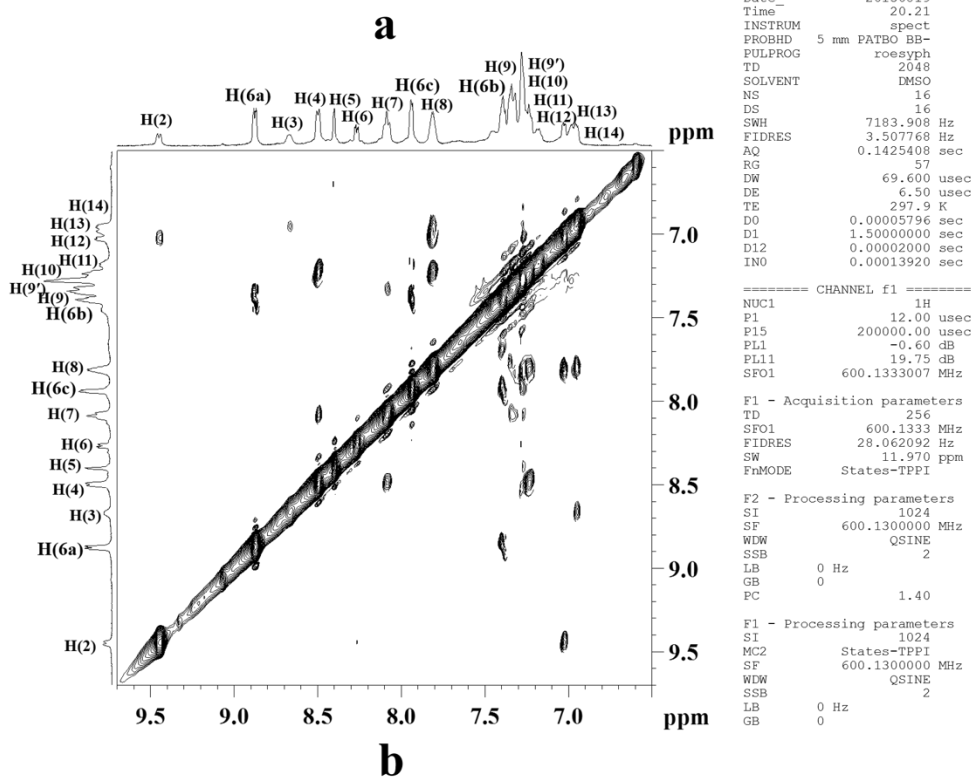
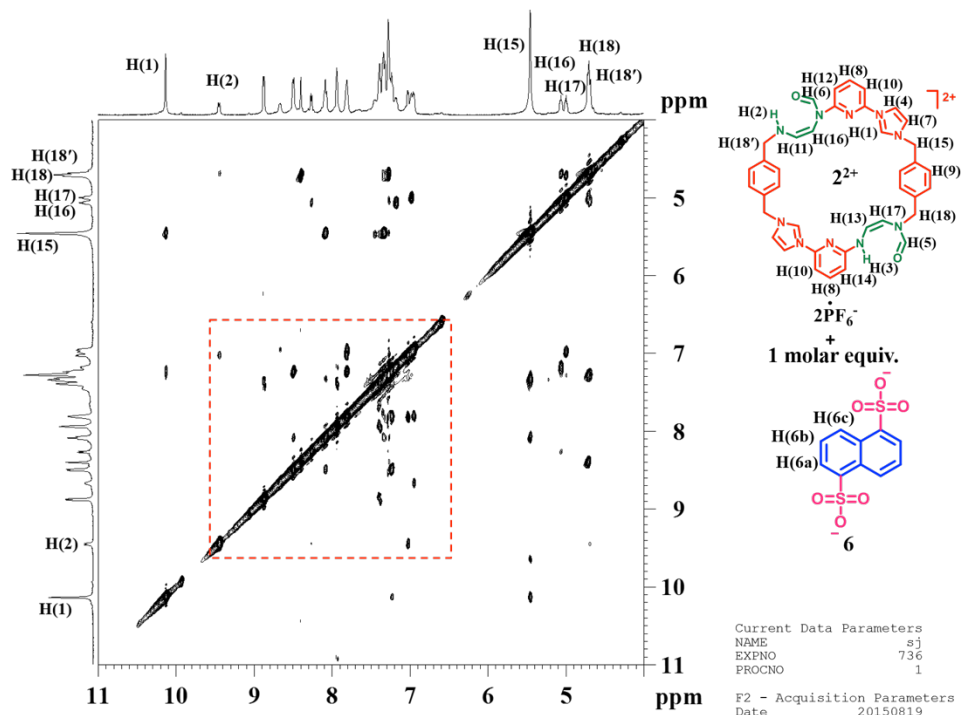


**Figure S58.** Full (a) and expanded view (b) of the 600 MHz ROESY NMR spectrum of  $2^{2+} \cdot 2PF_6^{-}$  ( $2.00 \times 10^{-2}$  M) recorded in the presence of 1 molar equiv. of 1,5-naphthalenedisulfonic acid and 2 molar equiv. of  $TMA^{+} \cdot OH^{-}$  in  $DMSO-d_6$  at 300K.

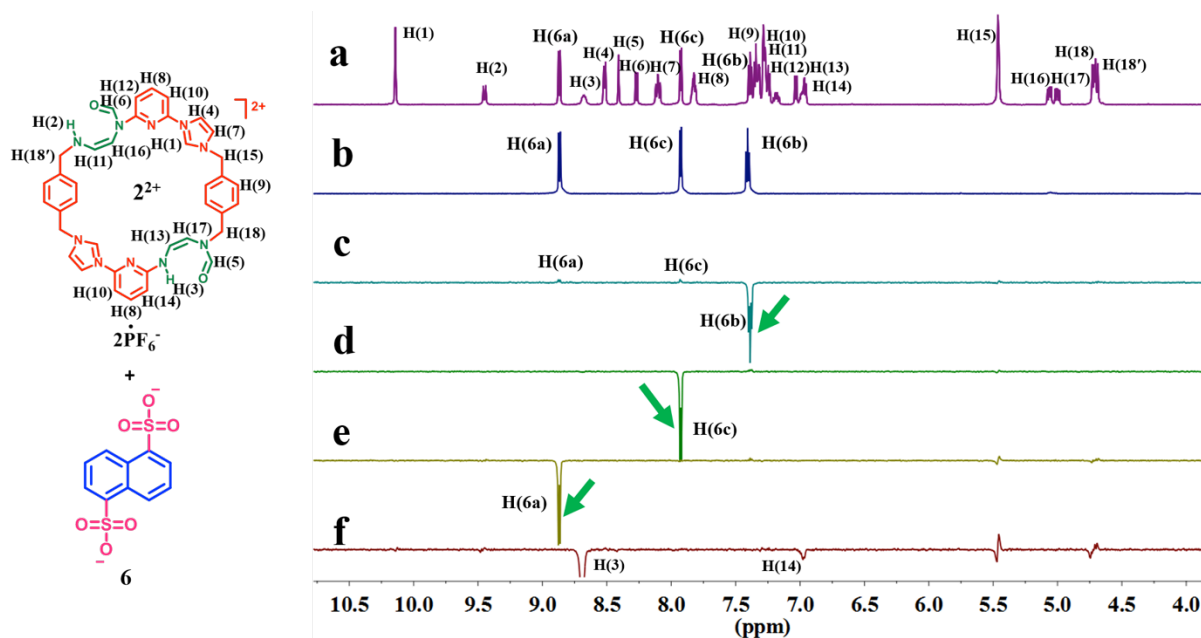


**Figure S59.** 600 MHz  $^1\text{H}$  NMR and 1D NOE NMR spectra recorded in DMSO- $d_6$  at 300K: (a)  $^1\text{H}$  NMR of  $2^{2+} \cdot 2\text{PF}_6^-$  in the presence of 1 molar equiv. of 1,5-naphthalenedisulfonic acid and 2 molar equiv. of TMA $^+$ ·OH $^-$  ([host] = [guest] =  $5.00 \times 10^{-3}$  M), (b)  $^1\text{H}$  NMR of the 1,5-naphthalenedisulfonic acid in the presence of 2 molar equiv. of TMA $^+$ ·OH $^-$ , and (c-e) 1D NOE NMR spectra of  $2^{2+} \cdot 2\text{PF}_6^-$  in the presence of 1 molar equiv. of 1,5-naphthalenedisulfonic acid and 2 molar equiv. of TMA $^+$ ·OH $^-$  ([host] = [guest] =  $5.00 \times 10^{-3}$  M). The green arrows indicate irradiation at the frequency of H(6a), H(6b) and H(6c) of 1,5-naphthalenedisulfonate. Shown in (f) is the 1D NOE NMR spectrum of  $2^{2+} \cdot 2\text{PF}_6^-$  ( $5.00 \times 10^{-3}$  M). The green arrow indicates irradiation at the frequency of H(3) of  $2^{2+} \cdot 2\text{PF}_6^-$ .

**Section S5:** Single crystal X-ray analysis of the complexes formed between  $2^{2+}$  and dianionic guest **5** or **6**

**Table S3.** Single crystal X-ray crystallographic data for  $[2^{2+}\cdot\mathbf{5}\cdot 5\text{H}_2\text{O}]$  and  $[2^{2+}\cdot\mathbf{6}\cdot 2.5\text{H}_2\text{O}]$ .

	$2^{2+}\cdot\mathbf{5}\cdot 5\text{H}_2\text{O}$	$2^{2+}\cdot\mathbf{6}\cdot 2.5\text{H}_2\text{O}$
CCDC No.	1433723	1433722
description	prism	needle
colour	colourless	colourless
From solution	DMF/water /acetonitrile	DMF/water /acetonitrile
empirical formula	$\text{C}_{48}\text{H}_{52}\text{N}_{10}\text{O}_{13}\text{S}_2$	$\text{C}_{48}\text{H}_{47}\text{N}_{10}\text{O}_{10.50}\text{S}_2$
<i>Mr</i>	1041.12	996.08
crystal size (mm <sup>3</sup> )	0.05 × 0.03 × 0.02	0.11 × 0.04 × 0.03
crystal system	Monoclinic	Triclinic
space group	P2(1)/n	P-1
<i>a</i> [Å]	13.490(3)	16.853(3)
<i>b</i> [Å]	18.126(4)	17.211(3)
<i>c</i> [Å]	20.197(4)	18.087(4)
<i>α</i> [deg]	90.00	99.16(3)
<i>β</i> [deg]	101.26(3)	91.70(3)
<i>γ</i> [deg]	90.00	96.78(3)
<i>V</i> [Å <sup>3</sup> ]	4843.4(17)	5136.5(18)
<i>d</i> [g/cm <sup>3</sup> ]	1.428	1.288
<i>Z</i>	4	4
<i>T</i> [K]	173(2)	173(2)
R1, wR2	0.1162	0.1539
<i>I</i> > 2 $\sigma$ ( <i>I</i> )	0.2200	0.3146
R1, wR2 (all data)	0.1480 0.2401	0.2232 0.3478
quality of fit	1.005	0.997

## Single-crystal X-ray structure of $[2^{2+}\cdot 5\cdot 5H_2O]$ :

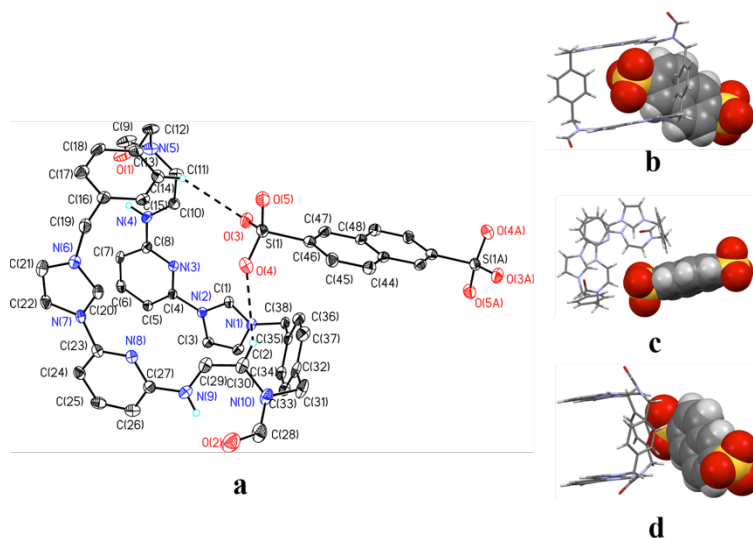


**Figure S60.** Structure of  $2^{2+}$  viewed from the top view in ellipsoid form (a), as well as top (b), side (c) and front views (d) of  $2^{2+}$  in stick form. In these structures,  $2^{2+}$  adopts a “clip-like” conformation with a molecule of **5** bound to its outer periphery in the final structure  $[2^{2+}\cdot 5\cdot 5H_2O]$ . Displacement ellipsoids are scaled to the 25% probability level. Some or all of the counter anions, solvent molecules and hydrogen atoms have been omitted for clarity. The symmetry transformation invoked by the additional "A" letter in the atom labels on the **5** is (1-x, 1-y, 1-z). Possible intermolecular hydrogen bonds: selected interatomic distances [Å]: O(4)...C(30) 3.501(8), O(3)...C(14) 3.627(7); selected bond angles: C(30)-H(30A)...O(4) 139.5°, C(14)-H(14A)...O(3) 148.8°.

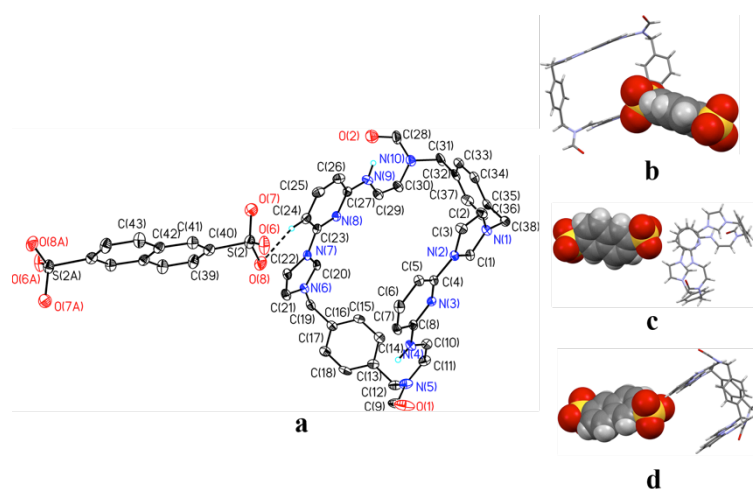


**Figure S61.** Structure of  $2^{2+}$  viewed from the top in ellipsoid form (a), as well as top (b), side (c) and front views (d) of  $2^{2+}$  in stick form. In these structures,  $2^{2+}$  adopts a “clip-like” conformation with a molecule of **5** bound to its outer periphery in the final structure  $[2^{2+}\cdot 5\cdot 5H_2O]$ . Displacement ellipsoids are scaled to the 25% probability level. Some or all of the counter anions, solvent molecules and hydrogen atoms have been omitted for clarity. The symmetry transformation invoked by the additional "A" letter in the atom labels on the **5** is (1-x, 1-y, 1-z). Possible intermolecular hydrogen bonds: selected interatomic distances [Å]: O(8)...C(24) 3.399(7); selected bond angles: C(24)-H(24A)...O(8) 167.2°.

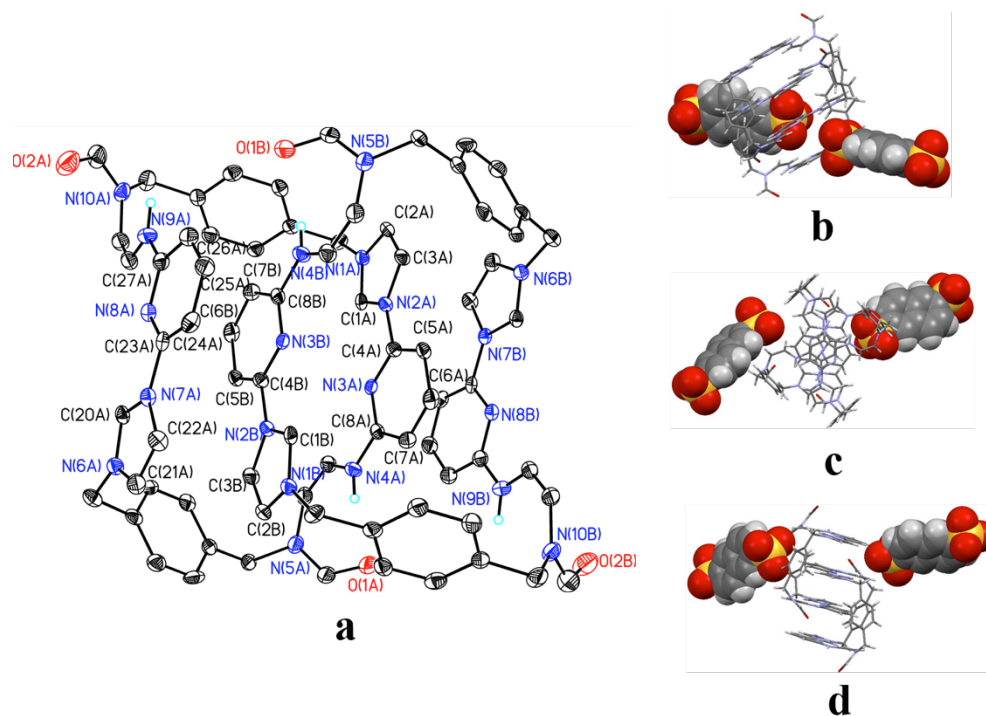


**Figure S62.** Structure of  $2^{2+}$  viewed from the top (a) in ellipsoid form, as well as top (b), side (c), and front views (d) in stick form. In these structures,  $2^{2+}$  is organized in a head-to-tail racemic dimer which is present in the final structure [ $2^{2+} \cdot 5 \cdot 5H_2O$ ]. Displacement ellipsoids are scaled to the 25% probability level. Some or all of the counter anions, solvent molecules and hydrogen atoms have been omitted for clarity. The symmetry transformation invoked by the additional "A" letter and "B" letter in the atom labels on the macrocycle  $2^{2+}$  are  $(x, y, z)$  and  $(-x, -y, 1-z)$ . Possible intramolecular  $\pi \dots \pi$  interaction: Selected interatomic distances [ $\text{\AA}$ ]: N(3B)...C(24A) 3.594(8), N(3B)...C(23A) 3.442(7), C(8B)...C(26A) 3.498(9), C(8B)...C(27A) 3.341(8), C(6B)...N(8A) 3.726(8), N(3B)...N(3A) 3.366(6), C(8A)...N(3B) 3.779(8), N(3B)...C(4A) 3.306(7), C(4B)...C(8A) 3.510(8), C(5B)...C(23A) 4.020(8), C(4B)...C(23A) 3.495(8), N(7A)...N(2B) 3.409(6), C(21A)...C(2B) 3.448(9), C(21A)...C(3B) 3.550(1), N(6A)...C(3B) 3.590(9).

Single-crystal analysis for structure  $[2^{2+} \cdot 6 \cdot 2.5H_2O]$ :

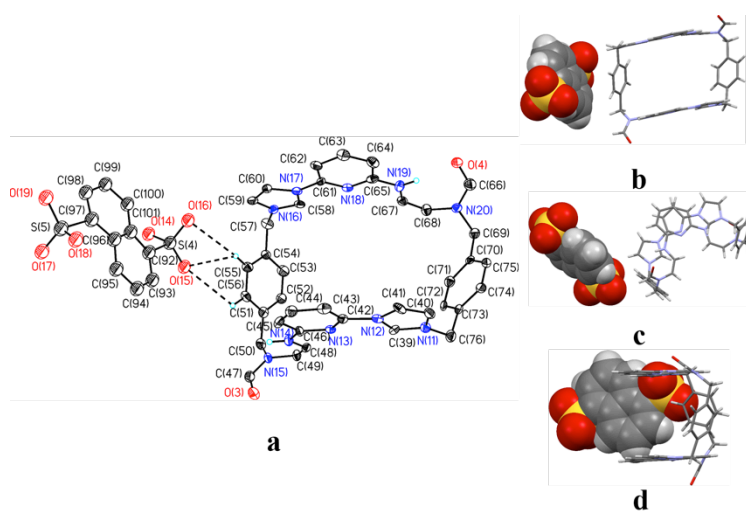


**Figure S63.** Structure of  $2^{2+}$  viewed from the top (a) in ellipsoid form, as well as top (b), side (c), and front views (d) in stick form. In these structures,  $2^{2+}$  adopts a “clip” conformation and **6** is bound to the outer periphery of the final structure  $[2^{2+} \cdot 6 \cdot 2.5H_2O]$ . Displacement ellipsoids are scaled to the 25% probability level. Some or all of the counter anions, solvent molecules and hydrogen atoms have been omitted for clarity. Selected bond distances between  $2^{2+}$  and the anion **6** are as follows. Intermolecular hydrogen bonds: selected interatomic distances [Å]: O(15)...C(55) 3.23(2), O(15)...C(56) 3.48(2), O(16)...C(55) 3.59(2). Selected bond angles: C(55)-H(55A)...O(15) 95.9°, C(56)-H(56A)...O(15) 85.8°, C(55)-H(55A)...O(16) 132.7°.

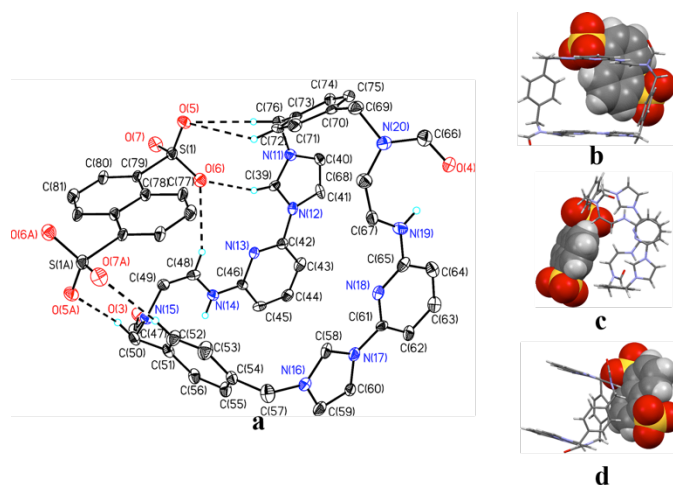


**Figure S64.** Structure of  $2^{2+}$  viewed from the top (a) in ellipsoid form, as well as top (b), side (c), and front views (d) shown in stick form. In these structures,  $2^{2+}$  adopts a “clip” conformation and **6** is bound to the outer periphery of the final structure  $[2^{2+} \cdot 6 \cdot 2.5H_2O]$ . Displacement ellipsoids are scaled to the 25% probability level. Some or all of the counter anions, solvent molecules and hydrogen atoms have been omitted for clarity. The symmetry transformation invoked by the additional "A" letter in the atom labels on the **6** is (1-x, 1-y, -z). Intermolecular hydrogen bonds: selected interatomic distances [Å]:

O(5A)...C(50) 3.53(1), O(5)...C(76) 3.77(1), O(5)...C(72) 3.59(1), O(6)...C(39) 2.97(1), O(6)...C(48) 3.57(1), O(7A)...C(52) 3.94(1). Selected bond angles: C(50)-H(50B)...O(5A) 163.5°, C(72)-H(72A)...O(5) 140.9°, C(76)-H(76A)...O(5) 156.3°, C(48)-H(48A)...O(6) 154.2°, C(39)-H(39A)...O(6) 152.7°, C(52)-H(52A)...O(7A) 159.0°.

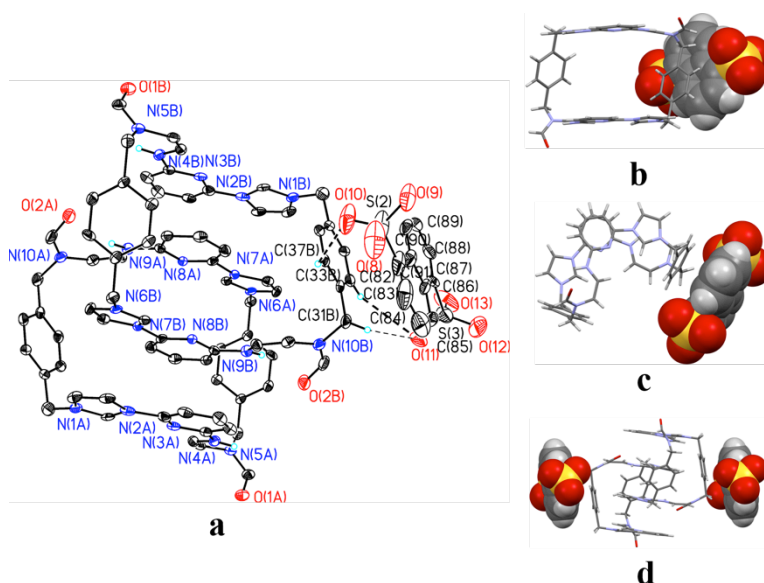


**Figure S65.** Structure of  $2^{2+}$  viewed from the top (a) in ellipsoid form, as well as top (b), side (c), and front views (d) shown in stick form. In these structures,  $2^{2+}$  adopts a “clip” conformation and **6** is bound to the outer periphery of the final structure [ $2^{2+} \cdot 6 \cdot 2.5\text{H}_2\text{O}$ ]. Displacement ellipsoids are scaled to the 25% probability level. Some or all of the counter anions, solvent molecules and hydrogen atoms have been omitted for clarity. The symmetry transformation invoked by the additional "A" letter and "B" letter in the atom labels on the  $2^{2+}$  are (x, y, z) and (1-x, 2-y, 1-z). Intermolecular hydrogen bonds: selected interatomic distances [Å]: O(11)...C(31B) 3.46(1), O(11)...C(33B) 3.68(2), O(10)...C(37B) 3.23(2); selected bond angles: C(31B)-H(31BA)...O(11) 164.5°, C(33B)-H(33BA)...O(11) 130.6°, C(37B)-H(37BA)...O(10) 115.9°. Possible intermolecular  $\pi \dots \pi$  donor-acceptor interactions: selected interatomic distances [Å]: C(90)...C(37B) 3.46(2), C(91)...C(37B) 3.51(2), C(86)...C(33B) 3.86(2), C(87)...C(33B) 3.51(2), C(88)...C(33B) 3.44(2).

**Section S6:** Mass spectrometric analysis of the complexes formed between  $2^{2+}$  and dianionic guest **4**, **5** or **6**

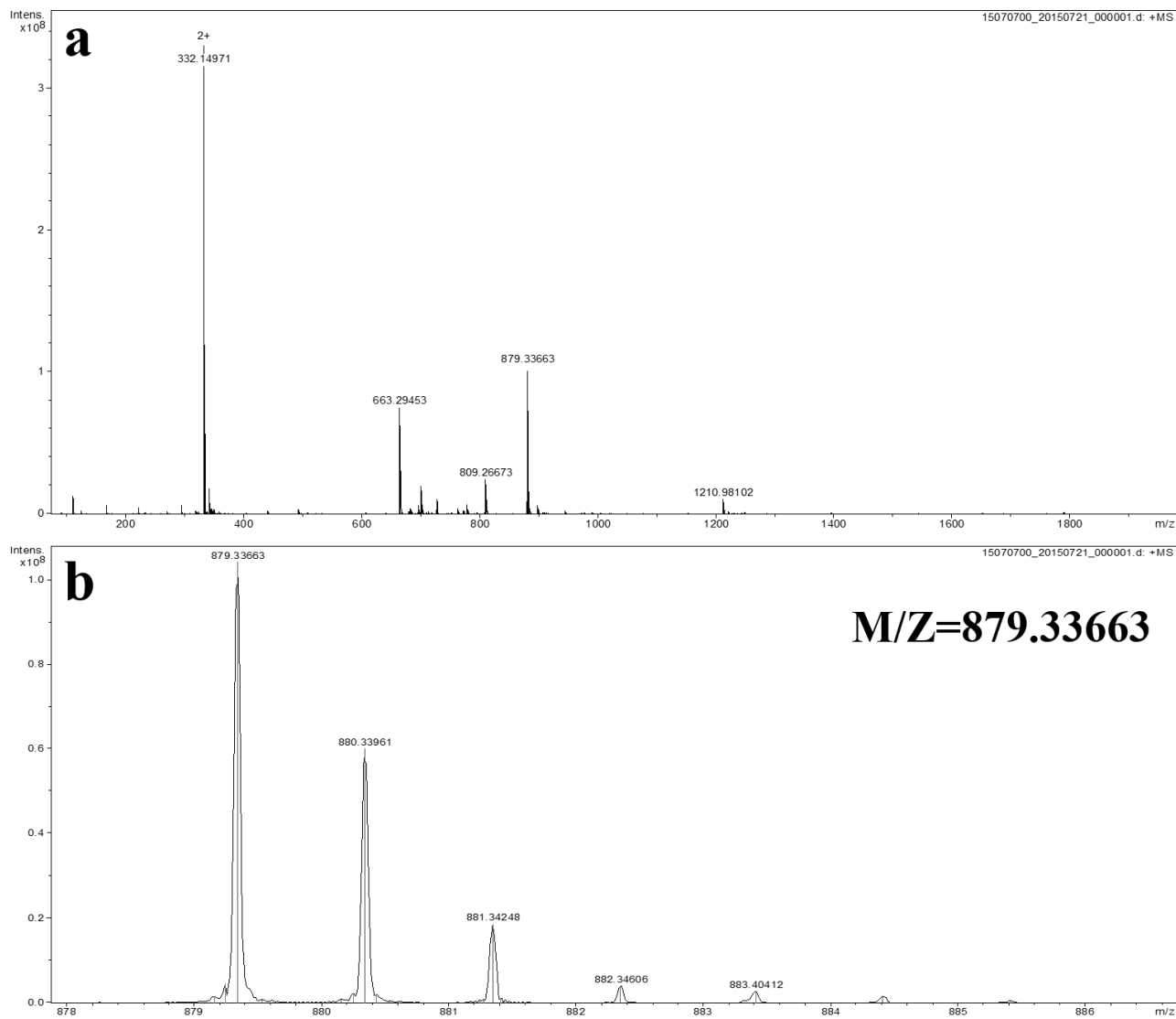


**Figure S66.** Full (a) and expanded view (b) of the ESI high resolution mass spectrum obtained from a mixture of  $2^{2+}$  and guest **4**.

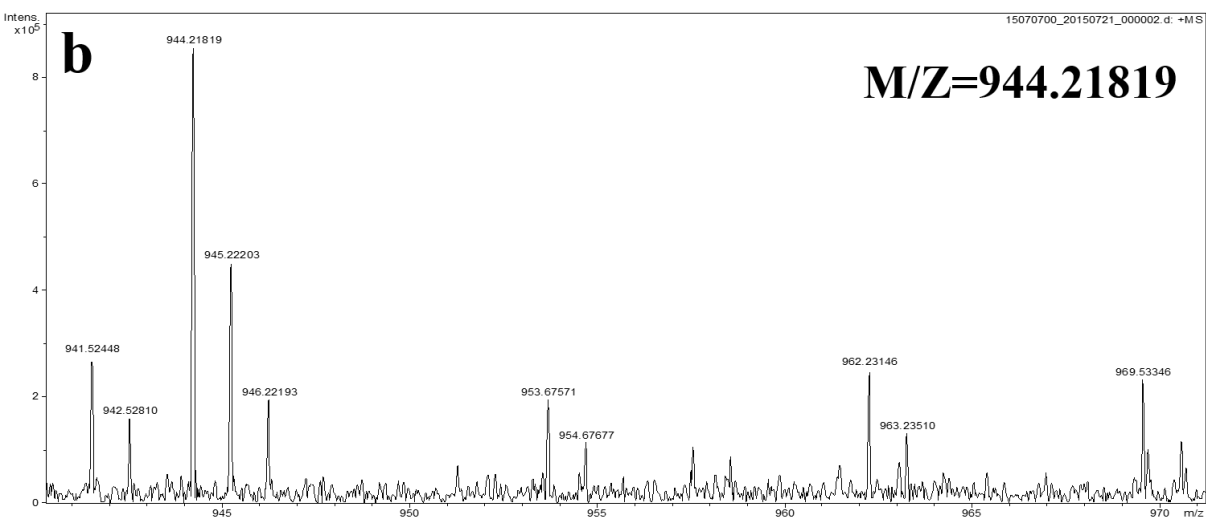
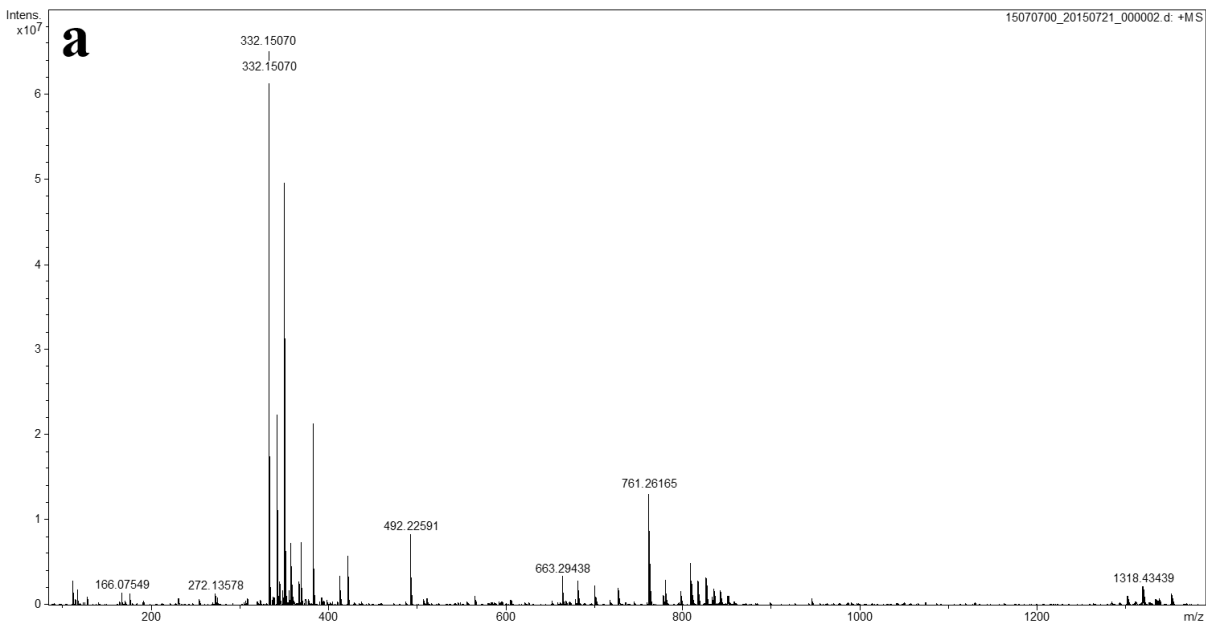


**Figure S67.** Full (a) and expanded view (b) of the ESI high resolution mass spectrum obtained from a mixture of  $2^{2+}$  and guest **5**.

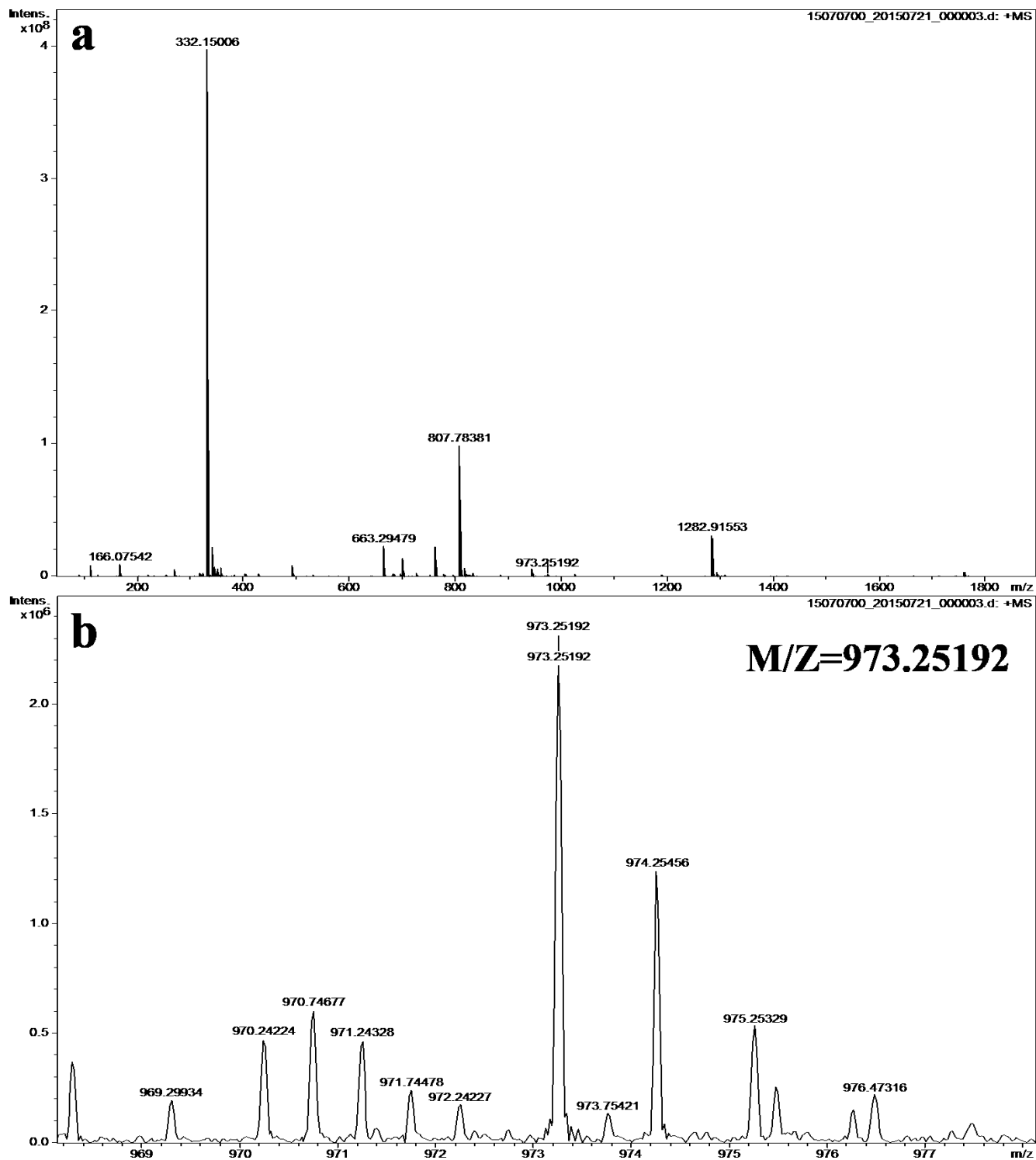
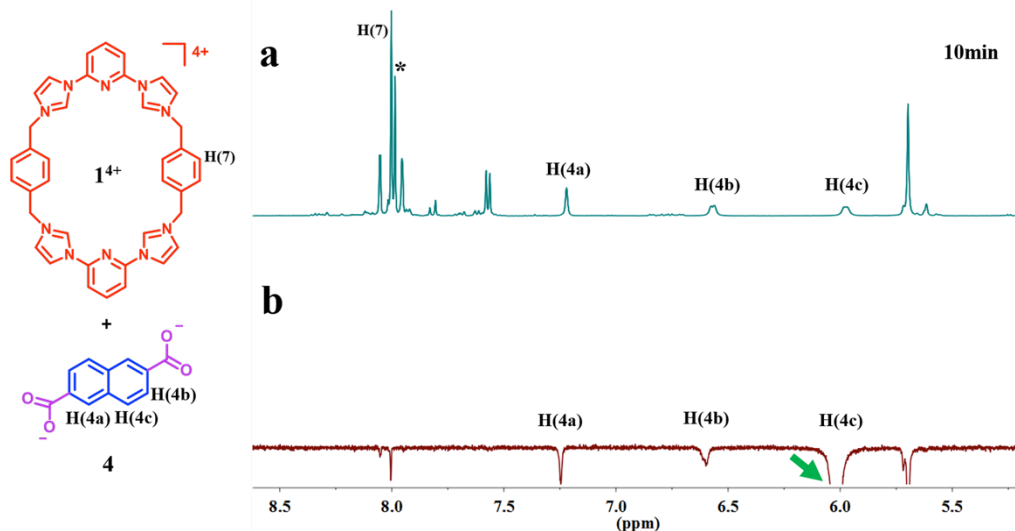


**Figure S68.** Full (a) and expanded view (b) of the ESI high resolution mass spectrum obtained from a mixture of  $2^{2+}$  and guest **6**.

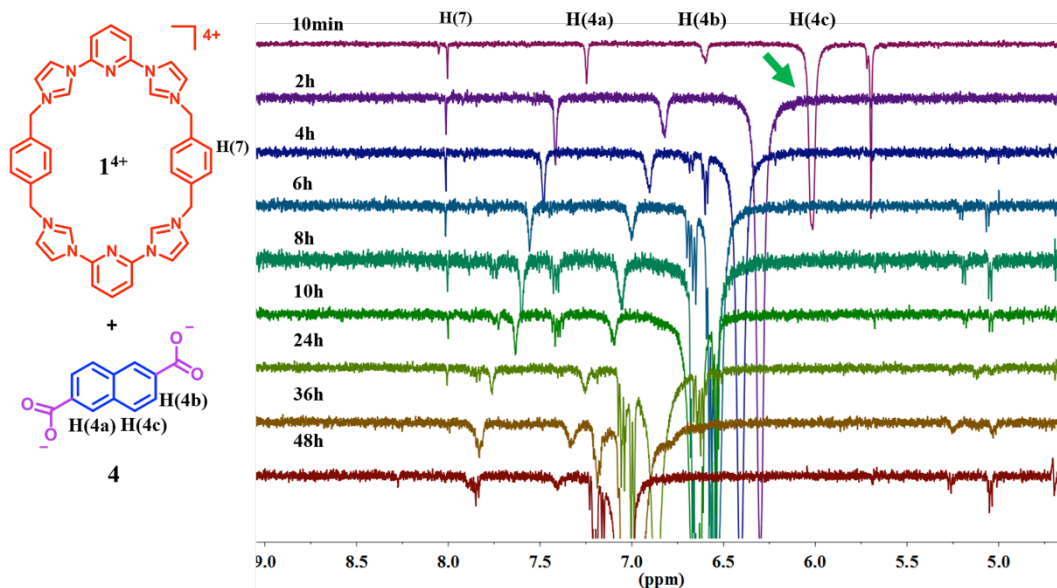
**Table S4.** Summary of ESI-MS results.

<b>Presumed Complex</b>	<b>Peak Assignment</b>	<b>Calculated m/z</b>	<b>Observed m/z</b>
[2 <sup>2+</sup> •4]	[2 <sup>2+</sup> +4+H] <sup>+</sup>	879.3367	879.3366
[2 <sup>2+</sup> •5]	[2 <sup>2+</sup> +5-6H] <sup>+</sup>	944.2159	944.2182
[2 <sup>2+</sup> •6]	[2 <sup>2+</sup> +6+Na] <sup>+</sup>	973.2526	973.2519

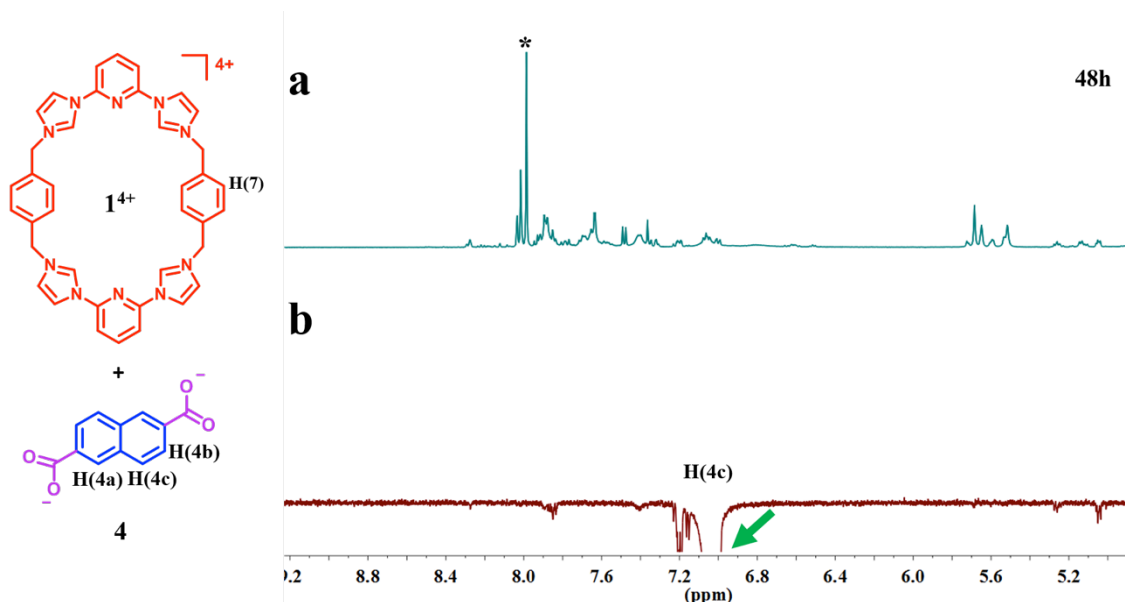
**Section S7: Solution binding studies and characterization of the OH ring-opening process leading to the irreversible disassembly of the interpenetrated structures  $[1^{4+}\cdot 4]$  and  $[1^{4+}\cdot 5]$**



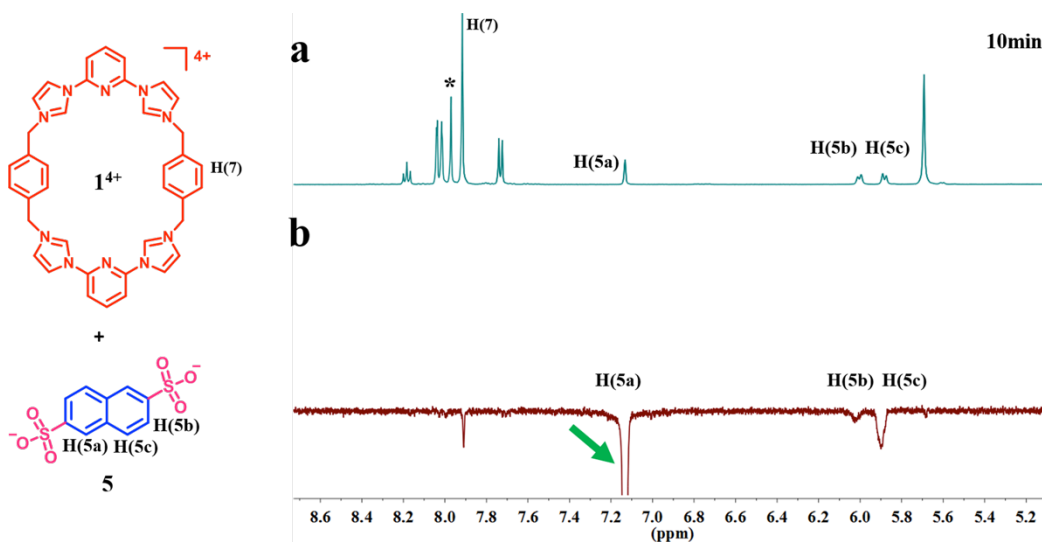
**Figure S69.** 600 MHz  $^1\text{H}$  NMR and 1D NOE NMR spectra recorded in  $\text{DMF-}d_7/\text{D}_2\text{O}/\text{ND}_3\cdot\text{D}_2\text{O}$  (1/0.98/0.02, v/v/v) at 298K: (a)  $^1\text{H}$  NMR spectrum of  $1^{4+}\cdot 4\text{PF}_6^-$  recorded in the presence of 1 molar equiv. of 2,6-naphthalenedicarboxylic acid and 2 molar equiv. of  $\text{TMA}^+\cdot\text{OH}^-$  at 10 min (reaction time) ( $[\text{host}] = [\text{guest}] = 5.00 \times 10^{-3}$  M), (b) 1D NOE NMR spectra of  $1^{4+}\cdot 4\text{PF}_6^-$  in the presence of 1 molar equiv. of 2,6-naphthalenedicarboxylic acid and 2 molar equiv. of  $\text{TMA}^+\cdot\text{OH}^-$  at 10 min (reaction time) ( $[\text{host}] = [\text{guest}] = 5.00 \times 10^{-3}$  M). There is one proton signal of the solvent  $\text{DMF-}d_7$  that is labeled with a “\*”. The green arrow indicates irradiation at the frequency of H(4c) of 2,6-naphthalenedicarboxylate (**4**).



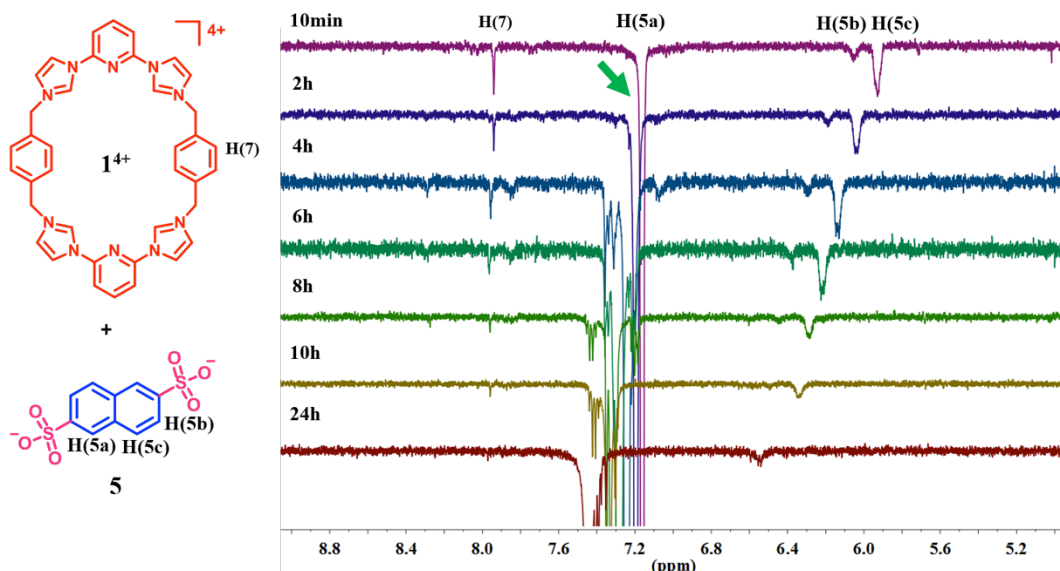
**Figure S70.** 1D NOE NMR spectra of  $1^{4+}\cdot 4\text{PF}_6^-$  recorded in the presence of 1 molar equiv. of 2,6-naphthalenedicarboxylic acid and 2 molar equiv. of  $\text{TMA}^+\cdot\text{OH}^-$  ( $[\text{host}] = [\text{guest}] = 5.00 \times 10^{-3}$  M) in  $\text{DMF-}d_7/\text{D}_2\text{O}/\text{ND}_3\cdot\text{D}_2\text{O}$  (1/0.98/0.02, v/v/v) at 298K (600 MHz). The green arrows indicate irradiation at the frequency of H(4c) of 2,6-naphthalenedicarboxylate (**4**). These findings are consistent with **4** dethreading from the pseudorotaxane structure  $[1^{4+}\cdot 4]$  as reaction proceeds.



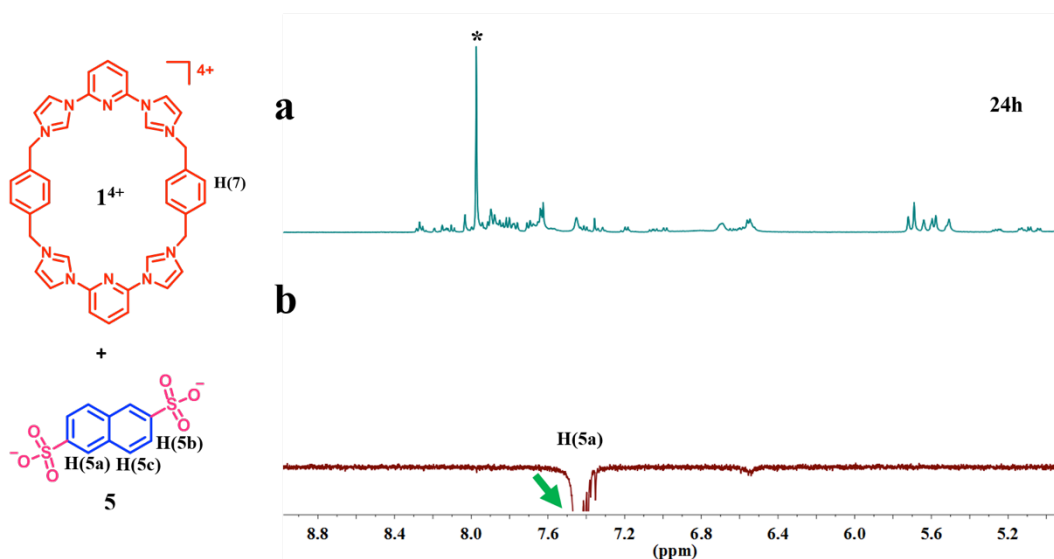
**Figure S71.** 600 MHz  $^1\text{H}$  NMR and 1D NOE NMR spectra recorded in  $\text{DMF-}d_7/\text{D}_2\text{O}/\text{ND}_3\cdot\text{D}_2\text{O}$  (1/0.98/0.02, v/v/v) at 298K: (a)  $^1\text{H}$  NMR of  $1^{4+}\cdot 4\text{PF}_6^-$  in the presence of 1 molar equiv. of 2,6-naphthalenedicarboxylic acid and 2 molar equiv. of  $\text{TMA}^+\cdot\text{OH}^-$  at 48 h (reaction time) ( $[\text{host}] = [\text{guest}] = 5.00 \times 10^{-3} \text{ M}$ ), (b) 1D NOE NMR spectra of  $1^{4+}\cdot 4\text{PF}_6^-$  recorded in the presence of 1 molar equiv. of 2,6-naphthalenedicarboxylic acid and 2 molar equiv. of  $\text{TMA}^+\cdot\text{OH}^-$  at 48 h (reaction time) ( $[\text{host}] = [\text{guest}] = 5.00 \times 10^{-3} \text{ M}$ ). The one proton signal of the solvent  $\text{DMF-}d_7$  is labeled with a “\*”. The green arrow indicates irradiation at the frequency of H(4c) of 2,6-naphthalenedicarboxylate (**4**).



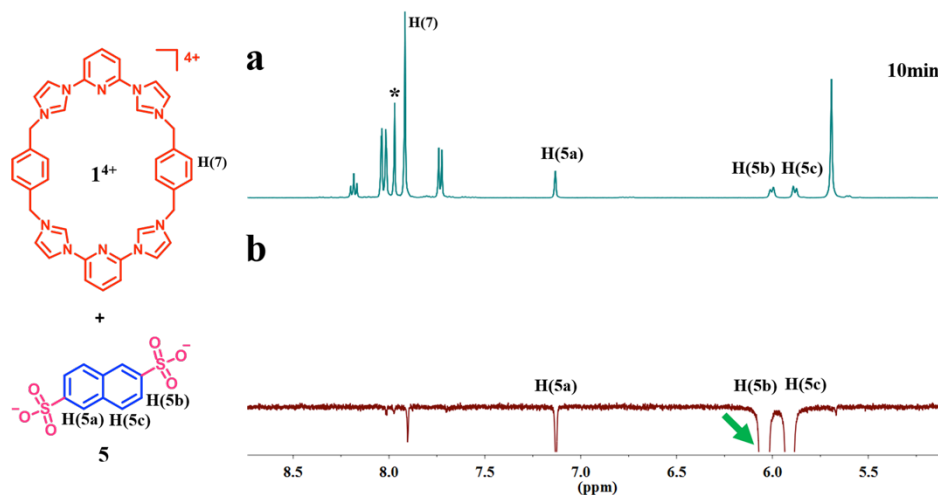
**Figure S72.** 600 MHz  $^1\text{H}$  NMR and 1D NOE NMR spectra recorded in  $\text{DMF-}d_7/\text{D}_2\text{O}/\text{ND}_3\cdot\text{D}_2\text{O}$  (1/0.98/0.02, v/v/v) at 298K: (a)  $^1\text{H}$  NMR of  $1^{4+}\cdot 4\text{PF}_6^-$  in the presence of 1 molar equiv. of 2,6-naphthalenedisulfonic acid and 2 molar equiv. of  $\text{TMA}^+\cdot\text{OH}^-$  at 10min (reaction time) ( $[\text{host}] = [\text{guest}] = 5.00 \times 10^{-3} \text{ M}$ ), (b) 1D NOE NMR spectra of  $1^{4+}\cdot 4\text{PF}_6^-$  in the presence of 1 molar equiv. of 2,6-naphthalenedisulfonic acid and 2 molar equiv. of  $\text{TMA}^+\cdot\text{OH}^-$  at 10min (reaction time) ( $[\text{host}] = [\text{guest}] = 5.00 \times 10^{-3} \text{ M}$ ). The one proton signal of the solvent  $\text{DMF-}d_7$  is labeled with a “\*”. The green arrows indicate irradiation at the frequency of H(5a) of 2,6-naphthalenedisulfonate (**5**).



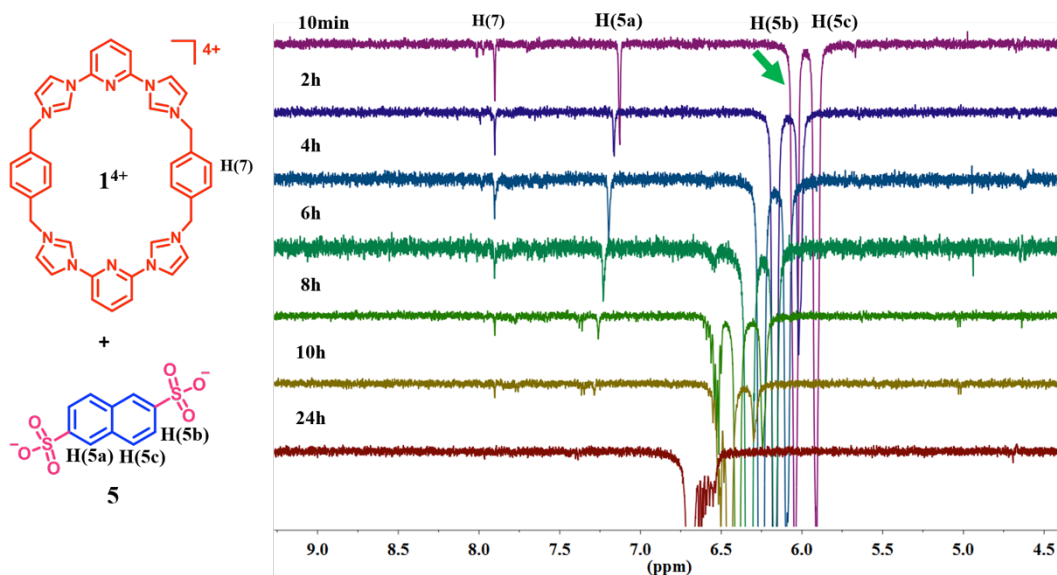
**Figure S73.** 1D NOE NMR spectra of  $1^{4+} \cdot 4PF_6^-$  recorded in the presence of 1 molar equiv. of 2,6-naphthalenedisulfonic acid and 2 molar equiv. of  $TMA^+ \cdot OH^-$  ( $[host] = [guest] = 5.00 \times 10^{-3} M$ ) in  $DMF-d_7/D_2O/ND_3 \cdot D_2O$  (1/0.98/0.02, v/v/v) at 298K (600 MHz). The green arrows indicate irradiation at the frequency of H(5a) of 2,6-naphthalenedisulfonate (**5**). These findings are consistent with **5** dethreading from the pseudorotaxane structure [ $1^{4+} \cdot 5$ ] as the reaction proceeds.



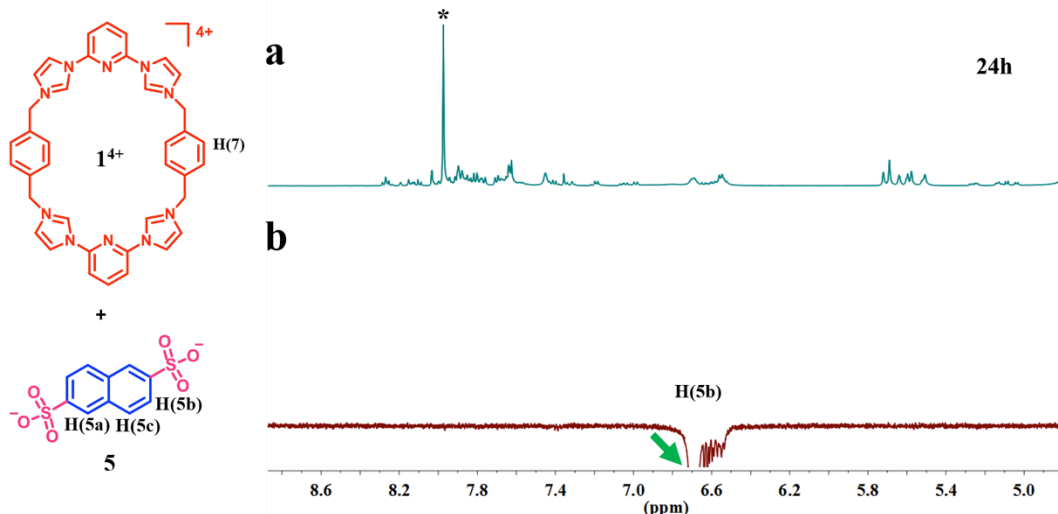
**Figure S74.** 600 MHz  $^1H$  NMR and 1D NOE NMR spectra recorded in  $DMF-d_7/D_2O/ND_3 \cdot D_2O$  (1/0.98/0.02, v/v/v) at 298K: (a)  $^1H$  NMR spectra of  $1^{4+} \cdot 4PF_6^-$  recorded in the presence of 1 molar equiv. of 2,6-naphthalenedisulfonic acid and 2 molar equiv. of  $TMA^+ \cdot OH^-$  at 24 h (reaction time) ( $[host] = [guest] = 5.00 \times 10^{-3} M$ ), (b) 1D NOE NMR spectra of  $1^{4+} \cdot 4PF_6^-$  in the presence of 1 molar equiv. of 2,6-naphthalenedisulfonic acid and 2 molar equiv. of  $TMA^+ \cdot OH^-$  at 24 h (reaction time) ( $[host] = [guest] = 5.00 \times 10^{-3} M$ ). The one proton signal of the solvent  $DMF-d_7$  is labeled with a “\*”. The green arrows indicate irradiation at the frequency of H(5a) of 2,6-naphthalenedisulfonate (**5**).



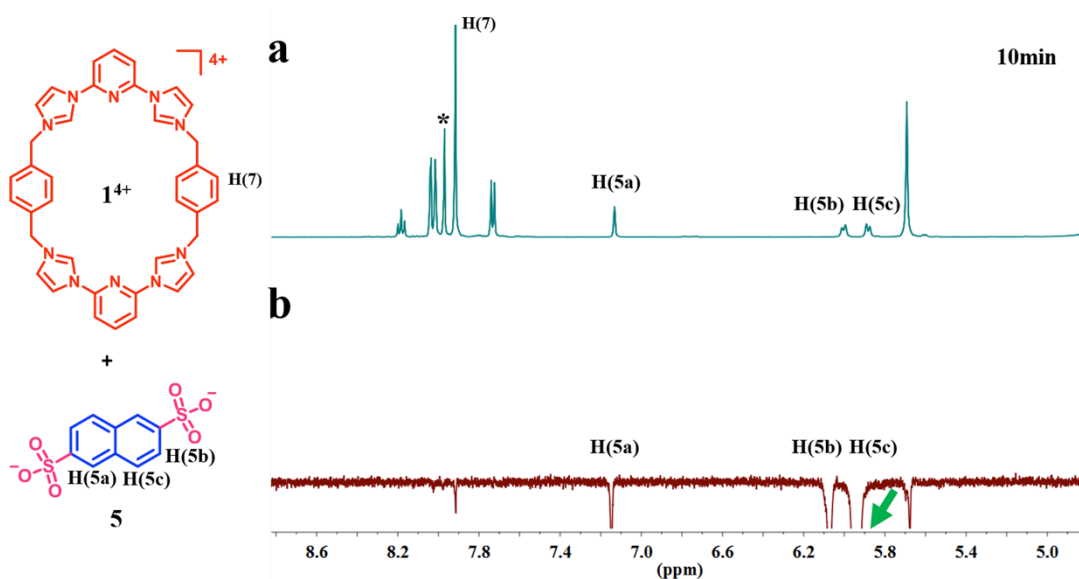
**Figure S75.** 600 MHz  $^1\text{H}$  NMR and 1D NOE NMR spectra recorded in  $\text{DMF-}d_7/\text{D}_2\text{O}/\text{ND}_3\cdot\text{D}_2\text{O}$  (1/0.98/0.02, v/v/v) at 298K: (a)  $^1\text{H}$  NMR of  $\mathbf{1}^{4+}\cdot 4\text{PF}_6^-$  in the presence of 1 molar equiv. of 2,6-naphthalenedisulfonic acid and 2 molar equiv. of  $\text{TMA}^+\cdot\text{OH}$  at 10min (reaction time) ( $[\text{host}] = [\text{guest}] = 5.00 \times 10^{-3}$  M), (b) 1D NOE NMR spectra of  $\mathbf{1}^{4+}\cdot 4\text{PF}_6^-$  in the presence of 1 molar equiv. of 2,6-naphthalenedisulfonic acid and 2 molar equiv. of  $\text{TMA}^+\cdot\text{OH}$  at 10min (reaction time) ( $[\text{host}] = [\text{guest}] = 5.00 \times 10^{-3}$  M). The one proton signal of the solvent  $\text{DMF-}d_7$  is labeled with a “\*”. The green arrow indicates irradiation at the frequency of H(5b) of 2,6-naphthalenedisulfonate (**5**).



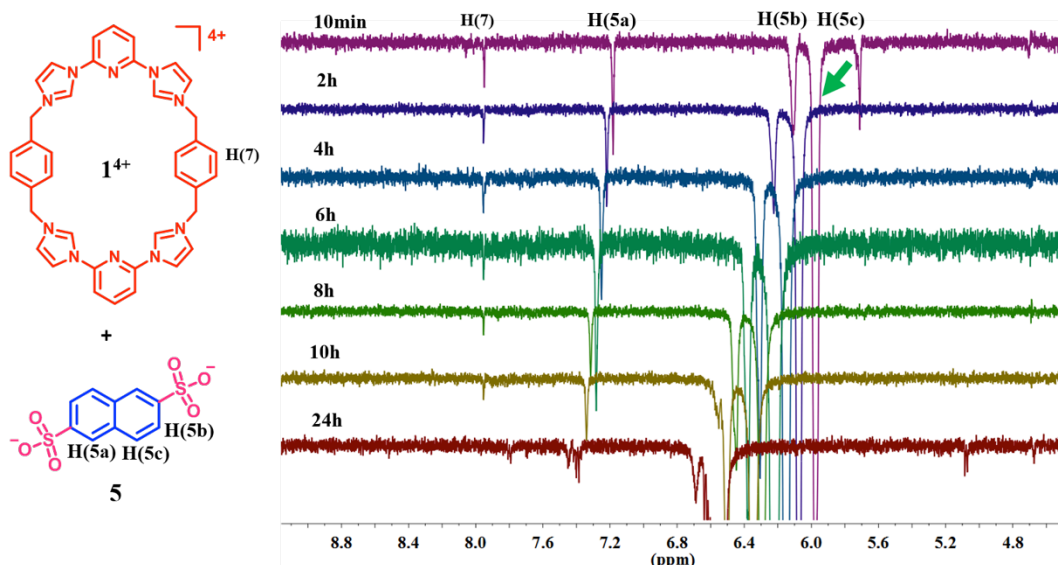
**Figure S76.** 1D NOE NMR spectra of  $\mathbf{1}^{4+}\cdot 4\text{PF}_6^-$  recorded in the presence of 1 molar equiv. of 2,6-naphthalenedisulfonic acid and 2 molar equiv. of  $\text{TMA}^+\cdot\text{OH}$  ( $[\text{host}] = [\text{guest}] = 5.00 \times 10^{-3}$  M) in  $\text{DMF-}d_7/\text{D}_2\text{O}/\text{ND}_3\cdot\text{D}_2\text{O}$  (1/0.98/0.02, v/v/v) at 298K (600 MHz). The green arrows indicate irradiation at the frequency of H (5b) of 2,6-naphthalenedisulfonate (**5**). These results are consistent with **5** dethreading from the pseudorotaxane structure  $[\mathbf{1}^{4+}\cdot\mathbf{5}]$  as the reaction proceeds.



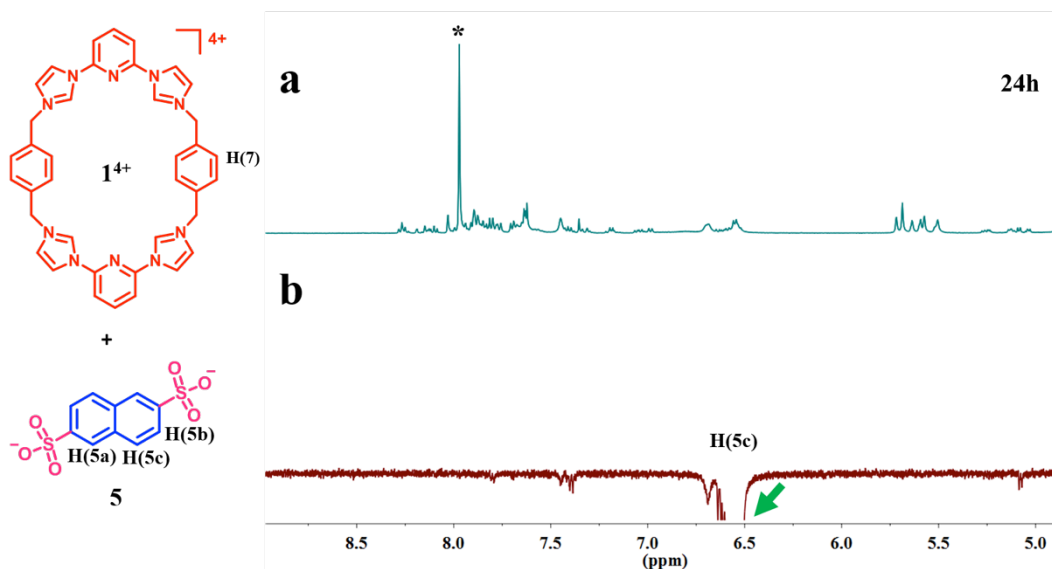
**Figure S77.** 600 MHz  $^1\text{H}$  NMR and 1D NOE NMR spectra recorded in  $\text{DMF-}d_7/\text{D}_2\text{O}/\text{ND}_3\cdot\text{D}_2\text{O}$  (1/0.98/0.02, v/v/v) at 298K: (a)  $^1\text{H}$  NMR of  $1^{4+}\cdot 4\text{PF}_6^-$  recorded in the presence of 1 molar equiv. of 2,6-naphthalenedisulfonic acid and 2 molar equiv. of  $\text{TMA}^+\cdot\text{OH}^-$  at 24 h (reaction time) ( $[\text{host}] = [\text{guest}] = 5.00 \times 10^{-3}$  M), (b) 1D NOE NMR spectra of  $1^{4+}\cdot 4\text{PF}_6^-$  in the presence of 1 molar equiv. of 2,6-naphthalenedisulfonic acid and 2 molar equiv. of  $\text{TMA}^+\cdot\text{OH}^-$  at 24 h (reaction time) ( $[\text{host}] = [\text{guest}] = 5.00 \times 10^{-3}$  M). The one proton signal of the solvent  $\text{DMF-}d_7$  is labeled with a “\*”. The green arrow indicates irradiation at the frequency of H (5b) of 2,6-naphthalenedisulfonate (5).



**Figure S78.** 600 MHz  $^1\text{H}$  NMR and 1D NOE NMR spectra recorded in  $\text{DMF-}d_7/\text{D}_2\text{O}/\text{ND}_3\cdot\text{D}_2\text{O}$  (1/0.98/0.02, v/v/v) at 298K: (a)  $^1\text{H}$  NMR of  $1^{4+}\cdot 4\text{PF}_6^-$  in the presence of 1 molar equiv. of 2,6-naphthalenedisulfonic acid and 2 molar equiv. of  $\text{TMA}^+\cdot\text{OH}^-$  at 10min (reaction time) ( $[\text{host}] = [\text{guest}] = 5.00 \times 10^{-3}$  M), (b) 1D NOE NMR spectrum of  $1^{4+}\cdot 4\text{PF}_6^-$  recorded in the presence of 1 molar equiv. of 2,6-naphthalenedisulfonic acid and 2 molar equiv. of  $\text{TMA}^+\cdot\text{OH}^-$  at 10 min (reaction time) ( $[\text{host}] = [\text{guest}] = 5.00 \times 10^{-3}$  M). The one proton signal of the solvent  $\text{DMF-}d_7$  is labeled with a “\*”. The green arrow indicates irradiation at the frequency of H (5c) of 2,6-naphthalenedisulfonate (5).

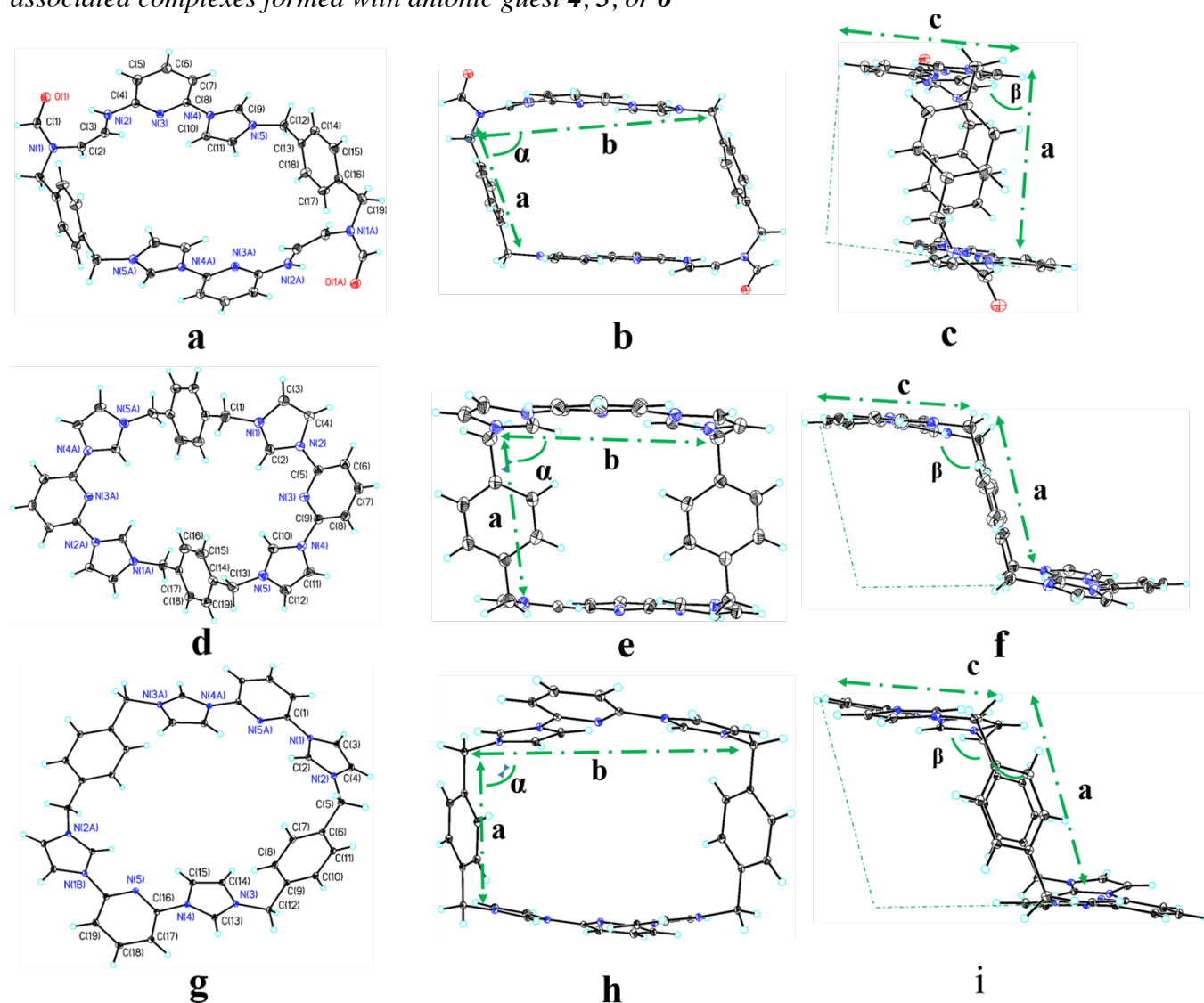


**Figure S79.** 1D NOE NMR spectra of  $1^{4+}\cdot 4\text{PF}_6^-$  recorded in the presence of 1 molar equiv. of 2,6-naphthalenedisulfonic acid and 2 molar equiv. of  $\text{TMA}^+\cdot\text{OH}^-$  ( $[\text{host}] = [\text{guest}] = 5.00 \times 10^{-3} \text{ M}$ ) in  $\text{DMF-}d_7/\text{D}_2\text{O}/\text{ND}_3\cdot\text{D}_2\text{O}$  (1/0.98/0.02, v/v/v) at 298K (600 MHz). The green arrows indicate irradiation at the frequency of H (5c) of 2,6-naphthalenedisulfonate (**5**). These findings are consistent with **5** dethreading from the pseudorotaxane structure  $[1^{4+}\cdot 5]$  as the reaction proceeds.

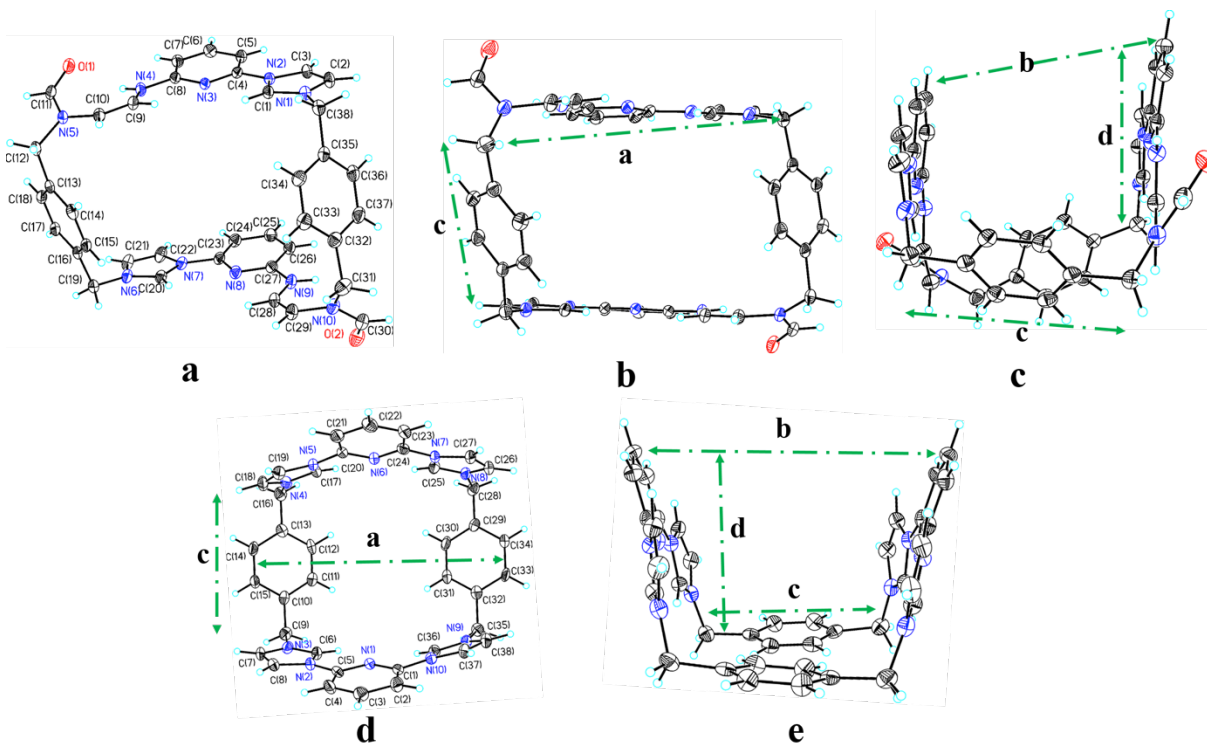


**Figure S80.** 600 MHz  $^1\text{H}$  NMR and 1D NOE NMR spectra recorded in  $\text{DMF-}d_7/\text{D}_2\text{O}/\text{ND}_3\cdot\text{D}_2\text{O}$  (1/0.98/0.02, v/v/v) at 298K: (a)  $^1\text{H}$  NMR of  $1^{4+}\cdot 4\text{PF}_6^-$  in the presence of 1 molar equiv. of 2,6-naphthalenedisulfonic acid and 2 molar equiv. of  $\text{TMA}^+\cdot\text{OH}^-$  at 24 h (reaction time) ( $[\text{host}] = [\text{guest}] = 5.00 \times 10^{-3} \text{ M}$ ), (b) 1D NOE NMR spectra of  $1^{4+}\cdot 4\text{PF}_6^-$  in the presence of 1 molar equiv. of 2,6-naphthalenedisulfonic acid and 2 molar equiv. of  $\text{TMA}^+\cdot\text{OH}^-$  at 24 h (reaction time) ( $[\text{host}] = [\text{guest}] = 5.00 \times 10^{-3} \text{ M}$ ). The one proton signal of the solvent  $\text{DMF-}d_7$  is labeled with a “\*”. The green arrow indicates irradiation at the frequency of H (5c) of 2,6-naphthalenedisulfonate (**5**).

**Section S8:** Comparative analysis of the conformation of  $[2^{2+} \cdot 2PF_6^-]$  and  $[1^{4+} \cdot 4PF_6^-]$ , and the associated complexes formed with anionic guest **4**, **5**, or **6**



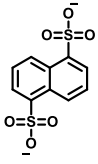
**Figure S81.** Comparison analysis of the conformations seen in “box-like” structures formed using macrocycle  $2^{2+}$  and  $1^{4+}$ . (a) full view, (b) top and (c) side views of the “box-like” conformation of  $2^{2+}$  in  $[2^{2+} \cdot 2PF_6^- \cdot 4\text{dioxane}]$ . (d) full view, (e) top and (f) side views of the “complete-chair” conformation of  $1^{4+}$  in  $[1^{4+} \cdot 4PF_6^- \cdot 4\text{DMF}]$ . (g) full view, (h) top and (i) side views of the “partial-chair” conformation of  $1^{4+}$  in  $[1^{4+} \cdot 4PF_6^- \cdot 2\text{CH}_3\text{CN}]$ . The important parameters for the cavity of  $2^{2+}$  are as follows: Selected distances [ $\text{\AA}$ ]  $a = 5.814$ ,  $b = 11.425$ ,  $c = 4.432$ ; selected angles:  $\alpha 73.36^\circ$ ,  $\beta 92.22^\circ$ . Important parameters for the cavities formed from  $1^{4+}$  in  $[1^{4+} \cdot 4PF_6^- \cdot 4\text{DMF}]$  are as follows: Selected distances [ $\text{\AA}$ ]  $a = 5.824$ ,  $b = 7.699$ ,  $c = 6.112$ ; selected angles:  $\alpha 85.34^\circ$ ,  $\beta 110.0^\circ$ .<sup>12</sup> Important parameters for the cavities formed from  $1^{4+}$  in  $[1^{4+} \cdot 4PF_6^- \cdot 2\text{CH}_3\text{CN}]$  are as follows: Selected distances [ $\text{\AA}$ ]  $a = 5.818$ ,  $b = 10.136$ ,  $c = 4.856$ ; selected angles:  $\alpha 82.53^\circ$ ,  $\beta 122.82^\circ$ .<sup>11</sup> It is noted that this molecular box  $2^{2+}$  has larger size than the box formed from  $1^{4+}$ . With same, if not, very similar width, the latter has a smaller length (9.374  $\text{\AA}$ ).



**Figure S82.** Comparison analysis of the conformations seen in “clip” structures formed using macrocycle  $2^{2+}$  and  $1^{4+}$ . (a) Full view, (b) top and (c) side views of the “clip” conformation of  $2^{2+}$  in  $[2^{2+} \cdot 2PF_6^- \cdot CH_3CN \cdot H_2O]$ . (d) Top and (e) side views of the “clip” conformation of  $1^{4+}$  in  $[1^{4+} \cdot 4PF_6^- \cdot CH_3CN]$ . Important parameters for the cavities of  $2^{2+}$  are as follows: Selected distances [Å]  $a = 9.787$ ,  $b = 7.485$ ,  $c = 5.817$ ,  $d = 5.532$ . Important parameters for the cavities of  $1^{4+}$  in  $[1^{4+} \cdot 4PF_6^- \cdot CH_3CN]$  are: Selected distances [Å]  $a = 10.314$ ,  $b = 9.370$ ,  $c = 5.770$ ,  $d = 5.863$ .<sup>11</sup> It is found that the top width of  $2^{2+}$  in its clip conformation is  $7.487 \text{ \AA}$ , which is smaller than for  $1^{4+}$  with a clip conformation of  $9.370 \text{ \AA}$ .

**Table S5.** Summary of the limiting binding modes for the complexes formed between  $2^{2+} \cdot 2PF_6^-$ ,  $1^{4+} \cdot 4PF_6^-$  and dianions (**4**, **5**, or **6**).

Guest	Binding mode with $1^{4+}$	Binding mode with $2^{2+}$
<p><b>4</b></p>	Pseudorotaxane	“Outside” mode
<p><b>5</b></p>	Pseudorotaxane	“Outside” mode

 <b>6</b>	“Outside” mode	“Outside” mode
---	----------------	----------------

**Table S6.** Summary of the calculated association constants,  $K_a$ , for the complexes formed between  $2^{2+} \cdot 2PF_6^-$ ,  $1^{4+} \cdot 4PF_6^-$  and dianions (**4**, **5**, or **6**).

Guest	Stoichiometric ratio and Association constants ( $K_a$ ) with $1^{4+}$	Stoichiometric ratio and Association constants ( $K_a$ ) with $2^{2+}$
<b>4</b>	1:1 (H:G) $K_a = (3.5 \pm 0.2) \times 10^4 \text{ M}^{-1}$	1:1 (H:G) $K_a = (2.0 \pm 0.1) \times 10^2 \text{ M}^{-1}$
<b>5</b>	1:1 (H:G) $K_a = (1.6 \pm 0.1) \times 10^3 \text{ M}^{-1}$	1:1 (H:G) $K_a = (1.7 \pm 0.2) \times 10^2 \text{ M}^{-1}$
<b>6</b>	1:1 (H:G) $K_a = (1.0 \pm 0.1) \times 10^3 \text{ M}^{-1}$	1:1 (H:G) $K_a = (4.0 \pm 0.5) \times 10^2 \text{ M}^{-1}$

**Section S8: References.**

- (1) W. L. F. Armarego, C. L. L. Chai, *Purification of Laboratory Chemicals* (Fifth Edition), Elsevier Science: USA, **2003**.
- (2) H. E. Gottlieb, V. Kotlyar, A. Nudelman, *J. Org. Chem.* **1997**, 62, 7512.
- (3) A. Altomare, M. C. Burla, M. Camalli, G. L. Cascarano, C. Giacovazzo, A. Guagliardi, A. G. G. Moliterni, G. Polidori, R. Spagna, *J. Appl. Cryst.* **1999**, 32, 115.
- (4) Sheldrick, G. M. SHELXL97. Program for the Refinement of Crystal Structures. University of Gottingen, Germany, **1994**.
- (5) R. I. Cooper, R. O. Gould, S. Parsons, D. J. Watkin, *J. Applied. Cryst.* **2002**, 35, 168.
- (6) L. J. Farrugia, *J. Applied. Cryst.* **1999**, 32, 837.
- (7) G. M. Sheldrick, *Acta Cryst.* **2008**, A64, 112.
- (8) P. Job, *Ann. Chim. Paris*, **1928**, 9, 113.
- (9) Hyperquad2003: P. Gans, A. Sabatini, A. Vacca, *Talanta*, **1996**, 43, 1739.
- (10) Ōki, M. *Applications of Dynamic NMR Spectroscopy to Organic Chemistry*; VCH, Weinheim, **1985**.
- (11) H.-Y. Gong, B. M. Rambo, E. Karnas, V. M. Lynch, J. L. Sessler, *Nature Chem.* **2010**, 2, 406.
- (12) H.-Y. Gong, B. M. Rambo, E. K. Karnas, V. M. Lynch, K. M. Keller, J. L. Sessler, *J. Am. Chem. Soc.* **2011**, 133, 1526.